

POLITECNICO DI TORINO

Master degree in Mechatronic Engineering

**Euclid High Gain Antenna Control Logic:  
flight code verification and validation**



**Supervisor**

Prof. Carlo Novara

**Internship tutors**

Eng. Andrea Bacchetta

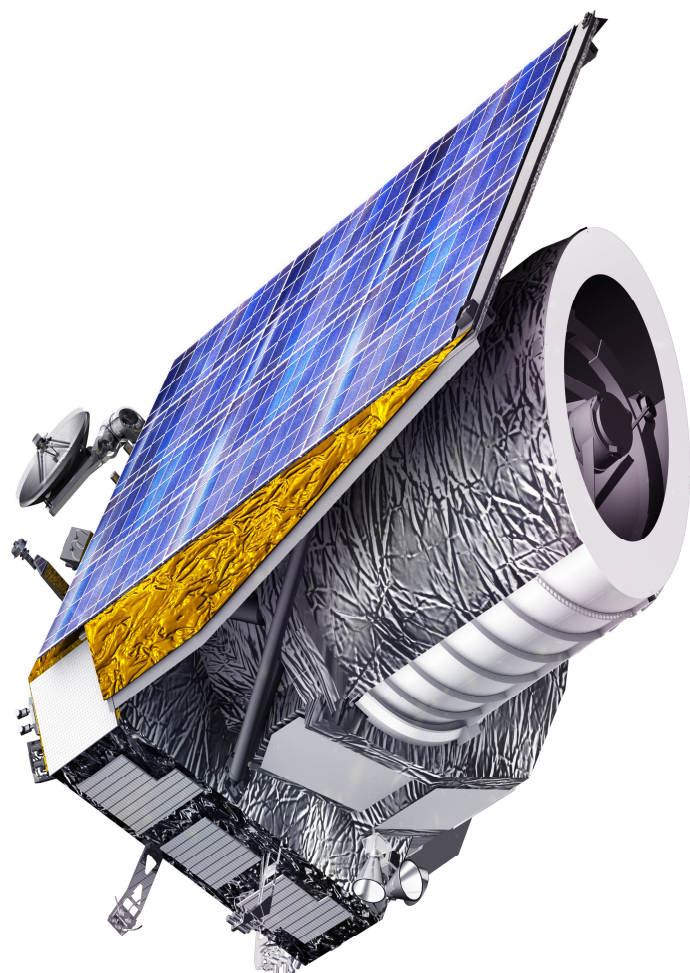
Eng. Francesco Simeoni

**Candidate**

Gabriele Vespa

July 2019





# **EUCLID spacecraft**

Credit: Thales Alenia Space



# Acknowledgements

I would like to acknowledge all the people supported me in my university journey. They have been in a special way fundamental to accomplish my work and enjoy my time.

During my six-months internship in Thales Alenia Space (site of Turin, Italy), I want to thank in particular Eng. Andrea Bacchetta and Eng. Francesco Simeoni which have entrusted in my capabilities introducing me in GNC division and giving me the honor to be involved in a so huge and ambitious project as ESA Euclid mission is.

A special gratitude goes to the academic supervisor Eng. Carlo Novara for his kindness and help.

Thank you to everyone which will spend some of their precious time to read this document.

Finally, a great heartfelt thanks to my family to keep advising me and give the opportunity to be the person I actually am.



# Abstract

The present document is meant to resume a six months internship in Thales Alenia Space, Turin, Italy for the Master degree in Mechatronic Engineering. In this period, I was involved in the European Space Agency (ESA) Euclid mission which it presents Thales Alenia Space as prime contractor.

This thesis has the goal to verify and validate the High Gain Antenna Control Logic (HGACL) simulation tool in Matlab environment as part of testing phase of the downlink antenna of Euclid spacecraft. Although the HGA system investigation was already developed from a functional point of view thanks to Euclid Engineering Group, my duty is to improve adherence of antenna software model and characterize an end to end performance test. The reader will be guided step by step through every study, analysis and test which shall reveal sufficient and necessary conditions in order to assure HGA pointing budget requirement. In particular, it will be highlighted the worsening due to misalignments on pointing performance of HGA, how the on-board Calibration of the antenna shall be implemented trying to adjust boresight alignment and if the resulting residuals are included in the expected pointing budget error.

To get the point, here it is presented the strategy pursued during the process:

- 1) ADPME testing;
- 2) Study about how antenna motors are commanded (Polynomial Law);
- 3) Calibration procedure analysis;
- 4) Simulation of a complete onboard Calibration by means of HGACL\_ESE Simulink model;
- 5) Verification of pointing performances.

The document outline is organized in the following chapters:

- Chapter 1 describes the main points of the thesis.
- Chapter 2 provides a global insight on Euclid mission overview focusing later on about characteristics of High Gain Antenna (HGA) dealing with its control logic (HGACL), electronics and mechanisms (ADPME and ADPM).
- Chapter 3 clarifies how HGACL Engineering Simulation Environment is designed.
- Chapter 4 gives emphasis to ADPME Simulink Model testing.
- Chapter 5 deals with misalignments between motors axes, polynomial correction law as relative corrective solution and how much HGA pointing performance are affected by these aspects.
- Chapter 6 studies elements affecting Calibration results.
- Chapter 7 simulates a complete 'in-flight' Calibration Procedure considering deductions from the previous chapter.
- Chapter 8 gives final conclusions.
- Annex 1 contains details on pointing error budget.



# Table of Contents

<b>LIST OF FIGURES .....</b>	<b>VII</b>
<b>LIST OF TABLES.....</b>	<b>VIII</b>
<b>DEFINITIONS AND ACRONYMS.....</b>	<b>IX</b>

## CHAPTER 1

<b>INTRODUCTION.....</b>	<b>1</b>
--------------------------	----------

## CHAPTER 2

<b>EUCLID MISSION AND HGA.....</b>	<b>3</b>
<b>2.1. Euclid mission .....</b>	<b>3</b>
2.1.1. Euclid overview .....	3
2.1.2. Scientific objectives .....	5
2.1.3. Mission Design .....	7
2.1.4. Mission Phases and SC Modes .....	9
2.1.5. Attitude and Orbit Control System (AOCS) .....	10
<b>2.2. High Gain Antenna (HGA and HGACL).....</b>	<b>12</b>
2.2.1. HGACL Mission Requirements & Design.....	12
2.2.2. Antenna Operation Analysis .....	13
2.2.3. HGACL modes .....	15
2.2.4. High Gain Major Assembly (HGAMA).....	16
2.2.5. ADPM.....	16
2.2.6. ADPME .....	17

## CHAPTER 3

<b>HGACL SIMULATION ENVIRONMENT .....</b>	<b>21</b>
<b>3.1. Description of the Model.....</b>	<b>21</b>

## CHAPTER 4

<b>ADPME MODEL TEST.....</b>	<b>25</b>
<b>4.1. Tests description.....</b>	<b>26</b>
<b>4.2. Results .....</b>	<b>27</b>

## CHAPTER 5

<b>POLYNOMIAL LAW EFFECT ON BORESIGHT</b> .....	<b>39</b>
<b>5.1. Scope and Purposes</b> .....	<b>39</b>
<b>5.2. Polynomial Correction Law assumption</b> .....	<b>39</b>
<b>5.3. Analysis of Polynomial Law effect</b> .....	<b>41</b>
<b>5.4. Analysis of results</b> .....	<b>45</b>

## CHAPTER 6

<b>STUDY OF ‘IN-FLIGHT’ HGA CALIBRATION</b> .....	<b>47</b>
<b>6.1. Scope and Purposes</b> .....	<b>47</b>
<b>6.2. Calibration procedure</b> .....	<b>47</b>
<b>6.3. Study of minimization problem and its boundary conditions</b> .....	<b>48</b>
6.3.1. General Mathematical Model.....	48
6.3.2. Errors in GS vector Estimation.....	49
6.3.3. Calibration Points.....	49
6.3.4. Calibration Minimization Problem.....	50
6.3.5. Analysis of Comparison.....	51
6.3.6. Are performances affected by the number of Calibration Points?.....	55
6.3.7. Are performances affected by different choice of Calibration Points?.....	57
6.3.8. How to choose the optimal Calibration Points.....	59
<b>6.4. Conclusions about the study</b> .....	<b>69</b>

## CHAPTER 7

<b>SIMULATION OF ‘IN-FLIGHT’ HGA CALIBRATION</b> .....	<b>71</b>
<b>7.1. Preliminary Steps</b> .....	<b>71</b>
<b>7.2. Measurements from Ground</b> .....	<b>74</b>
<b>7.3. Final Calibration Outcome</b> .....	<b>76</b>
<b>7.4. Conclusions of Chapter 7</b> .....	<b>79</b>

## CHAPTER 8

<b>FINAL CONCLUSIONS</b> .....	<b>81</b>
--------------------------------	-----------

<b>ANNEX 1: POINTING ERROR BUDGET</b> .....	<b>83</b>
---	-----------

<b>BIBLIOGRAPHY</b> .....	<b>8</b>
---------------------------	----------

# List of figures

FIGURE 2-1: EUCLID ARTISTIC IMPRESSION. CREDIT: ESA/ATG MEDIALAB .....	3
FIGURE 2-2: EUCLID AT THE STATE OF ART. CREDIT: THALES ALENIA SPACE.....	3
FIGURE 2-3: SC STEP & STARE MANEUVERS. CREDIT: THALES ALENIA SPACE .....	5
FIGURE 2-4: OBSERVATION PLAN. CREDIT: THALES ALENIA SPACE .....	5
FIGURE 2-5: UNIVERSE COMPOSITION. CREDIT: EUCLID ASSESSMENT STUDY.....	6
FIGURE 2-6: THE UNIVERSE EVOLUTION. CREDIT: EUCLID ASSESSMENT STUDY .....	6
FIGURE 2-7: ILLUSTRATION OF WEAK GRAVITATIONAL LENSING EFFECT. CREDIT: EUCLID CONSORTIUM .....	7
FIGURE 2-8: WEAK GRAVITATIONAL LENSING AND BARYONIC ACOUSTIC OSCILLATIONS. CREDIT: NASA, ESA, AND R. MASSEY .....	8
FIGURE 2-9: THE LOCATION OF THE FIELDS COPYRIGHT: ESA/GAIA/DPAC; EUCLID CONSORTIUM. ....	4
FIGURE 2-10: SUN EARTH LAGRANGIAN POINT L2. CREDIT: ESA .....	4
FIGURE 2-11: SPACECRAFT COMPONENTS. CREDIT: THALES ALENIA SPACE .....	9
FIGURE 2-12: SAA AND AA ANGLES DEFINITIONS. CREDIT: THALES ALENIA SPACE .....	11
FIGURE 2-13: INPUTS TO HGACL DESIGN .....	13
FIGURE 2-14: HGACL STATE MACHINE. CREDIT: THALES ALENIA SPACE.....	15
FIGURE 2-15: HGAMA CONCEPTUAL ARCHITECTURE. CREDIT: THALES ALENIA SPACE .....	16
FIGURE 2-16: ADPME SPEED PROFILE. CREDIT: THALES ALENIA SPACE.....	18
FIGURE 2-17: ADPME TARGET SPEED CASES (NOT REACHED IN CASE OF SMALL MOVEMENT). CREDIT: THALES ALENIA SPACE .....	18
FIGURE 3-1: HGACL ESE TOP LAYER. CREDIT: THALES ALENIA SPACE .....	21
FIGURE 4-1: ADPME SIMULINK MODEL. CREDIT: THALES ALENIA SPACE .....	25
FIGURE 4-2: TEST 1.....	28
FIGURE 4-3: TEST 2: AZ .....	28
FIGURE 4-4: TEST 2: EL .....	29
FIGURE 4-5: TEST 3: AZ .....	30
FIGURE 4-6: TEST 3: EL .....	31
FIGURE 4-7: TEST 4: AZ .....	32
FIGURE 4-8: TEST 4: EL .....	33
FIGURE 4-9: TEST 5.....	34
FIGURE 4-10: TEST 6.....	35
FIGURE 4-11: TEST 7: AZ .....	36
FIGURE 4-12: TEST 7: EL .....	36
FIGURE 4-13: TEST 7 WITH NO POLYNOMIAL LAW: AZ .....	37
FIGURE 5-1: BORESIGHT ORIENTATION IN INERTIAL REFERENCE SYSTEM (IRF).....	39
FIGURE 5-2: ERROR INDUCED BY ADPM AXES MISALIGNMENT .....	40
FIGURE 5-3: E_AZ (LEFT), E_EL (RIGHT) .....	41
FIGURE 5-4: BORESIGHT e_VEC without correction (left), e_VEC with correction (right).....	44
FIGURE 6-1: DOMAIN OF AZ/EL POINTS.....	50
FIGURE 6-2: TEST 1.....	52
FIGURE 6-3: TEST 2.....	53
FIGURE 6-4: TEST 3.....	54
FIGURE 6-5: TEST 4.....	54
FIGURE 6-6: CUMULATIVE DISTRIBUTION FUNCTIONS OBTAINED CONSIDERING 400 CASES.....	55
FIGURE 6-7: HISTOGRAM OF THE ERRORS OCCURRED; CUMULATIVE DISTRIBUTION FUNCTIONS OBTAINED CONSIDERING 400 CASES .....	55
FIGURE 6-8: GLOBAL BEHAVIOR OF THE ERRORS OCCURRED CONSIDERING 400 CASES .....	56
FIGURE 6-9: HISTOGRAM OF THE ERRORS OCCURRED; CUMULATIVE DISTRIBUTION FUNCTIONS OBTAINED CONSIDERING 400 CASES .....	56
FIGURE 6-10: GLOBAL BEHAVIOR OF THE ERRORS OCCURRED CONSIDERING 400 CASES .....	56
FIGURE 6-11: NO CALIBRATION .....	57
FIGURE 6-12: CALIBRATION WITH 1 <sup>ST</sup> SET.....	58

FIGURE 6-13: CALIBRATION WITH 2 <sup>ND</sup> SET .....	58
FIGURE 6-14: CALIBRATION WITH 3 <sup>RD</sup> SET .....	58
FIGURE 6-15: CALIBRATION WITH 4 <sup>TH</sup> SET.....	59
FIGURE 6-16: REGION COVERED BY SSCE VARIATION FROM 36° TO 7° (LEFT); RELATIVE TOP VIEW (RIGHT) .....	59
FIGURE 6-17: ACTUAL AZ/EL DOMAIN CONSIDERING SSCE CONSTRAINTS (RIGHT) .....	60
FIGURE 6-18: TEST 1 – RANDOM POINTS CALIBRATION .....	63
FIGURE 6-19: TEST 1 – FMINCON ATTEMPT 1 .....	63
FIGURE 6-20: TEST 1 – FMINCON ATTEMPT 2 .....	63
FIGURE 6-21: TEST 1 – GLOBAL SEARCH.....	64
FIGURE 6-22: TEST 1 – DIRECT SEARCH .....	64
FIGURE 6-23: TEST 1 – GENETIC ALGORITHM .....	64
FIGURE 6-24: TEST 1 – PARTICLE SWARM.....	65
FIGURE 6-25: TEST 1 – SURROGATE OPTIMIZATION .....	65
FIGURE 6-26: TEST 2 – RANDOM POINTS CALIBRATION .....	66
FIGURE 6-27: TEST 2 – FMINCON ATTEMPT 1 .....	66
FIGURE 6-28: TEST 2 – FMINCON ATTEMPT 2 .....	67
FIGURE 6-29: TEST 2 – GLOBAL SEARCH .....	67
FIGURE 6-30: TEST 2 – DIRECT SEARCH .....	67
FIGURE 6-31: TEST 2 – GENETIC ALGORITHM .....	68
FIGURE 6-32: TEST 2 – PARTICLE SWARM.....	68
FIGURE 6-33: TEST 2 – SURROGATE OPTIMIZATION .....	68
FIGURE 7-1: SPIRAL .....	72
FIGURE 7-2: TARGET QUATERNIONS .....	72
FIGURE 7-3: SC ANGULAR RATE .....	73
FIGURE 7-4: AZ/EL BEHAVIOR.....	73
FIGURE 7-5: 3-SPIRALS ACCOMPLISHMENT .....	74
FIGURE 7-6: BORESIGHT ERROR IN SC REFERENCE FRAME. ....	75
FIGURE 7-7: BORESIGHT ERROR ON GROUND.....	75
FIGURE 7-8: TEST 1 - SAA AND AA BEHAVIOR .....	77
FIGURE 7-9: TEST 1 - ALIGNMENT BTW HGA AND CEBREROS BORESIGHTS AFTER CALIBRATION .....	77
FIGURE 7-10: TEST 2 - SAA AND AA BEHAVIOR .....	78
FIGURE 7-11: TEST 2 - ALIGNMENT BTW HGA AND CEBREROS BORESIGHTS AFTER CALIBRATION .....	78
FIGURE 7-12: TEST 2 CONSIDERING 3-POINTS CALIBRATION, THE RED CURVE IS OBTAINED WITH 0.12°/S, THE BLUE CURVE WITH 0.10°/S .....	79
FIGURE 7-13: TEST 2 CONSIDERING 5-POINTS CALIBRATION, THE RED CURVE IS OBTAINED WITH 0.12°/S, THE BLUE CURVE WITH 0.10°/S .....	79

## List of tables

TABLE 2-1: HGA IN MISSION PHASES. CREDIT: THALES ALENIA SPACE .....	14
TABLE 3-1: HGACL SIMULATION ENVIRONMENT. CREDIT: THALES ALENIA SPACE .....	22
TABLE 4-1: TESTS FOR ADPME .....	26
TABLE 6-1: MINIMIZATION PROBLEM.....	48
TABLE 6-2: TESTS FOR COMPARISON IN CASE OF: NO CAL, CAL WITHOUT/WITH POLYNOMIAL CORRECTION.....	51
TABLE ANNEX 1: POINTING ERROR BUDGET .....	81

# Definitions and Acronyms

**AA:** Alpha Angle  
**AASW:** AOCS Application Software  
**HGACL:** Antenna Control Software  
**ADPM:** Antenna Deployment and Pointing Mechanism  
**ADPME:** Antenna Deployment and Pointing Mechanism Electronics  
**APE:** Absolute Pointing Error  
**ARA:** Antenna Reflector Assembly  
**ARF:** Attitude Reference Frame  
**AZ:** Azimuth angle  
**CASW:** CDMU Application Software  
**CDMS:** Command and Data Management System  
**DTCP:** Daily Telecommunication Period  
**EL:** Elevation angle  
**EME:** Earth Mean Equator and Equinox  
**ESE:** Engineering Simulation Environment  
**FDIR:** Fault Detection Isolation and Recovery  
**FGM:** Follow Ground station Mode  
**FPM:** Fine Pointing Mode  
**GS:** Ground Station  
**GTGM:** Go to Ground station Mode  
**GUI:** Guidance  
**HGAMA:** High Gain Antenna Major Assembly  
**HW:** Hardware  
**ICRF:** International Celestial Reference Frame  
**IRF:** Inertial Reference Frame  
**LEOP:** Launch and Early Orbit Phases  
**MPS:** Micro Propulsion System  
**OBT:** On Board Time  
**OCM:** Orbit Control Mode  
**SAA:** Sun Aspect Angle  
**SAM:** Sun Acquisition Mode  
**SBM:** Stand-By Mode  
**SC:** Spacecraft  
**SCM:** Science Mode  
**SFM:** Safe Mode  
**SRF:** Spacecraft Reference Frame  
**SSCE:** Sun Spacecraft Earth angle  
**SW:** Software  
**RCS:** Reaction Control System  
**RWL:** Reaction Wheels  
**TC:** TeleCommands



# Chapter 1

## Introduction

The Euclid mission is a medium class (M2) project part of the European Space Agency Cosmic Vision Program. Euclid is an optical/near-infrared survey mission designed to study the dark Universe and understand the origin of the accelerating expansion of the Universe. It will use cosmological techniques to investigate the nature of dark energy, dark matter and gravity by tracking their observational signatures on the geometry of the Universe and on the cosmic history of large structures formation. Such achievements can be attained by exploiting two different probes i.e. the weak gravitational lensing and the baryonic acoustic oscillations allowing to respectively measure shapes and redshifts of galaxies going back in time till 10 billion years ago.

The mission is scheduled to be launched in late 2022 (from Kourou by a Soyuz ST-2.1B) and will last more than 6 years orbiting around Sun-Earth Lagrangian point 2 (SEL2).

Thales Alenia Space, as prime contractor, is responsible for all the spacecraft subsystems development apart from the Payload Module instruments and the science ground segment.

As far as it concerns my role, I was involved in this project for six months internship in Thales Alenia Space (site of Turin). The core of the thesis is about the High Gain Antenna (HGA) whose function regards downlink scientific data to Earth. In detail, the end goal of the internship shall address verification and validation of the High Gain Antenna Control Logic (HGACL) in Matlab environment as part of testing phase of the downlink antenna of Euclid spacecraft.

After the preliminary chapter related to explain Euclid mission general overview and High Gain Antenna (HGA) peculiarities, the scope is to investigate a real-case problem coming from misalignments between elements of Antenna Deployment and Pointing Mechanism (ADPM). By continuing the Euclid Engineering group's HGA analysis, it will be highlighted how the actual misalignments concern pointing performance and in what manners the Onboard 'in-flight' Calibration of the antenna shall take them into consideration to lower the relative residuals. Furthermore, it must be assured such residuals are included in the expected pointing budget error (see Annex 1).

To get the point, here it is presented the strategy pursued during the process:

- 1) Consider the global Simulink Model HGACL\_ESE made up Thales Alenia Engineering Group whose scope is to reproduce the High Gain Antenna within a simplified spacecraft environment with only the needed functionalities.
- 2) Test the ADPME (Antenna Deployment and Pointing Mechanism Electronics) model block build by Sideral (one of Thales Alenia's subcontractors) pointing out eventual bugs or peculiar behaviors. Note that antenna motors are commanded in open loop with a start&stop strategy.
- 3) Study the Polynomial Law, a mathematical stratagem by Sideral to control Azimuth and Elevation motors of antenna compensating mechanical misalignments between HGA motors axes.

- 4) Analyze 'in-flight' Calibration procedure. The examination focuses on aspects which shall reveal critic as the more fitting number and/or the optimal choice of calibration points.
- 5) Simulate a complete 'in-flight' Calibration.
- 6) Check pointing requirements fulfillments and deduce final conclusions.

# Chapter 2

## Euclid mission and HGA

The first part of the paragraph has the aim of introducing Euclid mission such that the scientific objectives, the subsequent design choices and basic features are well clear to the reader. The second part deals with High Gain Antenna characteristics.

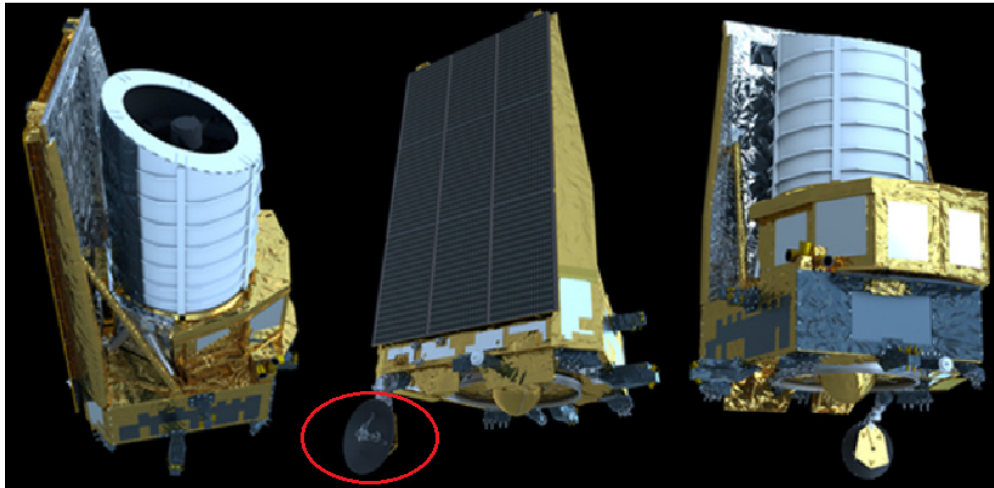


Figure 2-1: Euclid artistic impression, HGA highlighted in red. Credit: ESA/ATG medialab

### 2.1. Euclid mission

#### 2.1.1. Euclid overview

The Euclid mission is a medium class (M2) project which is part of the European Space Agency Cosmic Vision Program. Euclid emerged in 2007 during the ESA Cosmic Vision 2015-2025 Call for Proposals. The ESA advisory structure selected two interesting ideas evaluating them as equally pertinent for the investigation of dark universe: the DUNE (Dark Universe Explorer) and the SPACE (Spectroscopic All Sky Cosmic Explorer). Nowadays, the project has currently passed the Critical Design Review (CDR) under the lead of the European Space research and Technology Centre (ESTEC, Noordwijk, NL) and it is undergoing the integration and test phase in Turin (Italy) and Cannes (France) [8].

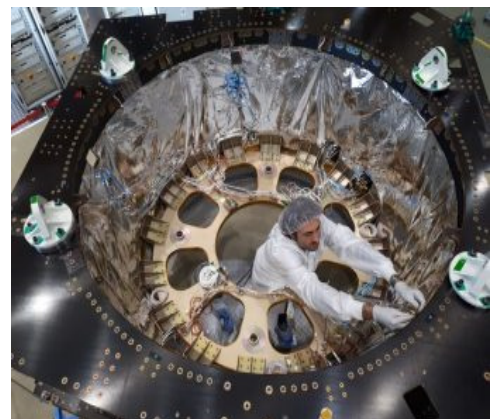


Figure 2-2: EUCLID at the state of art. Credit: Thales Alenia Space

The primary objective of the mission is trying to achieve the far ambitious goal of understanding the physics of the early universe, the formation of cosmic structures. Mission collected data will help to discriminate between concurrent cosmological theories and will be a unique resource for the scientific community impacting upon all areas of astronomy. Indeed, more than a thousand of scientists are expected to be involved from research centers all over the world.

Basically, Euclid will image billions of galaxies across the Universe to investigate the past ten billion years of our cosmic history. The largest fraction of the mission's observations will be devoted to a wide survey, covering 15 000 square degrees – more than one third of the sky. Euclid will also measure the redshifts of millions of galaxies, providing a 3D map of how galaxies are distributed in the Universe [7]. It uses a step-and-stare strategy of observation divided in Wide and Deep surveys. Each survey is organized in elementary pointing sessions (fields) which made up in their turn of four dithers whose correspondent exposure time allows instrument operating sequence [2].

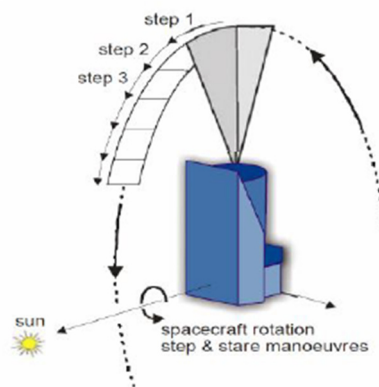


Figure 2-3: SC step & stare maneuvers. Credit: Thales Alenia Space

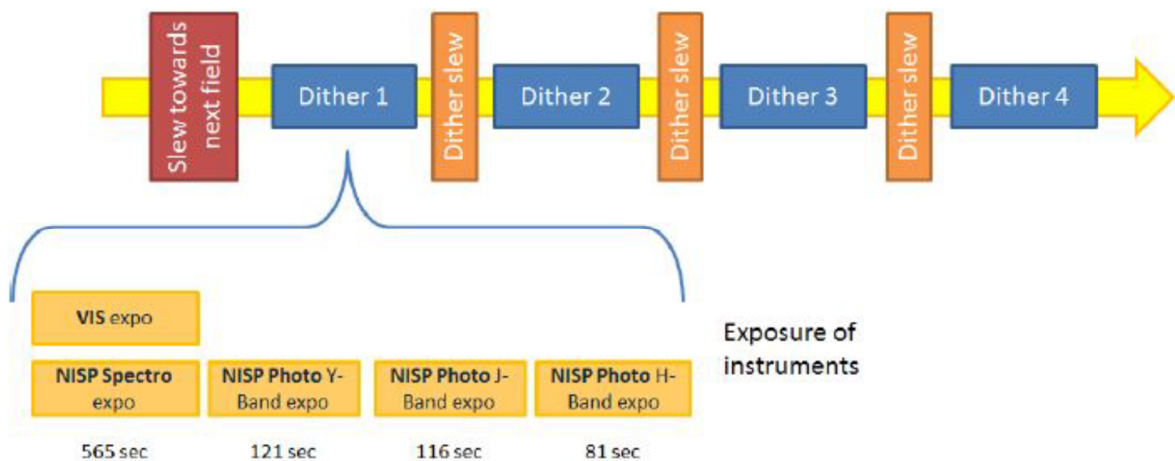


Figure 2-4: observation plan. Credit: Thales Alenia Space

The resulting spacecraft system will be at the forefront of satellite technology in several domains [1]:

- the telescope (large diameter, excellent image quality on a large FOV, free of stray-light and contamination);
- attitude measurement and control (high pointing accuracy and stability, dedicated Fine Guidance Sensor (FGS) at the telescope focal plane, fast and accurate slews);

- shape stability and temperature control (thermal stability of the focal planes, thermo-elastic stability, micro-vibration control);
- onboard data handling and communications.

### 2.1.2. Scientific objectives ([3],[4],[6],[7],[10])

The standard cosmological model works well but it includes three types of matter-energy. One of these is baryonic (ordinary) matter which represents barely ~4% of the total mass-energy according to the latest theories. The mass-energy budget of the Universe is actually dominated by two mysterious components whose nature is completely unknown and till now we do not have experimental clues but hints of their existence: dark energy and dark matter.

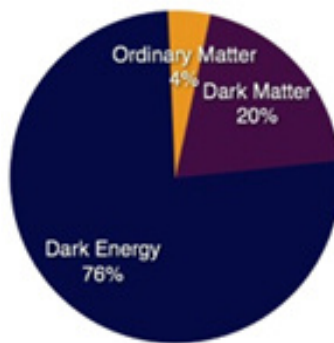


Figure 2-5: Universe composition. Credit: Euclid Assessment Study

Dark energy represents the vast majority (76%) and its signature should explain the ‘recent’ accelerating expansion of the Universe. The existence and energy scale of dark energy are out the current knowledge of fundamental physics. The remaining 20% is in charge of dark matter which, like baryonic matter, owns a gravitational field but, despite of it, not emit/absorb light. In particle physics, supersymmetric theory suggests as available candidates axion and the lightest supersymmetric particle for the cold dark matter while massive neutrinos as hot dark matter. For sure, whatever will be the result even the confirmed Einstein’s Theory of General Relativity and thus our understanding of gravity itself needs to be revised and completed.

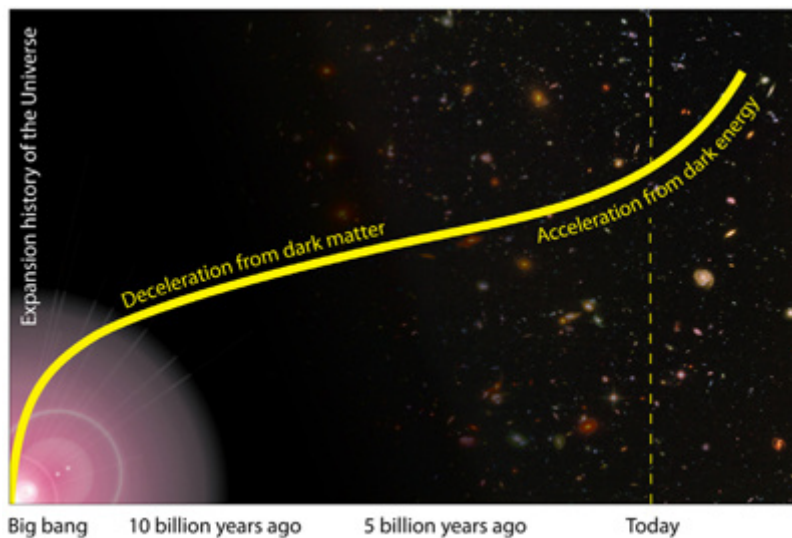


Figure 2-6: the Universe evolves from a homogeneous state after the big bang through cooling and expansion. The small initial inhomogeneities grow through gravity to produce the large-scale structures that we see today. Credit: Euclid Assessment Study

To plumb the universe, sophisticated scientific instruments are essential: a visible imager, a near-infrared photometer and a spectrograph. The first instrument is called Visual InStrument (VIS) and it works in 550-900 nm wavelength range, while the second and the third are integrated into Near-Infrared SPectrometer (NISP) that operates between 920 and 2000 nm. All these receive light from a 1.2 m Korsch telescope [2][19].

Such instruments allow analyzing the dark universe through two large-scale structures investigations:

- **Weak gravitational Lensing (WL):** “Weak lensing is a method to map the dark matter and estimate dark energy by measuring the distortions of galaxy images by mass inhomogeneities along the line-of-sight”. Extremely high image quality is required and is guaranteed by VIS.
- **Baryonic Acoustic Oscillations (BAO):** “BAOs are wiggle patterns, imprinted in the clustering of galaxies, which provide a standard ruler to measure dark energy and the expansion in the Universe”. The determination of the redshifts of galaxies to better than 0.1% accomplished through spectroscopy is achieved thanks to NISP.

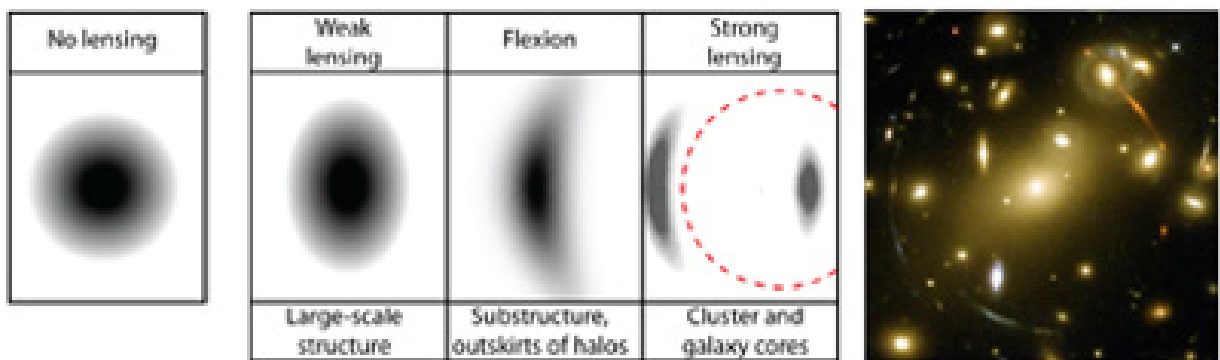


Figure 2-7: (left) Illustrations of the effect of a lensing mass on a circularly symmetric image; (right) In galaxy cluster Abell 2218, strongly lensed arcs can be seen around the cluster. Every background galaxy is weakly lensed. Credit: Euclid Assessment Study

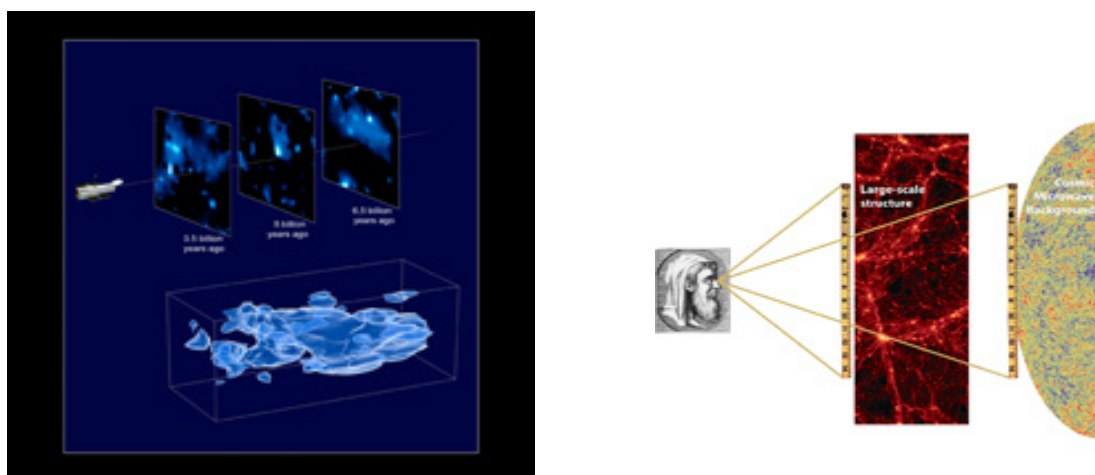


Figure 2-8: Illustration of the two primary cosmological probes of Euclid: weak gravitational lensing (left) and Baryonic Acoustic Oscillations (right). Credit: (right) NASA, ESA, and R. Massey.

In Figure 2.9, it is illustrated how scientists in the Euclid Consortium intend to scan the sky.

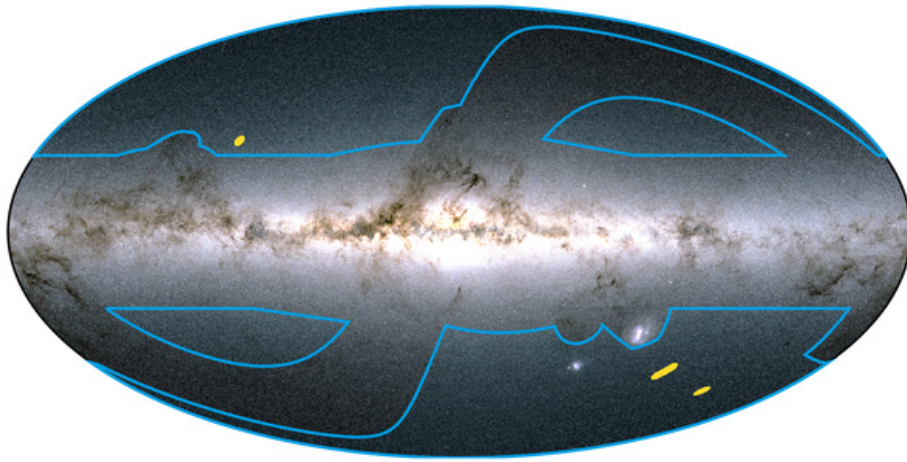


Figure 2-9: The location of the fields that will be covered by Euclid's wide (blue) and deep (yellow) surveys on an all-sky map based on data from ESA's Gaia mission. The sky is shown in the Galactic coordinate system, with the bright horizontal band corresponding to the plane of our Milky Way galaxy, where most of its stars reside. Copyright: ESA/Gaia/DPAC; Euclid Consortium. Acknowledgment: Euclid Consortium Survey Group

In Galactic coordinate system, this figure shows out the portions of the sky that will be considered so to have the best SNR (Signal to Noise Ratio) through wide and deep surveys. The wide survey is highlighted in blue and comprise the two large portions to the upper left and lower right of the Galactic Centre, and the two smaller portions to the upper right and lower left. Other regions are avoided because of deceptive influence of Milky Way stars, interstellar matter or zodiacal light i.e. diffuse dust in the Solar System. The wide survey is complemented by a deep survey. It consists of observing just three patches of the sky consuming about 10% of the total observing time: the Euclid Deep Fields, highlighted in yellow in the image. These fields have not been covered yet by any sky survey, so they have a huge scientific interest as place for new, exciting discoveries.

### 2.1.3. Mission Design ([9],[17],[19])

Driven by the demanding requirements of the wide and deep surveys, some design choices are here stated:

- The survey speed requirement, 15,000 deg<sup>2</sup> (more than a third of the sky) to be covered in 6 years, leads to:
  - Large Telescope Field of View of about 0.5 deg<sup>2</sup>
  - Optimized sky survey strategy with fast slews and fast settling times.
- The survey depth and signal to noise ratio requirements demand:
  - Mission at L2
  - Permanently shaded telescope
  - Well baffled telescope design
  - Low detector temperatures.
- The size reconstruction and stability requirements of the Point Spread Function lead to:
  - high image quality
  - high thermo-elastic stability
  - high pointing stability.

- The number of exposures per field, the high-resolution image sampling and a daily telecom period of 4 hours leads to:
  - large onboard memory
  - high science telemetry data rate (CFDP Protocol).

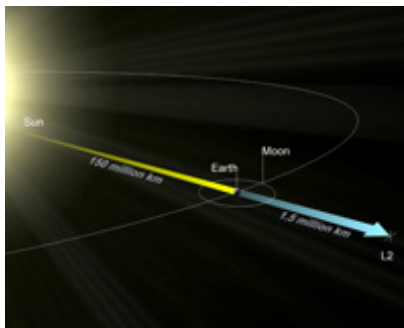


Figure 2-10: The second Sun-Earth Lagrange point (L2) is situated some 1.5 million km from the Earth on the line defined by the Sun and Earth. Credit: ESA

As already said, Euclid will be launched from Kourou, French Guyana and in about 30 days the spacecraft will reach the orbit around SEL2 by means of a Fregat ascent trajectory. The final orbit will lie in a plane nearly perpendicular to ecliptic and in such a way the SC can maintain its orbit without excessive station-keeping and attitude big adjustments. A fundamental constraint is represented by direct sun-light: a sun-shield must always keep telescope and all the electronics inside a tolerable range to prevent from overheating.

In charge of the overall SC control, Attitude and Orbit Control System (AOCS) relies on a combination of star trackers, gyroscope, cold gas micro-propulsion, reaction wheels and a Fine Guidance Sensor. Instead, chemical (hydrazine) propulsion is necessary only for dedicated maneuvers like transfer corrections, station-keeping and for Sun Acquisition maneuver at the beginning of the mission and as a principle actuator during Safe Mode.

To establish communications, three low gain antennas in X band support telecommands and real-time station-keeping, while a steerable high gain antenna in K band is used to downlink science data. In order to interact with the Earth, two ground stations (GS) are selected: one on the Northern hemisphere (Cebreros, Spain) and the other on the Southern hemisphere (Malargue, Argentina).

Solid-state mass memory stores and encodes the compressed instrument data. SpaceWire links are enrolled of reception of instrument science and housekeeping telemetry from onboard computers, collected and distributed via MIL-Std-1553 buses.

Thermal design is critical as anticipated before. An active control for payload (heaters commanded with pulse width modulation) is needed in order to guarantee high isolation and stability. In special areas, thermal baffle, radiators and blankets complete the configuration.

As source of energy, solar panels are body-mounted on sun-shield coupled with a Lithium-Ion battery.

At last, the SerVice Module (SVM) presents 6 panels and a central cone which accommodates propellant tanks. Each panel has a functional role: Telemetry and

Telecommand (TT&C), Attitude and Orbit Control (AOCS), Central Data Management (CDMS) and Electric Power (EPS), payload and Fine Guidance Sensor (FGS) warm electronics.

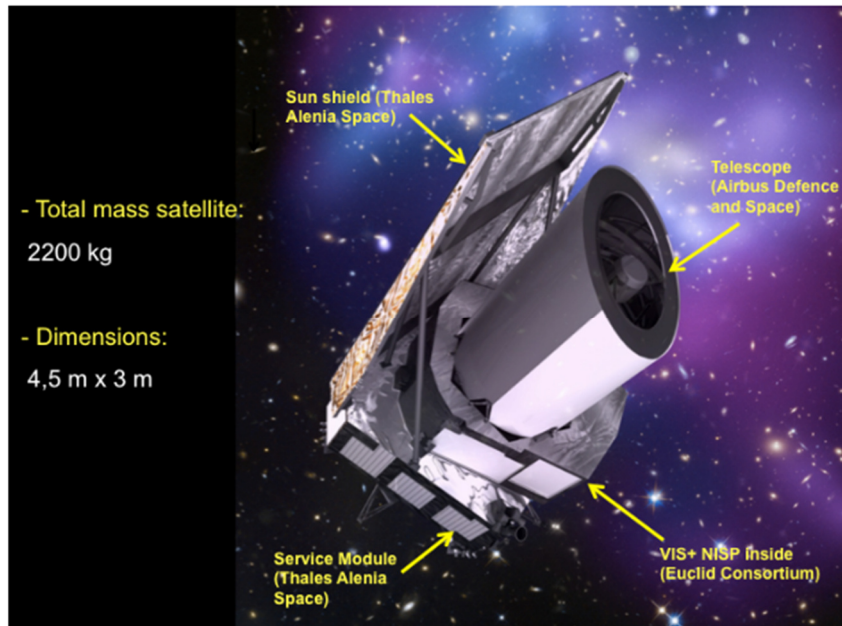


Figure 2-3: spacecraft components. Credit: Thales Alenia Space

#### 2.1.4. Mission Phases and SC Modes ([2],[17])

A brief description of the mission phases and spacecraft's operating modes is presented. The mission timeline identifies the following phases:

- *Launch (15min)*
- *Ascent (40min)*
- *Launch and Early Orbit Phases (LEOP) (1 to 4 days):* the spacecraft acquires the Sun position, reaches the target attitude, adjusts its orbit and deploys the antenna.
- *Transfer & S/C Commissioning (1 month):* the spacecraft moves to its default mode, de-ices and cools down the payload, performs further orbit adjustments.
- *Nominal Operation Phase (6 years and 2 month):* instrument commissioning happens in the first 2 months. Then the scientific observation and the orbit control are alternated. The scientific observation can be performed autonomously or during the Daily Telecommunication Period.
- *S/C Decommissioning*

The system level operating modes are the following (notice how they are strictly related to AOCS which will be highlighted later):

- *Launch Mode:* the corresponding AOCS mode is SBM
- *Sun Acquisition Mode:* the corresponding AOCS mode is SAM
- *Nominal Mode:* the corresponding AOCS modes are FPM-RCS, FPM-RWL, OCM, SCM
- *Safe Mode:* the corresponding AOCS mode is SFM
- *Attitude Hold Mode:* the corresponding AOCS mode is FPM-RCS or FPM-RWL

### 2.1.5. Attitude and Orbit Control System (AOCS) ([17],[19])

A challenging feature from engineering point of view is represented by the Attitude and Orbit Control System (AOCS). Euclid AOCS is based on a hybrid control to manage every phase and it includes:

- Star Tracker with 3 orthogonal optical heads (STR);
- Inertial Measurement Unit;
- Coarse Rate Sensors;
- Sun Sensors;
- Fine Guidance Sensor (FGS);
- 5 reaction wheels (RWL) (4 in tetrahedral configuration + 1 apart);
- redundant micro-propulsion thrusters set (2 x 6) (MPS);
- redundant chemical propulsion thrusters set (2 x 10): hydrazine Reaction Control System (RCS);

Note that all these components don't work simultaneously but in combinations for specific scopes. In fact, the SC shall perform two types of slew:

- Long slew
- Dither/Field slew

Spacecraft must guarantee long rotations are sun-safe slews, meaning that the Sun vector is nominally included in a domain such that:

- $87^\circ \leq \text{SAA} \leq 121^\circ$  where SAA stands for Sun Aspect Angle;
- $-8^\circ \leq \text{AA} \leq 8^\circ$  where AA stands for Alpha Angle.

The control problem is then rather complex. On the one hand, there is the necessity of fast and accurate large slews for survey's plan and, on the other one, of very precise pointing and small jitter for quality image purposes. These considerations provoke another important design choice: the definition of absolute and relative attitude measurement requirements.

The delivered strategy implies of determining spacecraft attitude in the Inertial Celestial Reference Frame coordinates by checking stars with respect to an on-board star catalog. Such procedure shall periodically be invoked, watch over SC stability and estimate current attitude relative to the foreseen one.

Since the requirement of high torque, actuators like the Reaction Wheels appear ideal for fast slew but they are not fitting for stable pointing performance because of noise-insertion into the system (micro-vibrations). So that only a hybrid solution can be the optimal trade-off and for example in this case RWL and Micro-Propulsion Subsystem are used in synergy to cope with both the agility and stable pointing.

Depending on the mission phase and system mode, the AOCS can move to different operating modes.

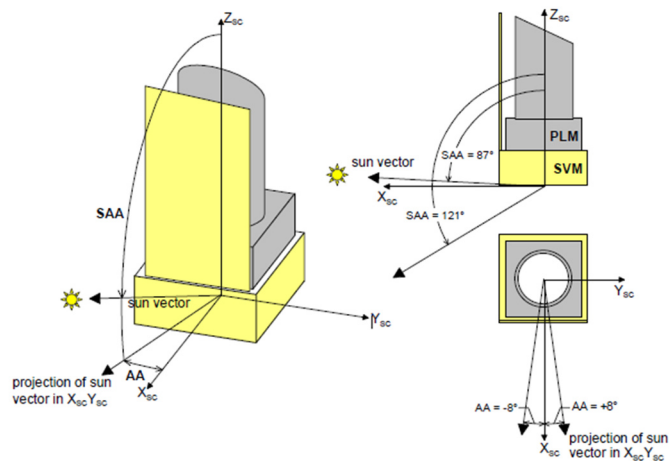


Figure 2-4: SAA and AA angles definitions. Credit: Thales Alenia Space

The main capabilities are summarized hereafter:

- **Stand-By Mode (SBM):** in this condition no active control is performed.
- **Sun Acquisition Mode (SAM):** it is entered after the launcher separation and after any on-board failure or violation of the attitude/angular rate constraints.
- **Fine Pointing Mode (FPM):** it is the mode which provides three axes stabilized attitude before the transition to other modes. It is also used as fallback mode facilitating the return to normal operation when the payload is not at risk. FPM functionalities are:
  - three axes inertial pointing during transfer and commissioning phases;
  - slew capability to achieve the proper attitude with respect to the Sun to complete the sky coverage;
  - slew capability to achieve the required attitude for orbit correction and station keeping maneuvers;
  - maintain the reference attitude during transfer and commissioning phases, during slew maneuvers, etc. in line with power, communication and PLM restricted zone requirements;
- **Orbit Control Mode (OCM):** it is in charge of executing  $\Delta V$  maneuvers for orbit injection and orbit station keeping, providing also three axis inertial pointing. Its main functionalities are:
  - three axes inertial pointing during orbit correction maneuvers;
  - maintain the attitude error within the allowed error in  $\Delta V$  inertial direction;
- **Science Control Mode (SCM):** it is in charge of performing three axes inertial pointing during scientific observations. It provides:
  - three axes inertial pointing with the scientific performance observation constraints defined by the Absolute Pointing Error (APE): 7.5 arcsec around X/Y, 22.5 arcsec around Z;
  - spacecraft slews and dithers according to planned scanning law.
- **Safe Mode (SFM):** it is activated after major on-board failure requiring full reconfiguration.

## 2.2. High Gain Antenna (HGA and HGACL)

From now on, the focus concerns the communication antenna of EUCLID for downlink. It has been estimated during its lifetime the Euclid mission will deliver an unprecedented large volume of data for a space mission: about 850 Gbit of compressed data per day for a total of more or less 30 Petabytes. To cope with such huge science data volume, K-band (25.5-27 GHz) communications will be used at a transfer rate of 55 Mbit/s. As a consequence of the large variations in the Sun-spacecraft-Earth angle, a two-degrees-of-freedom mechanism for the antenna is needed to maintain the science telemetry link to Earth.

Hereafter, all aspects related to the peculiarities of the High Gain Antenna (HGA) is going to be clarified and its control logic (HGACL) will be explained. Therefore, any misbehavior (both software and hardware) from this component is going to be deeply investigated avoiding the worst scenarios as far as predictable and assuring to fulfil high level requirements and correctly interface with SC equipment and subsystem.

### 2.2.1. HGACL Mission Requirements & Design ([2],[17])

The High Gain Antenna Control Logic (HGACL) needs to point the High Gain Antenna towards the Ground Station for 4 hours of Daily Telecommunication Period (DTCP) so that globally, at the end of the mission, the HGACL shall deliver the 98% instruments data generated onboard. It means that the HGA has to maintain the pointing during DTCP constantly with an accuracy of at least 0.4 deg or conversely 24 arcmin (see ANNEX 1) assuming the nominal downlink EIRP 51.8W. Note that the apparent circle of the Earth from L2 is smaller than the cone of the HGA lobe. This means that is not sufficient to orient towards the Earth center, but it is necessary to select properly the GS (Cebreros or Malargue) to be targeted.

Due to stringent directivity requirement, a parabolic antenna seems to be the most fitting choice since it characterizes by the narrowest beam-width and high gain for point to point communications. Nevertheless, several external error sources may impact the pointing requirement e.g. the AOCS introduces attitude errors and computes the ground station vector in a discrete way. Other errors are related to the approximated knowledge of the Euclid position and of orbit environment which takes into account Sun-Spacecraft-Earth angle (SSCE), Solar Aspect Angle (SAA) and Alpha Angle (AA). All these contributions have to be considered in the HGACL pointing budget.

As a further matter, the High Gain Antenna shall be compatible with at least 60000 Scientific Observations. This entails either the HGACL and HGA pointing performances shall be well-suited with lifetime constraints of Antenna Deployment and Pointing Mechanism Electronics (ADPME) and Antenna Deployment and Pointing Mechanism (ADPM) otherwise a degradation compromising mission functions can occur, i.e. the total sweep angle of the single motor cannot be larger than 228800 deg.

It is worth to highlight the antenna movements aiming for exact alignment during DTCP can take place only during a SC slew (in SCM/FPM-RWL) or when the SC is pointing in FPM-RWL, in other words it's mandatory the operations of the HGA shall not disturb the Scientific observation and not introduce any delay.

Another feature is the HGACL support for both SC autonomous operations and commands delivered by ground stations through Mission Timeline (MTL).

The design of HGACL depends on many elements which are summarized in Figure 2.13 and then briefly highlighted:

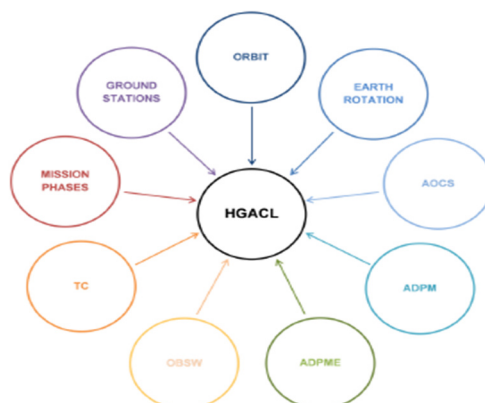


Figure 2-5: inputs to HGACL design

- Mission phases determine when the antenna needs to be commanded during the Euclid mission.
- Ground stations, orbit and Earth rotation are related to the GS vector computation.
- AOCS controls the spacecraft attitude and so affects the GS position in the SC reference frame. The kinematic of the slew maneuvers also affects the performance of the control law of the antenna.
- ADPM is the mechanical actuator and provides kinematic and dynamic constraints. It introduces disturbances due to micro-vibrations and thermoelastic deformations, affecting the pointing budget. The lifetime of the ADPM can influence control strategy.
- ADPME is the ADPM FPGA-based electronic driver. It is in charge to control ADPM motors in order to follow the reference provided by HGACL. The ADPME generates a profile to be followed by the ADPM motors. This profile drives the control strategies and the achievable performance. The performance of the ADPME control in terms of resolution in angle and velocity impacts on the overall pointing performance.
- OBSW (CASW) is where HGACL Application Software will be included. The HGACL shall use the interfaces, the variables available in the Data Bank and the scheduling capabilities provided by CASW.
- Telecommands (TCs) are the interfaces that Ground uses to command the HGACL.

### 2.2.2. Antenna Operation Analysis [17]

Depending on the mission phase, system and AOCS mode, it can be necessary to move the antenna:

- *Launch and Ascent:*
  - during SBM, the antenna is stowed.
- *LEOP:*
  - during SAM, there is no possibility to point the antenna (the attitude quaternion is not available).
  - during TCM1 (AOCS is in OCM), it is not foreseen to command the HGA.
- *Transfer & Commissioning:*
  - The HGA (mechanism + electronics + HGA Control Logic) will be commissioned. It includes calibration activities.

- During FPM-RWL, HGA shall be pointed towards the Ground Station (GS) during DTCP. There are no specific requirements since there will not be Science activities.
- During FPM-RWL out of DTCP there are no requirements on HGA pointing and no requirements on time before pointing availability
- During OCM, it is not foreseen to command the HGA.
- When AOCS is in SCM, there are no specific requirements in DTCP.
- When AOCS is in SCM, there are no specific requirements out of DTCP.
- **Nominal Operational Phase:**
  - During SCM, the S/C shall be able to point HGA automatically during slews and keep the link budget during DTCP (Daily Telecommunication Period).
  - During SCM and out of DTCP there are not specific requirements, except to not interrupt/compromise the science operations. This includes also that the re-pointing before the next DTCP shall be performed with disturbing Science Observations
  - During OCM, it is not foreseen to command the HGA.
  - During SAM, HGA it is not foreseen to be commanded, since the attitude quaternion is not verified.
- **Safe Mode**
  - When the SC enters in SFM there are no means to point the antenna to GS.
  - When the S/C enters in SFM the ADPME sends a command to drive the antenna in safe position.
- **Attitude Hold Mode**
  - When S/C falls back to AHM, the Antenna is pointed to a default position defined in body axes (target AZ, EL stored onboard). The target angles are maintained by Ground.
  - When in Attitude Hold Mode, it is possible to command the HGA in order to point the GS with nominal accuracy ensuring K-Band downlink.

Table 2.1 summarizes all the relations between the different mission phases, system and AOCS sub-modes, DTCP, slews and if antenna movements are foreseen or not.

Table 2.1. Credit: Thales Alenia Space

Mission Phase	Mission Event or sub-phase	SYSTEM MODE	AOCS MODE	SO	DF Slew	Long Slew	Antenna movement
Launch	Pre-launch	LM	SBM				
Ascent	Ascent	LM	SBM				
LEOP	Initial Attitude Acquisition	SAM	SAM				
LEOP	sun Pointing	SAM	SAM				
LEOP	TCM1 Preparation	Nominal	FPM-RCS				
LEOP	TCM1	Nominal	OCM				
LEOP	RWL commissioning	Nominal	FPM-RWL				Deploy
Transfer and S/C Commissioning	SVM commissioning & FLM Decontamination	Nominal	FPM-RWL			Yes	Yes
Transfer and S/C Commissioning	FLM de-icing	Nominal	FPM-RWL			Yes	Yes
Transfer and S/C Commissioning	FLM cool down + FGS Instruments Cool Down	Nominal	FPM-RWL			Yes	Yes
Transfer and S/C Commissioning	FLM cool down + FGS Instruments Cool Down	Nominal	SCM			Yes	Yes
Transfer and S/C Commissioning	TCM2	Nominal	OCM				
Transfer and S/C Commissioning	TCM3	Nominal	OCM				
Nominal Phase	Operation	Autonomous Operations	SCM	Yes	Yes	Yes	Yes
Nominal Phase	Operation	Autonomous Operations	FPM-RWL			Yes	Yes
Nominal Phase	Operation	Station Keeping	OCM				

S/C Decommissioning	Decommissioning	Nominal	OCM				
Safe mode	Safe Mode	SFM	SFM				
Attitude Hold Mode	Attitude Hold Mode	Attitude Hold Mode	FPM				Yes

### 2.2.3. HGACL modes [17]

Now an analysis of antenna modes and their description is furnished. Five operating modes are conceived:

- 1) Standby Mode (SBM)
- 2) Hold Mode (HM)
- 3) Follow GS Mode (FGM)
- 4) Go To GS Mode (GTGM)
- 5) Go To Next DTCP Mode (GTDM)

The brief description of the modes is the following:

- 1) SBM is necessary in order to put the HGACL in standby conditions, after the HGACL initialization or if the other modes have received an abort telecommand. If the ADPME is not operative, rejects all the incoming commands otherwise accepts only “Go to Hold Mode” telecommand.
- 1) HM is a waiting mode which detects AOCS and switches to other operating modes if certain conditions are verified as soon as possible.
- 3) Follow GS Mode is in charge to command the ADPME in such a way to follow autonomously the ground station when the spacecraft is slewing during DTCP.
- 4) GTGM was designed in order to align the HGA as fast as possible towards the selected ground station.
- 5) During science, GTDM checks if the targets provided by Ground are reachable in an amount of time equal to the slew duration, otherwise it computes the achievable angles and provides them to the ADPME. If the AOCS is in FPM-RWL, FPM-RCS or OCM, the HGACL in GTDM moves the HGA towards an AZ-EL target provided by Ground as fast is possible.

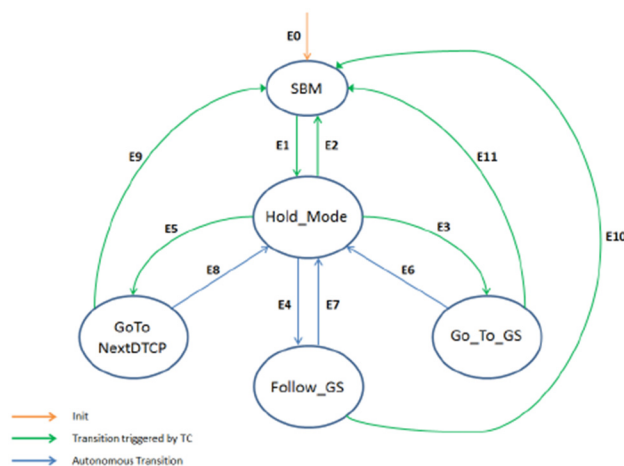


Figure 2-6: HGACL state machine. Credit: Thales Alenia Space

It is worth to put in evidence that no transitions are allowed between low-level operating modes: each one must return to Hold Mode. This choice reduces the design complexity, the difficulties related to the change of mode when the mechanism is being commanded

and last but not least, reduces the number of tests. SBM can be reached from any mode upon the arrival of an “abort” TC.

#### 2.2.4. High Gain Major Assembly (HGAMA) [17]

The High Gain Major Assembly (HGAMA) is composed by the Antenna Assembly and the driving electronics ADPME (Antenna Deployment and Pointing Mechanism Electronics). The HGAMA design is able to fulfill all the static (i.e. angle ranges) and kinematics (i.e. angular rates) requirements imposed by the Euclid mission, in particular the S/C attitude domain and orbit.

The Antenna Deployment and Pointing Mechanism (ADPM) is composed by three independent actuators, mutually perpendicular. The Deployment Mechanism will be commanded only at the deployment of the Antenna, while the Azimuth and Elevation motors will be commanded through the ADPME for all SC lifetime in order to correctly point the GS. The HGACL shall compute the commands to be sent to ADPME through CASW fulfilling this task during nominal SC operations.

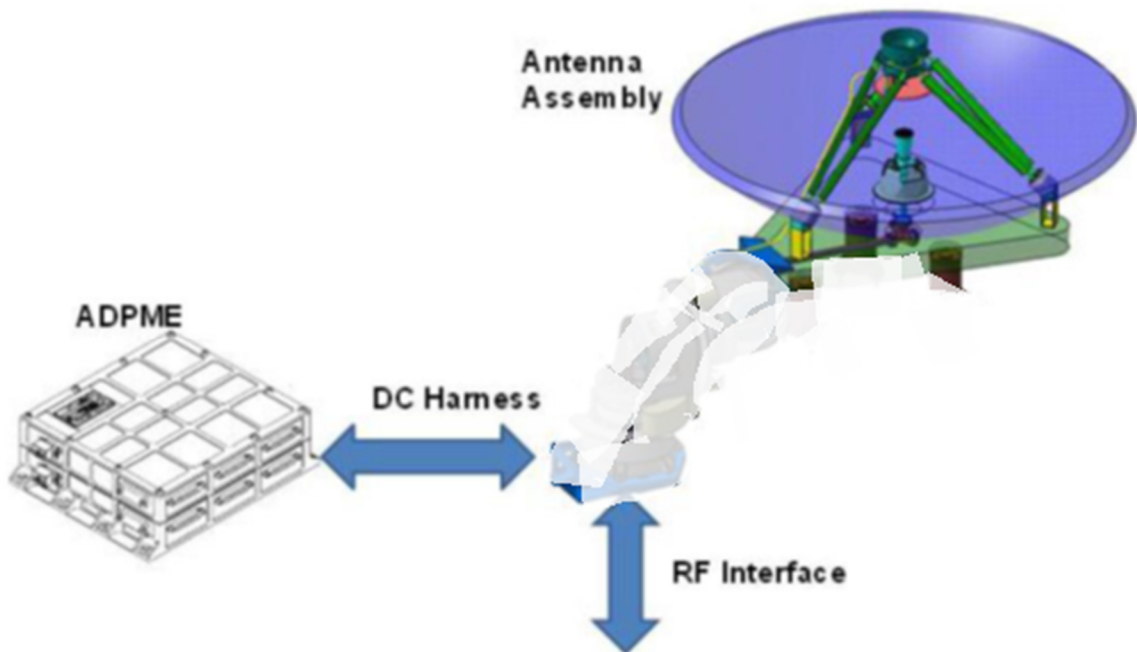


Figure 2-7: HGAMA conceptual architecture. Credit: Thales Alenia Space

The ARA (Antenna Reflector Assembly) gathers together the HGA (High Gain Antenna) and its support structure.

The ADPME is a box containing two electronic boards (internally redundant) used to control the ADPM. This electronic component is controlled by the Command and Data Management System (CDMS) via MIL-STD-1553B, specific High Priority Commands (HPC) and Bi-level Status Monitor (BSM) interfaces.

The CDMU Application Software (CASW) is in charge of dispatching the proper commands to the ADPME in order to steer the Azimuth and Elevation actuators during SC slews and follow the GS position with the antenna.

#### 2.2.5. ADPM [17]

The ADPM is composed by three independent actuators (mutually perpendicular) and a specific system for communicating:

- 
- 1) One linked to the S/C is the 1st axis. It's used to deploy the Antenna Reflector Assembly;
  - 2) One intermediate actuator in the 2nd axis. It's used for Azimuth steering;
  - 3) One actuator linked to the Antenna Reflector Assembly (3rd axis). It's used for Elevation steering.
  - 4) Rotary Joints (for K band) and twist-capsule/wrap-cable system (for X band)

Static and dynamic capabilities are summarized hereafter:

- Angles:
  - Angles range:
    - $-55^{\circ} \leq AZ \leq 55^{\circ}$  in Azimuth
    - $-70^{\circ} \leq EL \leq 40^{\circ}$  in Elevation
  - Final angle accuracy: 1 arcmin (including calibration error);
  - 1 step =  $1^{\circ}/160 = 0.00625^{\circ}$ ;
  - Micro-step control: 1 micro-step=step/64
- Angular rate
  - Maximum angular rate: 0.3 deg/s for each axis;
- Angular acceleration:
  - Maximum angular acceleration:  $0.04 \text{ deg/s}^2$ , for each axis;

As far as it concerns the lifetime of the ADPM, the total angle of rotation of the single motor has been identified as the limiting factor and it shall correspond to 228800 deg. This angle has been defined as the total sweep angle and it is linked to the performances of the potentiometer.

### 2.2.6. ADPME [17]

The ADPME (Antenna Deployment and Pointing Mechanism Electronics) is an electronic equipment in charge to control target angles and angular velocities to the ADPM.

The functionalities related to the HGACL are:

- Drive ADPM actuators during antenna Azimuth and Elevation steering;
- Provide acquisition, formatting and reporting of internal HK (Housekeeping);
- Provide HPC (High Power Command) and BSM (Bi-level Switch Monitor) direct TM/TC interfaces;
- Interface the CDMU through MIL-STD-1553B I/F.

It was verified what control strategy would be able to guarantee the pointing requirement. Analysis led to choose an open loop control strategy which behaves in a different way depending on the situation:

- When the antenna tracks the ground station during a SC slew, HGACL sends new references to the ADPME every 15s. Every position reference is reached by ADPME with a trapezoidal velocity profile in such a way to perform a sequence of start&stop movements. HGA is commanded also during dither slews.
- When the antenna needs to be pointed towards a given target or has to be aligned fast with the ground station vector, HGACL sends a position reference and a target coasting rate which is equal to the maximum allowed rate.

The major drawbacks are the readiness of the system and a poorer pointing accuracy with respect to more sophisticated control methods e.g. closed loop strategies. Both limitations are nevertheless mitigated by providing a sequence of intermediate targets every 15 seconds. And by the presence of the “stop” phase which compensates for the residual errors caused by the ADPME erroneous rates and velocity resolution. Overall, this control solution was selected thanks to its design and testing simplicity.

For what concern the actuation during any type of slews, it was verified that the HGA motion shall not endanger the APE performance since the inertia moment of the HGA is 2000 times lower than the S/C provoking only a negligible S/C angular rate with no impact on Science survey.

Deepening about trajectory generation, the ADPME allows the simultaneous motion of both Azimuth and Elevation actuators in order to reach the Target Position by generating the velocity profile shown in Figure 2.16:

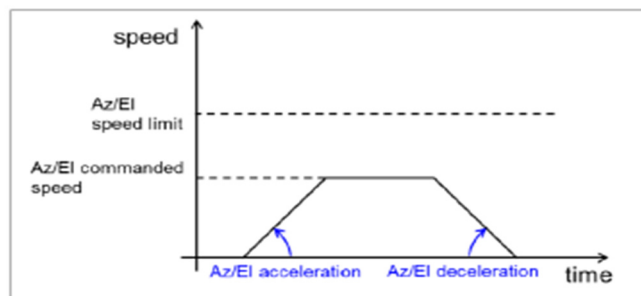


Figure 2-8: ADPME speed profile. Credit: Thales Alenia Space

The trapezoidal profile is obtained by considering a constant default acceleration/deceleration value of  $0.04^{\circ}/s^2$  with a resolution of  $0.005^{\circ}/s^2$ . For what concern the velocity, ADPME shall use a well-defined speed parameter as default while it shall use a different speed value only when requested.

The velocity is constrained by a maximum value of:

- 48steps/s (equivalent to  $0.3^{\circ}/s$ ) around Azimuth axis
- 48steps/s (equivalent to  $0.3^{\circ}/s$ ) around Elevation axis

In any case, the target angular speed shall have a resolution of 0.08 step/s (or equivalently  $5e-4^{\circ}/s$ ) even if the unit is able to achieve a resolution of  $3e-4^{\circ}/s$ .

In case of small movements with a duration such that the target speed cannot be reached, ADPME manages the actuators’ speed profile according triangular speed profile:

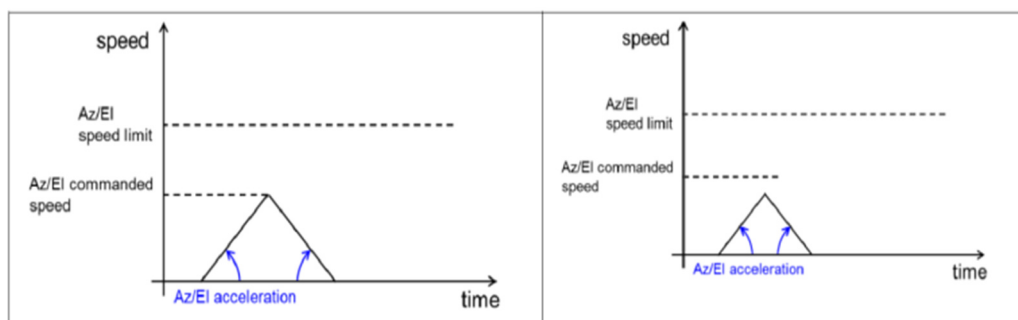


Figure 2-9: ADPME target speed cases (not reached in case of small movement). Credit: Thales Alenia Space

---

ADPME performs degree to step conversions using the conversion factors  $1 \text{ step/s} = 0.00625^\circ/\text{s}$  and  $1 \text{ step} = 0.00625^\circ$ . Moreover, the ADPME has a polynomial law that translates angles in steps and steps in angle. In this way the misalignment between nominal Azimuth rotation and Elevation rotation axis can be reduced. The polynomial law couples the AZ and EL steps, so it can happen that if only one axis rotation is commanded, both axes need to be moved. Finally, ADPME commands the actuators through the micro-step technique which implements 64 micro-steps per step.



# Chapter 3

## HGACL Simulation Environment

This chapter describes the HGACL Engineering Simulation Environment providing a general overview of the simulator. The HGACL\_ESE was developed with MATLAB 2014a 32bit by the Euclid Engineering group in order to support the HGACL software development and testing. It uses a fixed step size solver and will be largely used for the scopes of the thesis.

Here the top layer structure (Reference-Control-Plant) shown in Figure 3.1.

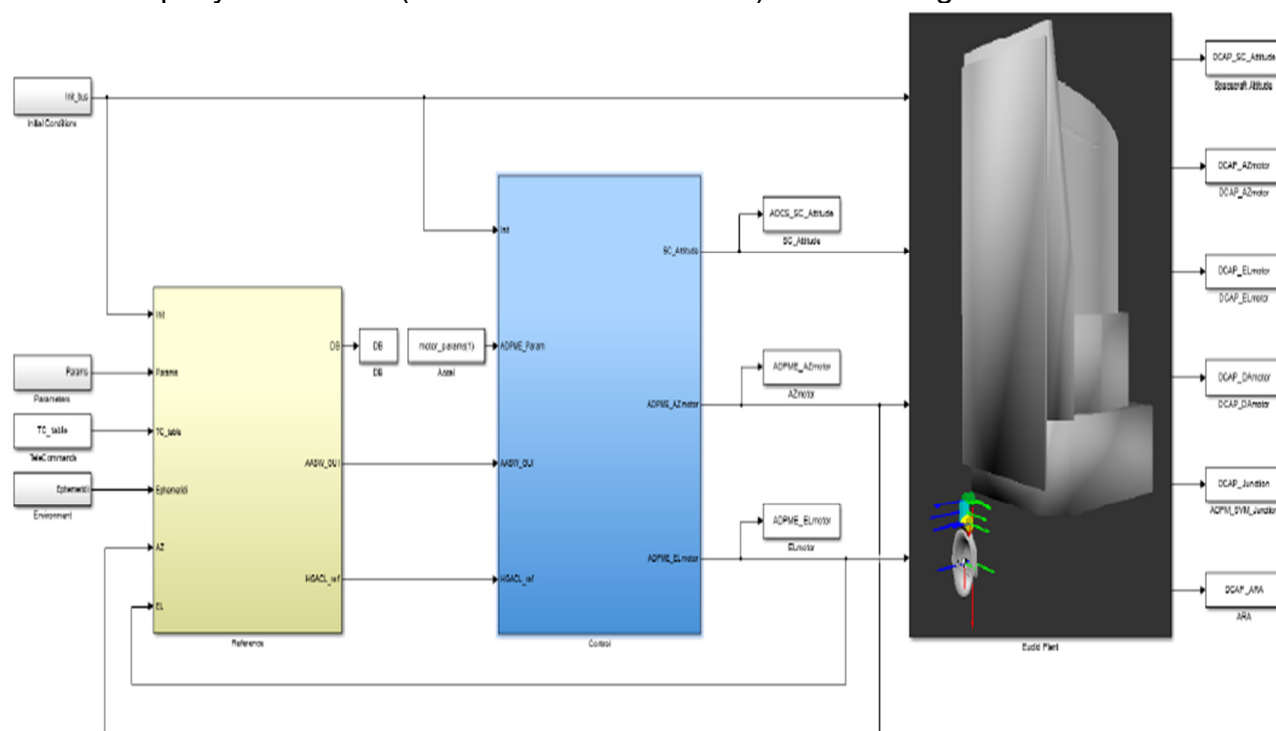


Figure 3-1: HGACL ESE top layer. Credit: Thales Alenia Space

### 3.1. Description of the Model [16]

‘External Inputs’ are essentially the initial conditions, general parameters and orbit-related quantities: in specific the ‘TC\_Table Block’ provides an input list of telecommands while the ‘Environment Block’ computes the Earth, Sun and GS vectors with respect to the IRF according to the spacecraft’s orbit.

The ‘Reference Block’ contains a simplified model of the AOCS Guidance (derived from a complete one done by SENER, one of Euclid mission subcontractors) and SW Data Handling in in such a way to reproduce only the needed functionalities and reduce the overall complexity. The AOCS Guidance is composed by three blocks: the AOCS manager (which reproduces the AOCS state machine and manages the incoming requests), the AOCS GUI (which builds the attitude quaternion during sun-safe long slews and dither slews) and the GS SRF block which rotates the ground station vectors from the IRF to the SRF with the attitude quaternion. Moreover, the ‘Reference Block’ contains the HGACL, whose functions are written in C functions.

The ‘Control Block’ contains the ADPME model and AOCS controller. The first one is provided by SYDERAL (another Euclid mission subcontractors) and it directly controls the ADPM according to the references provided by the HGACL. Instead, the AOCS controller is assumed to be an ideal one which tracks perfectly the input guidance signal. This choice was done in order to reduce the ESE complexity, anyway the errors associated to AOCS control were considered in the HGACL pointing budget.

The ‘Plant Block’ is essentially a S-function developed with the aid of DCAP (Dynamics and Control Analysis Package) which, as Fortran-oriented software, autonomously writes the dynamic equations of motion starting from a user defined configuration of bodies and hinges.

In the Table 3.1, more details from Figure 3.1. are unfolded:

Table 3.1. Credit: Thales Alenia Space

<b>Block Name</b>	<b>Description</b>	<b>Input</b>	<b>Output</b>
<i>Initial Conditions</i>	Block that reads the initial conditions from the MATLAB workspace	-	Initial conditions for each block
<i>Telecommands</i>	A table which contains a list of telecommands that are provided during the simulation	-	TC table
<i>Environment</i>	A block which interpolates the Euclid trajectory provided by ESOC and computes Sun, Earth and GS vectors according to the actual position of the spacecraft.	-	Sun, Earth, GS vectors and unit vectors in the inertial reference frame
<i>Reference Generator</i>	Contents: <ul style="list-style-type: none"> <li>• Dummy TC Handler</li> <li>• Dummy AOCS Guidance derived from the complete one provided by SENER</li> <li>• HGACL</li> </ul>	<ul style="list-style-type: none"> <li>• Initial conditions</li> <li>• Parameters</li> <li>• TCs</li> <li>• Sun/Earth/GS vectors</li> <li>• ADPME AZ-EL angles</li> </ul>	<ul style="list-style-type: none"> <li>• Reference attitude quaternion of the spacecraft</li> <li>• Azimuth and Elevation reference angles</li> <li>• Azimuth and Elevation reference coasting rates</li> </ul>

			<ul style="list-style-type: none"> <li>• DB structure saved into the MATLAB workspace and used for plots and debug.</li> </ul>
<i>Control</i>	<p>Contents:</p> <ul style="list-style-type: none"> <li>• Dummy AOCS controller (an ideal controller which tracks perfectly the reference signal)</li> <li>• ADPME model provided by SYDERAL</li> </ul>	<ul style="list-style-type: none"> <li>• Initial conditions</li> <li>• Reference attitude quaternion of the spacecraft</li> <li>• Azimuth and Elevation reference angles</li> <li>• Azimuth and Elevation reference coasting rates</li> </ul>	<ul style="list-style-type: none"> <li>• Spacecraft RPY acceleration</li> <li>• Azimuth motor acceleration</li> <li>• Elevation motor acceleration</li> </ul>
<i>EUCLID Plant</i>	<p>Euclid's simplified multi-body dynamic model realized with DCAP</p>	<ul style="list-style-type: none"> <li>• Initial conditions</li> <li>• Spacecraft acceleration in terms of RPY angles</li> <li>• Azimuth motor acceleration</li> <li>• Elevation motor acceleration</li> </ul>	<ul style="list-style-type: none"> <li>• Spacecraft attitude</li> <li>• Position and velocity of the Azimuth motor</li> <li>• Position and velocity of the Elevation motor</li> <li>• Position and velocity of the Deployment motor</li> <li>• Forces and torques at the SVM-ADPM junction</li> <li>• ARA CoM position and velocity wrt SRF</li> <li>• Boresight axis wrt SRF</li> </ul>

After explaining each important element, from the next chapters on, the focus will be centered on the proposed solution strategy.



# Chapter 4

## ADPME model test

When I was introduced to this project at the state of the art of that time, ADPME Simulink model (one of *Control* blocks) was already functionally tested. Though it was the first step where I was actively involved in and, as soon as I got acquainted, my duty was to analyze it furtherly adding new probative tests.

Then, this chapter has the role to describe the most significant test-cases performed on the ADPME Simulink model in order to stress the simulator and examine if results match with what shall be expected (check with results in [15]).

Syderal's ADPME model was designed in Simulink-Stateflow. It receives as inputs:

- The target azimuth angle [deg];
- The reference coasting rate modulus [deg/s] for the azimuth motor;
- The target elevation angle [deg];
- The reference coasting rate modulus [deg/s] for the elevation motor.

With these inputs, the antenna electronic equipment (ADPME) plans the path for each motor in such a way to reach the target angles with a trapezoidal velocity profile.

The outputs are:

- The Azimuth Motor angular velocity;
- The Elevation Motor angular velocity;
- The Azimuth Motor angular position;
- The Elevation Motor angular position.

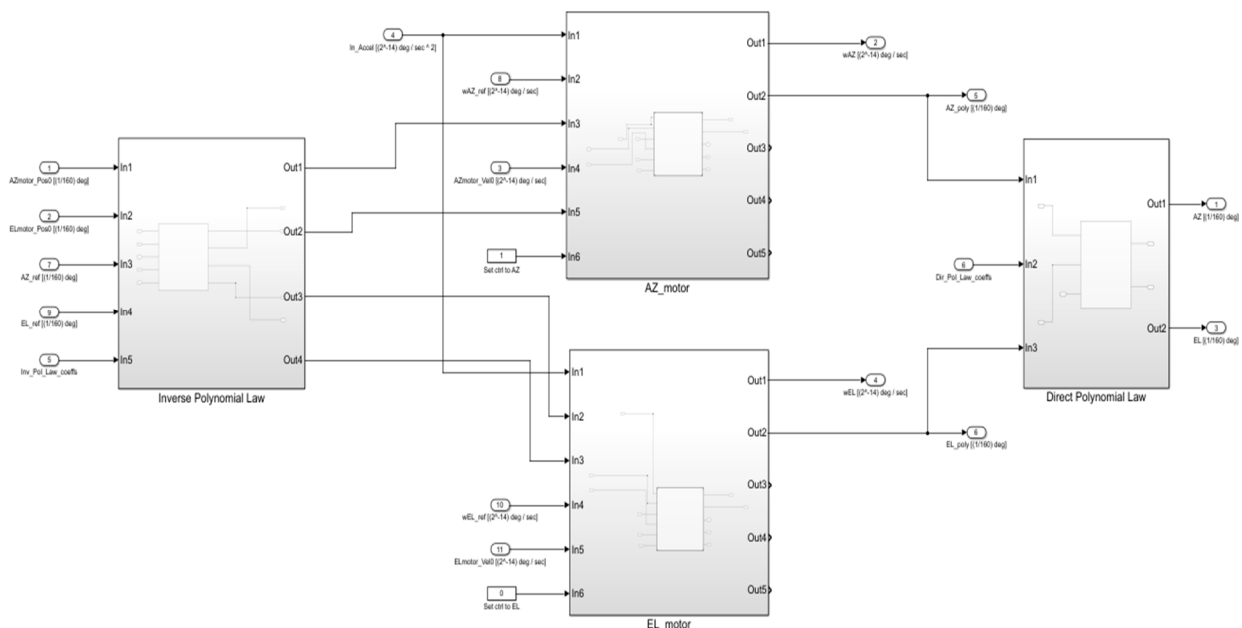


Figure 4-1: ADPME Simulink model. Credit: Thales Alenia Space

## 4.1. Tests description

Considering the design constraints for ADPME model summarized hereafter:

- Angles:
  - Angles range:
    - 60° ≤ AZ ≤ 60° in Azimuth (-55° ≤ AZ ≤ 55° in Azimuth instead for ADPM)
    - 75° ≤ EL ≤ 45° in Elevation (-70° ≤ EL ≤ 40° in Elevation instead for ADPM)
  - Final angle accuracy: 1 arcmin (including calibration error);
    - 1 step = 1°/160 = 0.00625°;
    - Micro-step control: 1 micro-step=step/64
- Angular rate
  - Maximum angular rate: 0.3 deg/s for each axis;
- Angular acceleration:
  - Maximum angular acceleration: 0.04 deg/s<sup>2</sup>, for each axis;

The conceived tests are the following:

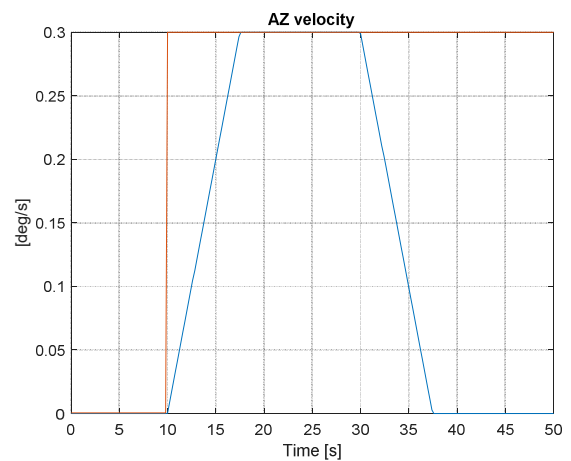
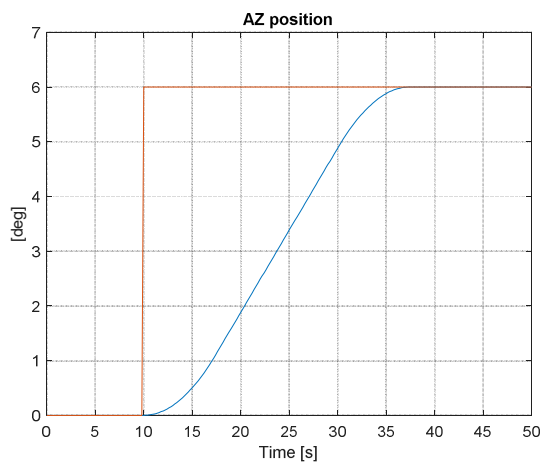
*Table 4-1: ADPME tests*

Tests	Description	Goal
	Command only a motor (the other motor is at reference)	
1 and 2	A target position and coasting rate are provided in order to verify if a start&stop movement is accomplished. The very same test is performed again considering motors viceversa.	<ul style="list-style-type: none"> <li>• Check if ADPME reaches the target with a trapezoidal velocity profile. Depending on the initial condition, the velocity profile should be positive for Test 1. negative for Test 2.</li> <li>• Check if the model introduces an error lower than the motor step.</li> </ul>
3	Constant reference velocity, the reference position changes every 15 s.	<ul style="list-style-type: none"> <li>• Output position should reach every intermediate reference within 15 s with a trapezoidal velocity profile unless out of bounds.</li> <li>• Check if the model introduces an error lower than the motor step.</li> </ul>
4	Constant target position, the reference velocity changes every 15 s.	<ul style="list-style-type: none"> <li>• Output velocity should follow the reference unless out of bounds.</li> <li>• Check if the model introduces an error lower than the motor step.</li> </ul>

Command both motors		
5	A sequence of targets is provided as if it would be commanded by the HGACL in the Follow GS Mode.	<ul style="list-style-type: none"> <li>• Output should follow the reference.</li> <li>• Check if the model introduces an error lower than the motor step.</li> </ul>
6	A sequence of targets is provided as if it would be commanded by the HGACL during a Long Slew.	<ul style="list-style-type: none"> <li>• Output should follow the reference.</li> <li>• Check if the model introduces an error lower than the motor step.</li> </ul>
7	Both motors are commanded focusing on possible each other interferences in following their references.	<ul style="list-style-type: none"> <li>• Output should follow the reference.</li> <li>• Check if the model introduces an error lower than the motor step.</li> </ul>

## 4.2. Results

Test 1	Sim Time [s]	Initial Condition [deg deg/s]	Ref angle [deg]	Ref velocity [deg/s]	Acc [deg/ s <sup>2</sup> ]
AZ	50	[0 0]	6 (10-50 s)	0.3	0.04
EL	50	[5 0]	5 (15-50 s)	0.3	0.04



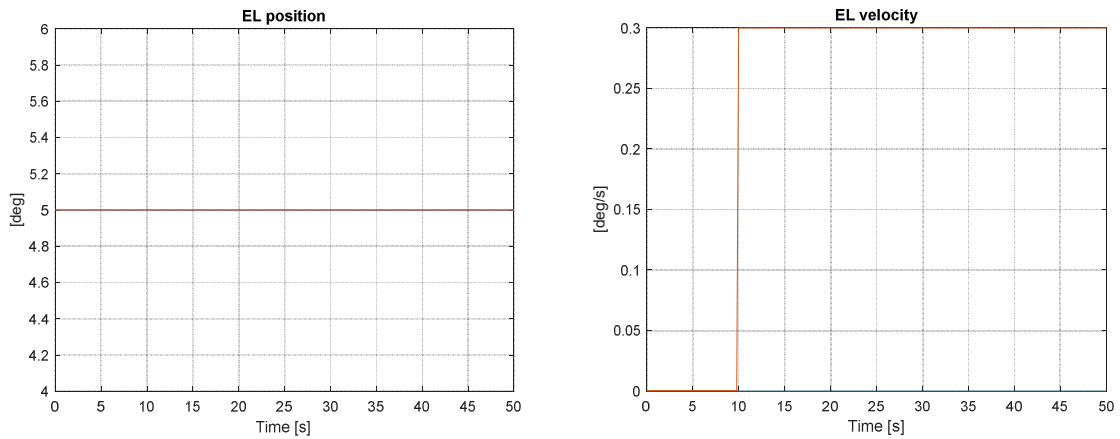


Figure 4-2: on top AZ position (left), AZ velocity (right), on bottom EL position (left), EL velocity (right); RED is the reference and BLUE is the actual profile.

Azimuth target (see Figure 4.2 on top) is correctly reached with a trapezoidal velocity profile while Elevation position (see Figure 4.2 on bottom) keeps constant, although coasting rate is 0.3 deg/s from 10 sec on, since EL is already at reference.

Test 2	Sim Time [s]	Initial Condition [deg deg/s]	Ref angle [deg]	Ref velocity [deg/s]	Acc [deg/ s <sup>2</sup> ]
AZ	50	[30 0]	25(10-50 s)	0.3	0.04
EL	50	[48 0]	48(15-50 s)	0.3	0.04

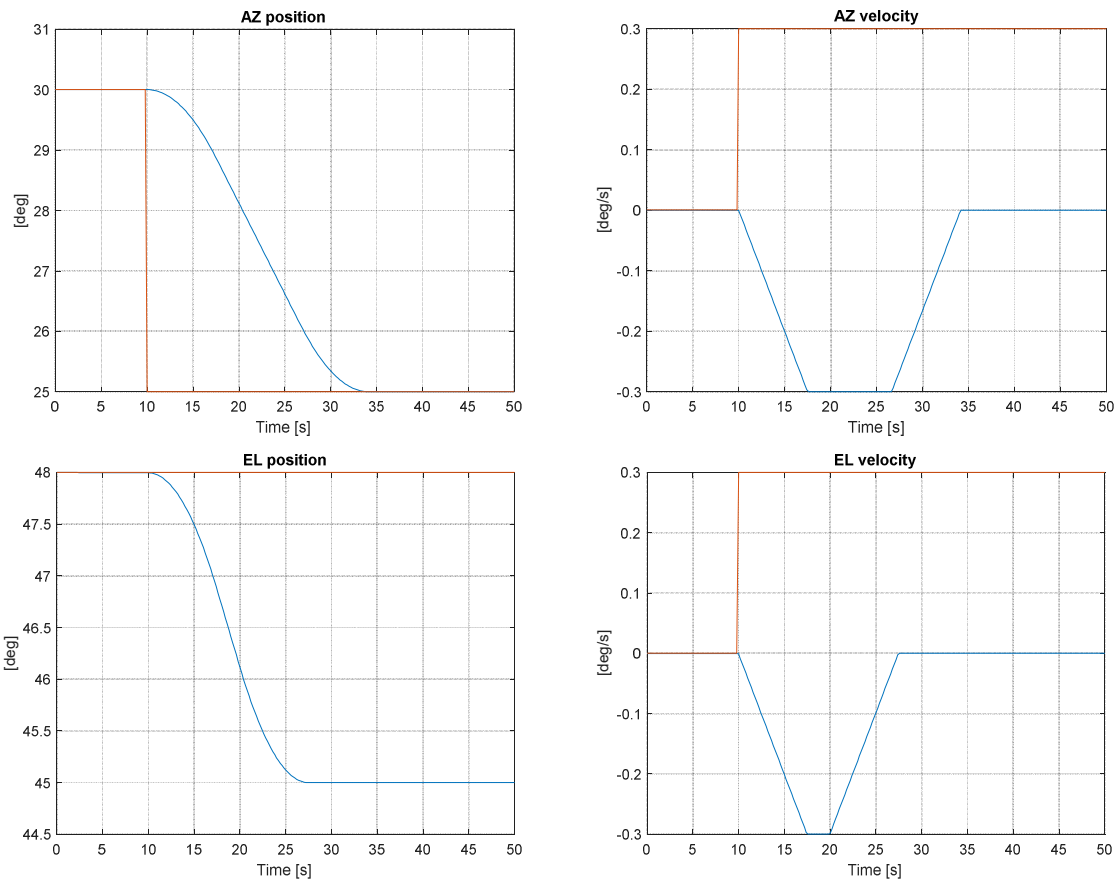


Figure 4- 3: on top AZ position (left), AZ velocity (right); on bottom EL position (left), EL velocity (right); RED is the reference and BLUE is the actual profile.

Instead of Test 1, Azimuth target (see Figure 4.3 on top) is correctly reached but with a negative trapezoidal velocity profile since it was lower than the initial position. It is worth to notice that the reference coasting rate is indicated as modulus so that it is always positive, on the contrary the actual velocity profile is not. As far as it concerns Elevation (see Figure 4.3 on bottom), the indicated initial position (48 deg) is out of boundaries but the model does not saturate the value to its upper bound (45 deg for EL). Though as soon as possible (from 10 sec on, EL coasting rate is not more null), it reacts reaching 45 deg. Investigating in more details, in the very same test conditions but with now EL reference coasting rate maintained constant during the whole simulation (see Figure 4.4), EL motor starts to move unexpectedly at its minimum velocity ( $3e-4$  deg/s) trying to close the distance with its upper bound (45 deg). This behavior could be erroneous if not considered in the rest of the model.

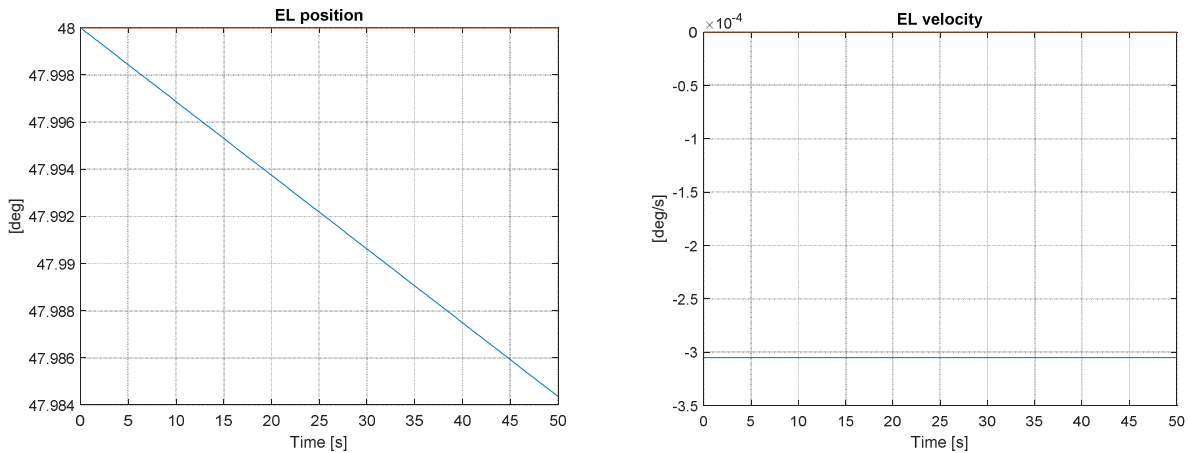


Figure 4- 4: EL position (left) trying to reach 45 deg at EL velocity of  $3e-4$  deg/s (right)

<b>Test 3</b>	Sim Time [s]	Initial Condition [deg deg/s]	Ref angle [deg]	Ref velocity [deg/s]	Acc [deg/ s <sup>2</sup> ]
AZ	70	[0 0]	5 (2-70 s)	0.3 (2-10 s) 0.5 (10-15 s) -0.3 (15-25 s) 0.03 (25-40 s) 0 (40-45 s) 0.1 (45-50 s) 6e-4 (50-55 s) 1e-4 (55-60 s) 0.15 (60-70 s)	0.04
EL	70	[10 0]	10(10-70 s)	0.3	0.04

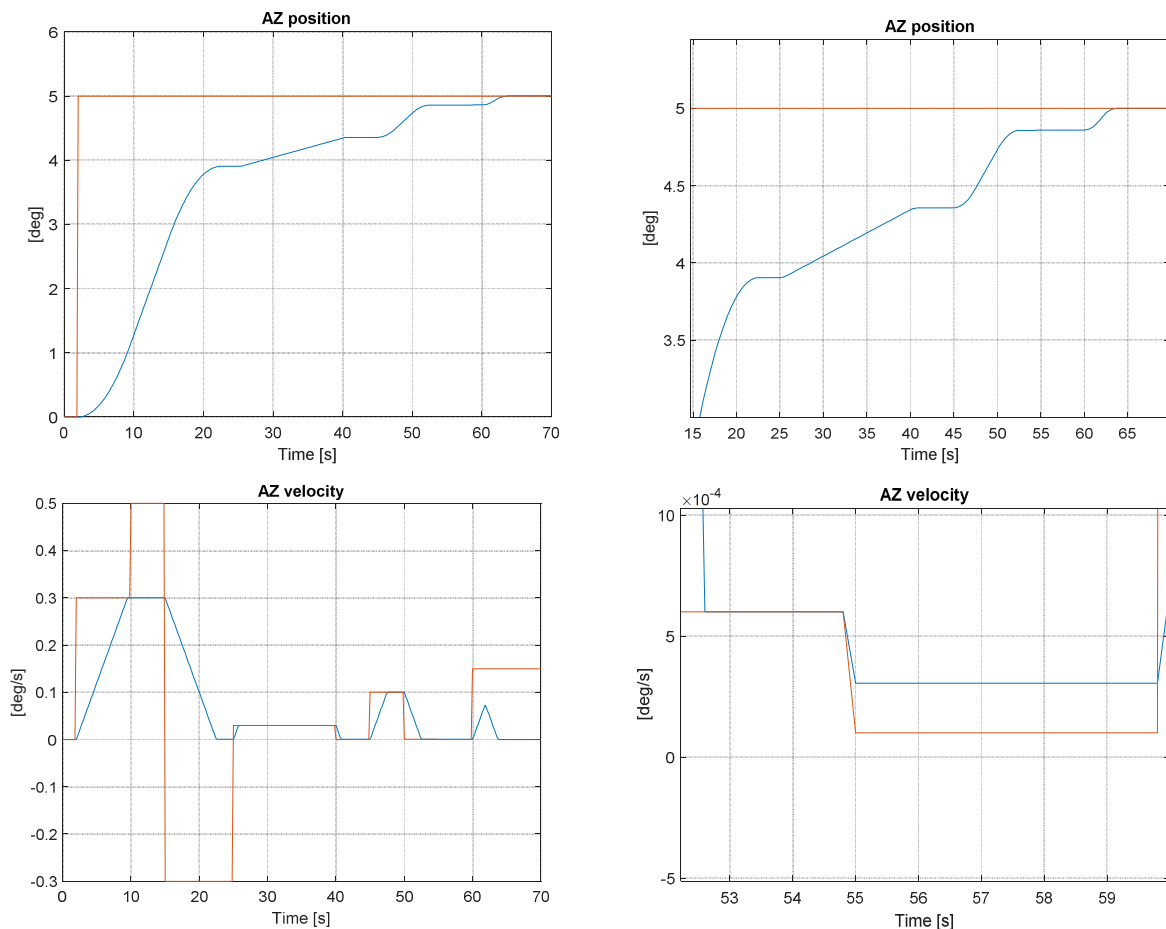


Figure 4-5: on top AZ position (left) and a detail (right); on bottom AZ velocity (left) and a detail (right); RED is the reference and BLUE is the actual profile.

In Figure 4.5, a single target position is provided to the ADPME with a sequence of different velocity coasting rates. The ADPME output is a trapezoidal profile in terms of velocity and a S-profile in terms of position in each time interval. Some sensitive cases must be pointed out:

- when at 10 sec the actual velocity profile reaches the maximum possible coasting rate, a further increase of speed is required to achieve 0.5 deg/s. The model correctly saturates at 0.3 deg/s;
- at 15 sec, the new velocity target is -0.3 deg/s. Once again, the model reacts as expected rejecting the command (remember target coasting rate is a modulus so that it can be only positive) and decelerating till to stop, provoking a flat region in position;
- after a correct start&stop actuation between 25-40 sec, AZ motor is still as driven;
- after another correct start&stop actuation between 45-50 sec, in order to excite low dynamics, two consecutive velocity targets are given. The first ( $6e-4$  deg/s) is just higher than the minimum velocity ( $5e-4$  deg/s as requirement,  $3e-4$  deg/s as model resolution), the latter ( $1e-4$  deg/s) is just smaller. As the detail in Figure 4.5 shows, both targets are admitted approximating in particular  $1e-4$  deg/s to  $3e-4$  deg/s;
- at 60 sec, a triangular velocity profile is sufficient to reach the target position, moreover with a lower coasting rate than the conceived one.

In Figure 4.6, in the meanwhile Elevation motor is at reference.

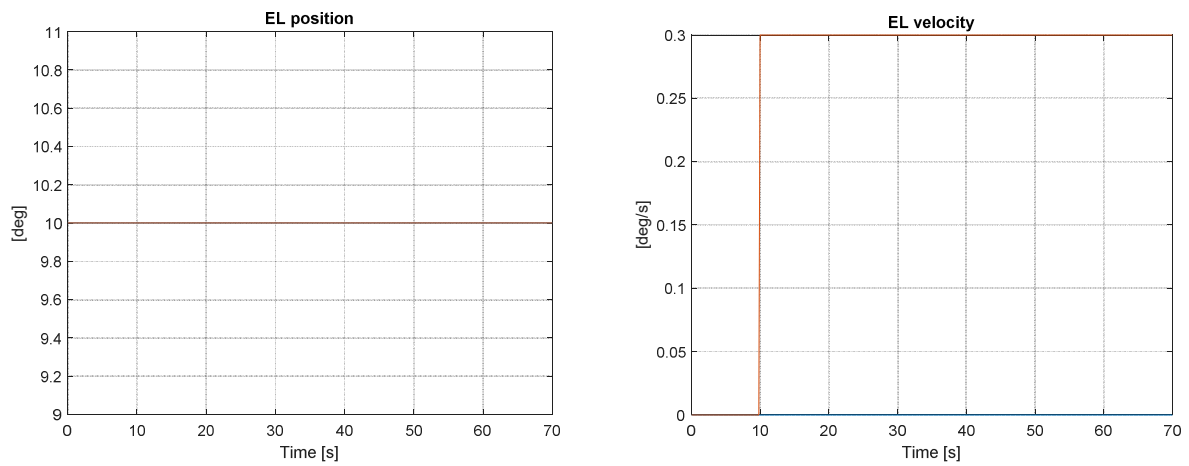


Figure 4- 6: EL position (left) and EL velocity (right); RED is the reference and BLUE is the actual profile.

<b>Test 4</b>	Sim Time [s]	Initial Condition [deg deg/s]	Ref angle [deg]	Ref velocity [deg/s]	Acc [deg/s <sup>2</sup> ]
AZ	120	[55 0]	56.5 (5-20 s) 56 (20-22 s) 58 (22-40 s) 61 (40-60 s) 55 (60-70 s) 59 (70-75 s) 58.8 (75-80 s) 58.5 (80-90 s) 58 (90-110 s) 58.007(110-111.5s) 58.0075(111.5-120s)	0.2(5-120s)	0.04
EL	120	[10 0]	10(10-120 s)	0	0.04

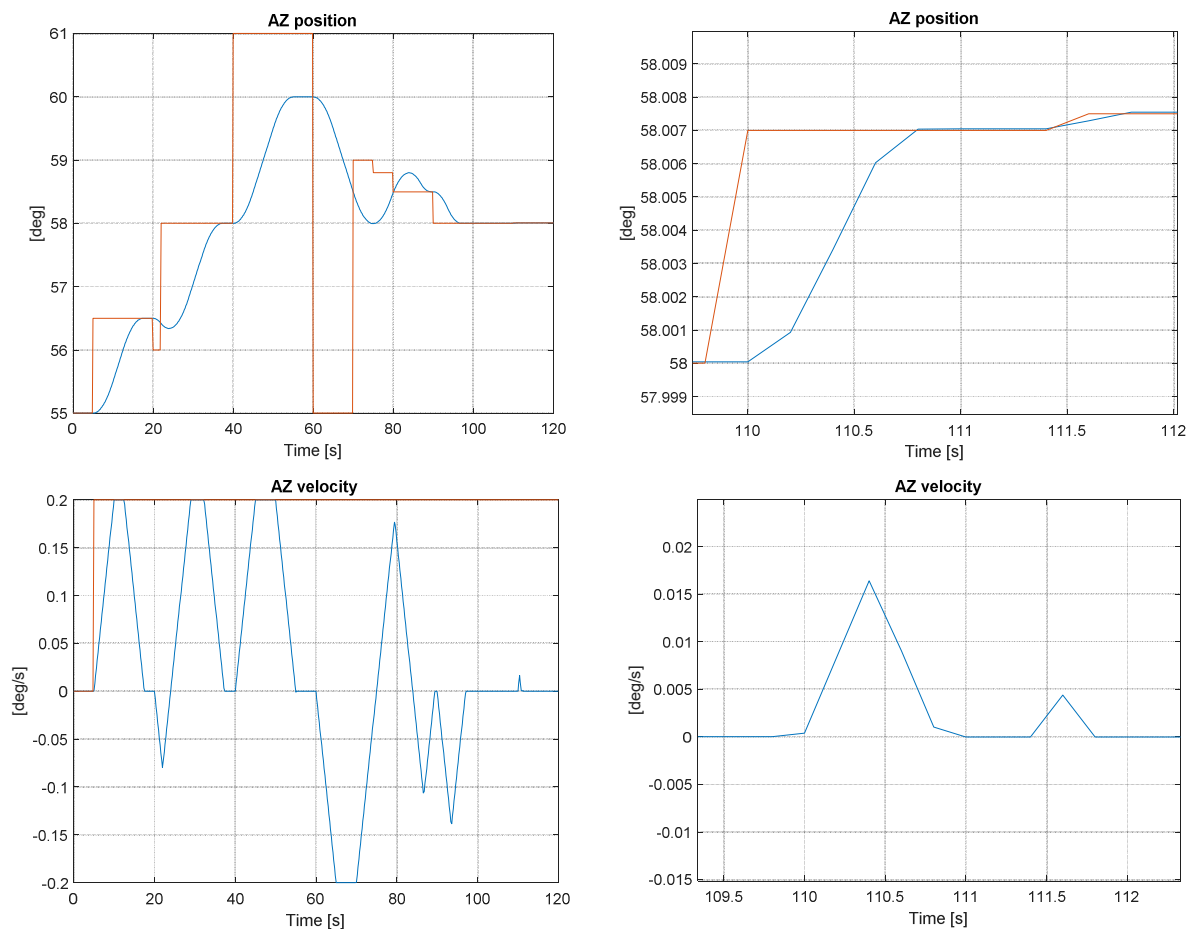


Figure 4-7: on top AZ position (left) and a detail (right); on bottom AZ velocity (left) and a detail (right); RED is the reference and BLUE is the actual profile.

In Figure 4.7, a sequence of step positions is provided to the ADPME with a single target modulus velocity as coasting rate. The ADPME output results to be a trapezoidal or triangular profile in terms of velocity and a S-profile in terms of position in each time interval. Here some crucial passages are highlighted:

- After correctly reaching the first AZ target, at 20 sec a new lower target is given. Since after just 2 sec a further higher angular position is delivered, ADPME aborts the first command picking out the latter due to the strict timeline. Indeed, if an initial decrease of velocity is performed after the abortion a new sudden acceleration is present at 22 sec;
- at 40 sec, the new target is towards 61 deg. Once again, the model reacts as expected saturating in its maximum model upper bound, it means 60 deg;
- from 60 sec on, a sequence of consecutive far-distance targets is conceived. ADPME manages to meet only the fourth and the fifth angular positions of this series. Velocity profile is coherent with respect to the relative position profile;
- finally, small variations as much as the motor-step resolution ( $1^\circ/160 \text{ steps}=0.0063 \text{ deg}$ ) are proposed in position. The first is equal to 0.007 deg, the latter is just 0.0005 deg. As shown in the details of Figure 4.7, both variations are not omitted.

In Figure 4.8, in the meanwhile Elevation motor is not commanded.

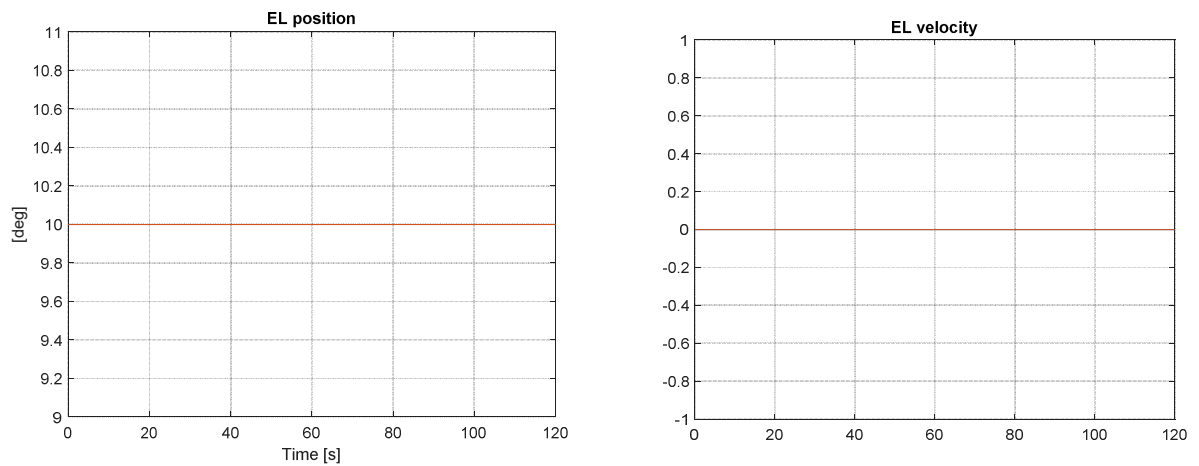


Figure 4- 8: EL position (left) and EL velocity (left); RED line is the reference and BLUE line is the actual profile.

<b>Test 5</b>	Sim Time [s]	Initial Condition [deg deg/s]	Ref angle [deg]	Ref velocity [deg/s]	Acc [deg/s <sup>2</sup> ]
AZ	70	[10 0]	0.18125 (5-20 s) 0.71875 (20-35 s) 1.2625 (35-50 s) 1.44375 (50-70 s)	0.012512 (5-20 s) 0.038452 (20-35 s) 0.039001 (35-50 s) 0.012512 (50-70 s)	0.04
EL	70	[-10 0]	-0.00625 (5-20 s) -0.00625 (20-35 s) 0 (35-50 s) 0.00625 (50-70 s)	0.000488 (5-20 s) 0.000488 (20-35 s) 0.000488 (35-50 s) 0.000488 (50-70 s)	0.04

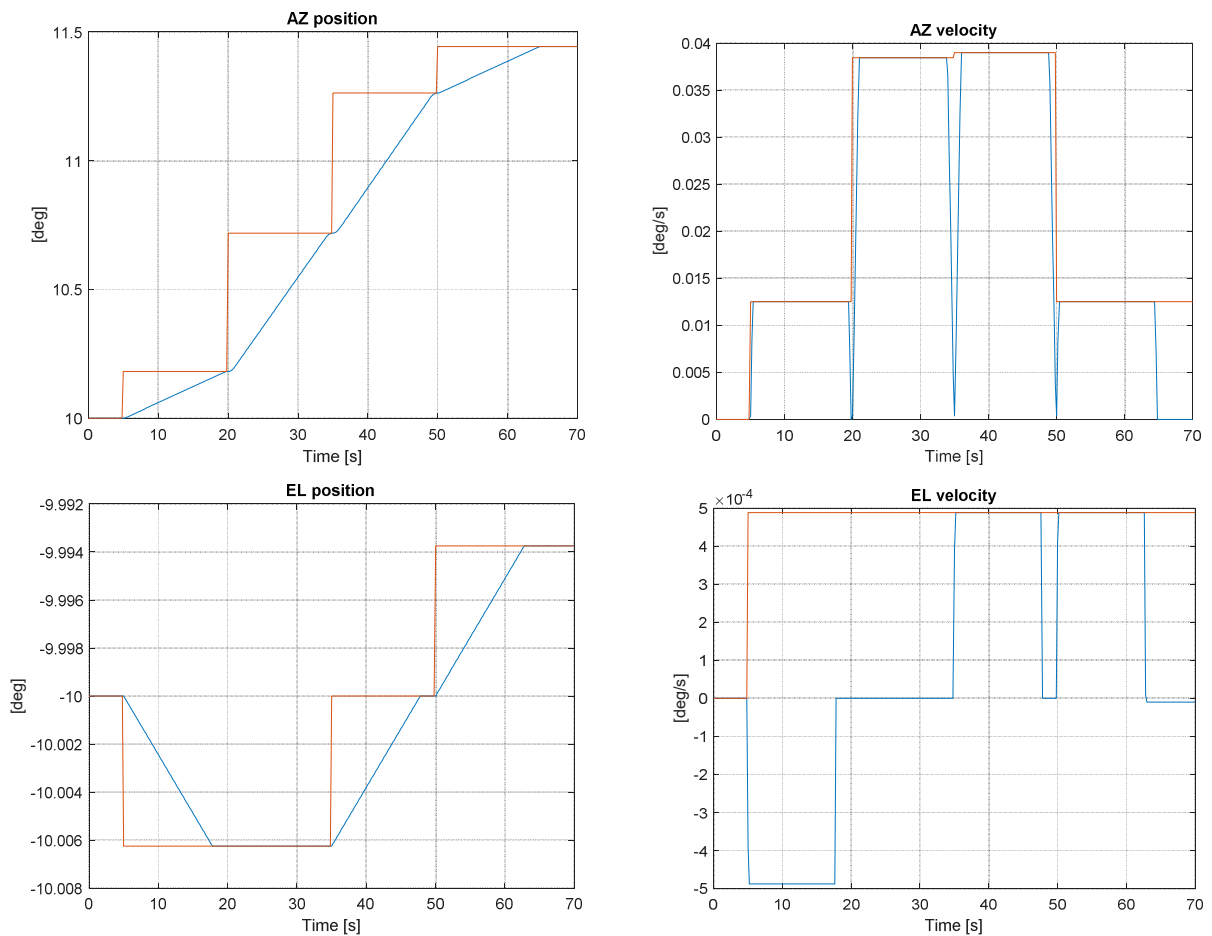


Figure 4-9: on top AZ position (left) and AZ velocity (right); on bottom EL position (left) and EL velocity (right); RED line is the reference and BLUE line is the actual profile.

In Test 5, both motors are driven in such a way to reproduce more faithfully, with respect to the previous tests, how ADPME would be commanded by HGACL in the Follow Ground Station Mode.

In Figure 4.9, a stair of reference positions is provided to the ADPME with a new target every 15 sec. The ADPME output is a trapezoidal profile in terms of velocity and a S-profile in terms of position. Each trapezoid is correctly closed at 0 deg/s, this means that the start&stop actuation is achieved correctly and that the reference positions are reached without any residual velocity.

## Test 6: Example of Long Slew

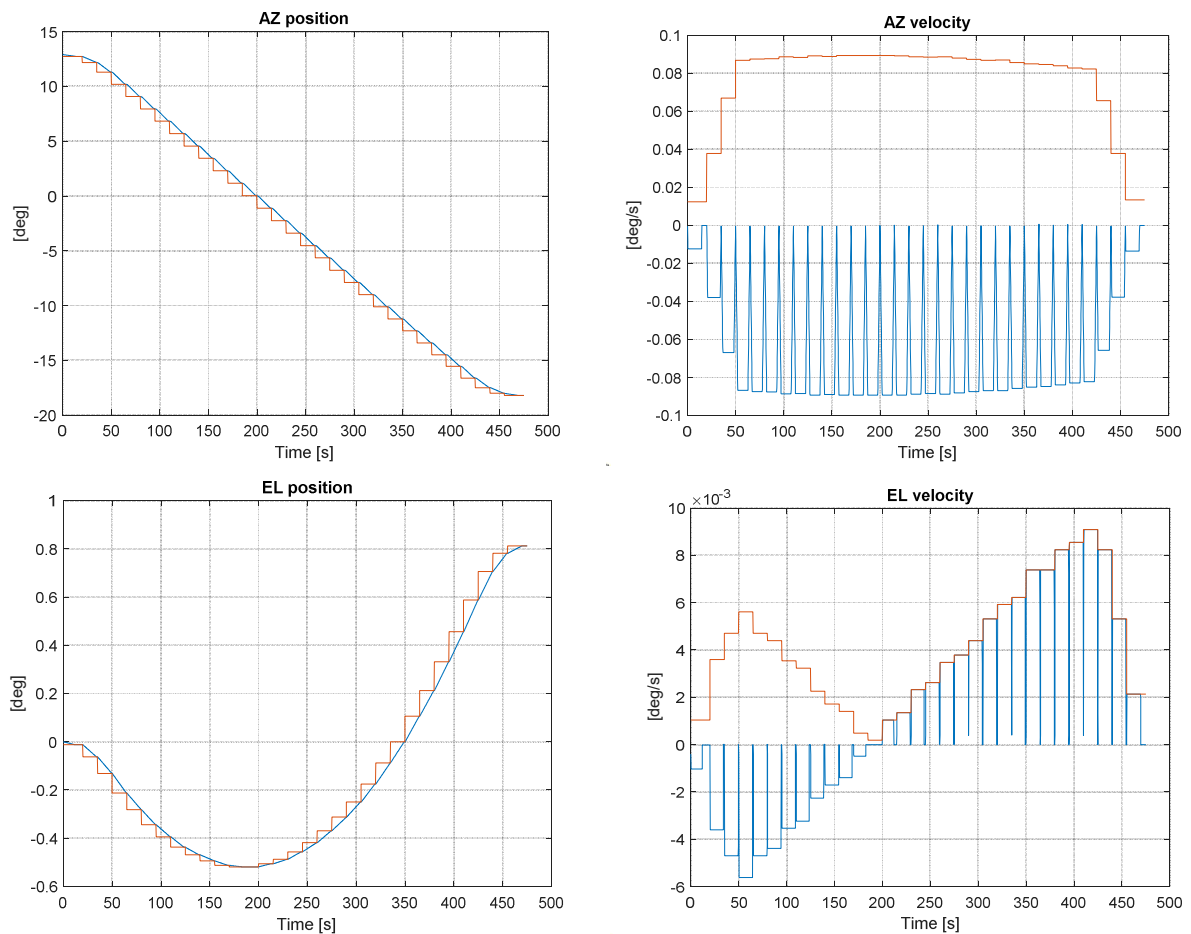


Figure 4-10: on top AZ position (left) and AZ velocity (right); on bottom EL position (left) and EL velocity (right); RED line is the reference and BLUE line is the actual profile.

In Figure 4.10, a sequence of reference positions similar to those that HGACL provides during a long slew is provided to the ADPME.

As far as it deals with Azimuth, since a descending stair appears in position, each trapezoid is negative in velocity provoking the motor moves backwards. They are also correctly closed at 0 deg/s, this means that the start&stop actuation is achieved correctly and that the reference positions are reached without any residual velocity.

As far as it deals with Elevation, a sequence of reference targets with an overall amplitude of about 1 deg is provided. A negative slope occurs until 190s, then it becomes positive. Again, the ADPME builds correctly the trapezoidal velocity profile in such a way it reaches 0 deg/s before the new position reference.

<b>Test 7</b>	Sim Time [s]	Initial Condition [deg deg/s]	Ref angle [deg]	Ref velocity [deg/s]	Acc [deg/ s <sup>2</sup> ]
AZ	300	[0 0]	5 (5-100 s) 10 (100-300 s)	0.3 (5-100 s) 0.3 (100-300 s)	0.04
EL	300	[0 0]	45 (130-300 s)	0.3 (130-300 s)	0.04

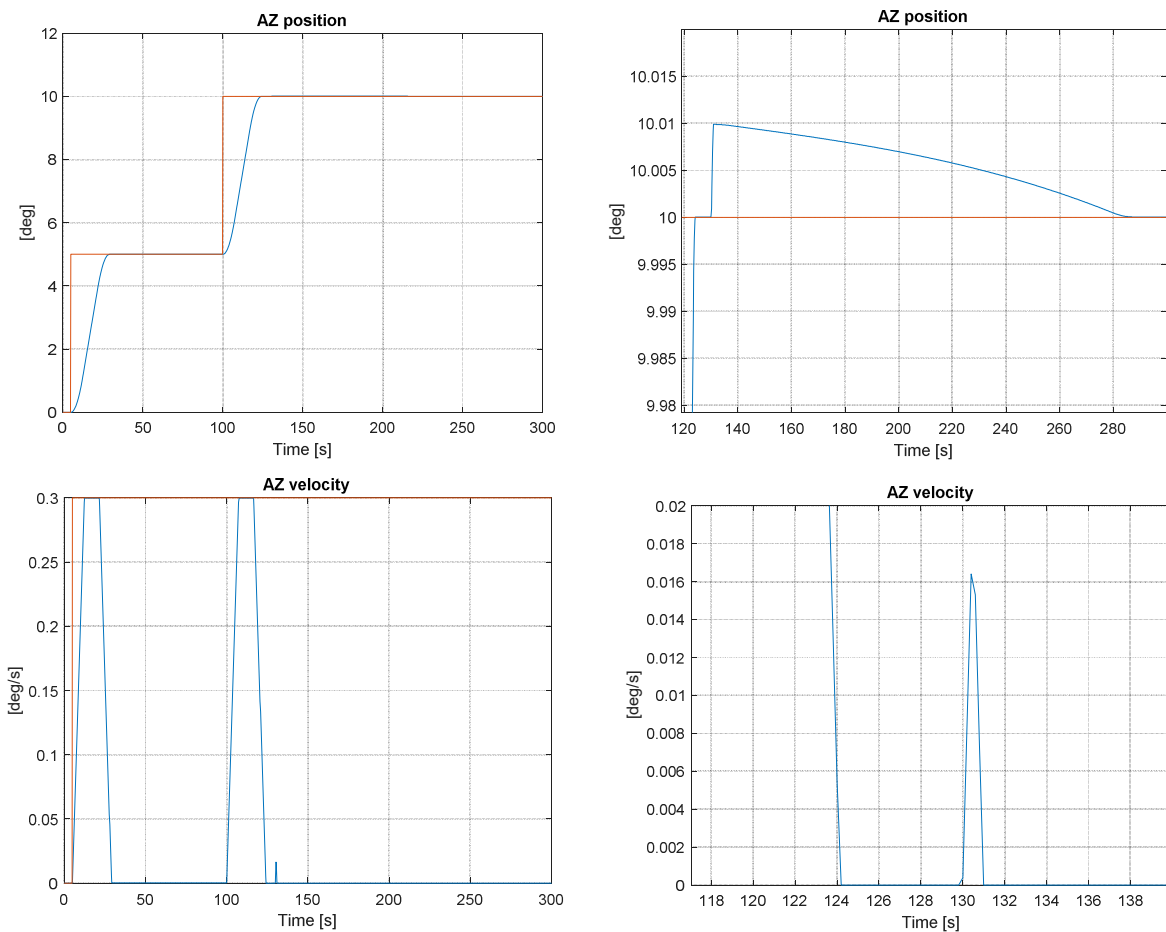


Figure 4-11: on top AZ position (left) and a detail (right); on bottom AZ velocity (left) and a detail (right); RED line is the reference and BLUE line is the actual profile.

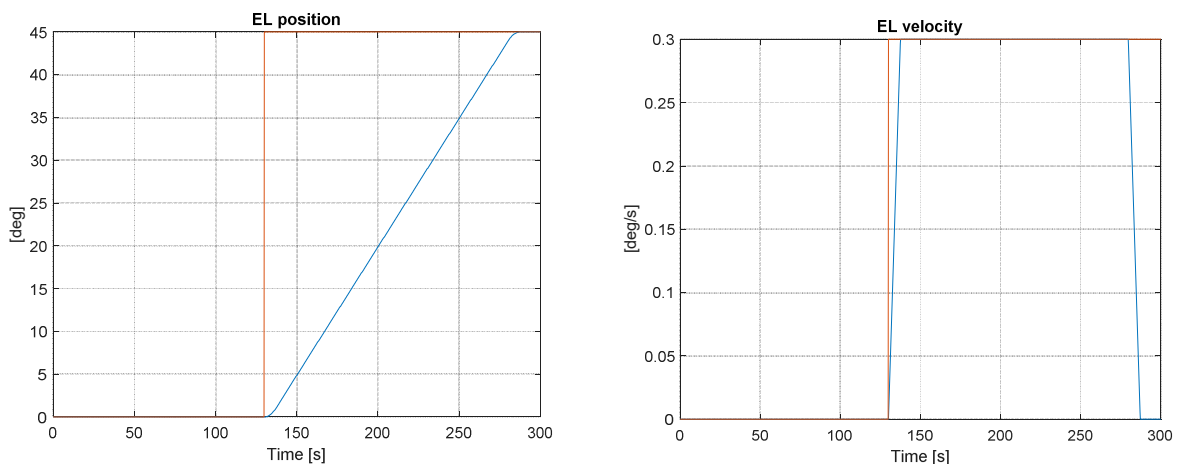


Figure 4-12: EL position (left) and EL velocity (right); RED line is the reference and BLUE line is the actual profile.

In Test 7, the aim is to verify if the two motors interfere with each other. It is important to point out the role of the Polynomial correction law, which will be largely explained in Chapter 5. From ADPME point of view, the Polynomial law represents the function which couples Azimuth and Elevation. Furthermore, the ADPME Simulink model under investigation is only the latest version of a series of ADPME Simulink models. Despite the previous variants, its peculiarity is to just insert the dependency of Azimuth with respect to Elevation which were decoupled up until this model.

## POLYNOMIAL LAW

$$AZ = A_1 APM1 + B_1 APM2 + C_1 APM1^2 + D_1 APM1 APM2 + E_1 APM1^2 + F_1 APM1^3 + G_1 APM1^2 APM2 + H_1 APM1 APM2^2 + I_1 APM2^3 + AB_1$$

$$EL = A_2 APM1 + B_2 APM2 + C_2 APM1^2 + D_2 APM1 APM2 + E_2 APM1^2 + F_2 APM1^3 + G_2 APM1^2 APM2 + H_2 APM1 APM2^2 + I_2 APM2^3 + AB_2 = B_2 APM2$$

Where APM1, APM2 are respectively EL and AZ variable in motor-steps dimension.

Considering now Test 7 results in Figure 4.12, a not-negligible variation of 0.01 deg manifests at 130 sec in AZ position when, on the contrary, Azimuth motor should be already at ease without any new income AZ command. Looking at the AZ velocity profile, it shows an unexpected peak at the same time. It is evident the discrepancy is greater than motor-step resolution ( $1^\circ/160=0.0063$  deg) and it nullifies only at more or less 280 sec, it means when Elevation target position is achieved.

The explanation of this behavior is due to the Polynomial law since any such phenomenon occurs in previous versions of ADPME Simulink model. As counterproof, the same test is performed without using AZ/EL relation (see Figure 4.13):

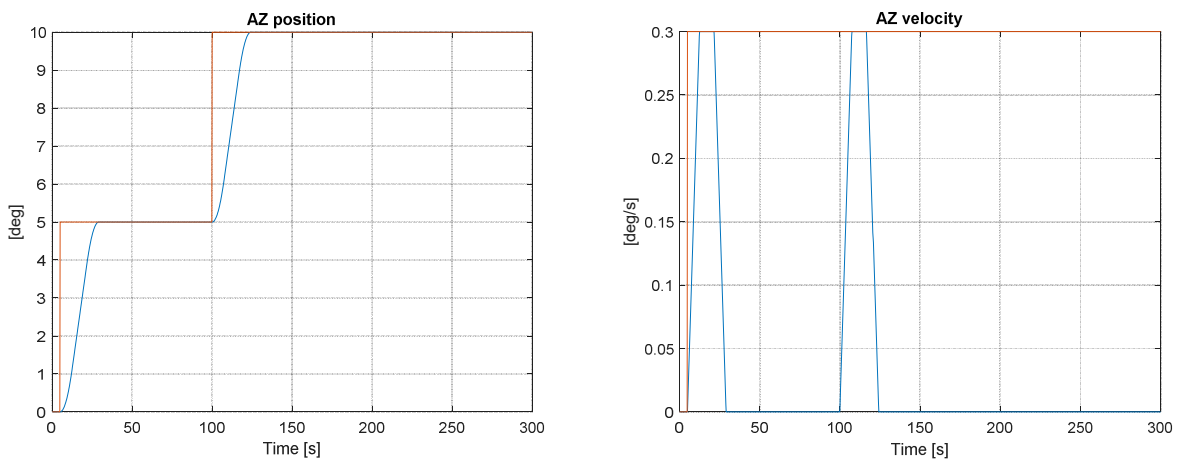


Figure 4-13: AZ position (left) and AZ velocity (right) without Polynomial law.

By means of several tests maintaining AZ motor at ease while commanding EL motor and repeating the same tests the other motor around, it is possible to state the discrepancy occurs only on Azimuth position and velocity and not on Elevation values and it lasts till the attainment of EL targets. Further considerations imply that mismatches width is as larger as much the increasing distance between two consecutive EL targets while mismatches time-length is as longer as much the decreasing relative EL velocity. Nevertheless, this model is limited and fictitious as every mathematical modeling. Actually AZ/EL commands shall be delivered in couple to motors by the actual ADPME so that this solution guarantees a reliable improvement in performance.



# Chapter 5

## Polynomial Law effect on boresight

### 5.1. Scope and Purposes

The aim of this paragraph is to investigate the relation between the actual boresight orientation and mounting misalignments errors between Azimuth and Elevation motor axes.

### 5.2. Polynomial Correction Law assumption ([13],[14])

It is worth to remember the ADPM shall be composed by three independent actuators, mutually perpendicular:

- One linked to the S/C is the 1st axis. It is used to deploy the Antenna Reflector Assembly,
- One intermediate actuator in the 2nd axis. It is used for Azimuth (AZ) steering.
- One actuator linked to the Antenna Reflector Assembly (3rd axis). It is used for Elevation (EL) steering.

While the 1<sup>st</sup> axis shall work only during the deployment of antenna after launch in *Transfer & Commissioning* phase, the alignment between the AZ rotation axis and the EL rotation axis is critical for pointing performance.

As Antenna Deployment and Pointing Mechanism (ADPM) sub-contractor, Sener shall deliver a parabolic antenna as much accurate as possible contributing to satisfy the strict mission pointing requirement (0.4 deg or 24 arcmin). In this regard, Sener assumptions are presented by explaining the advantages of the usage of a polynomial correction law.

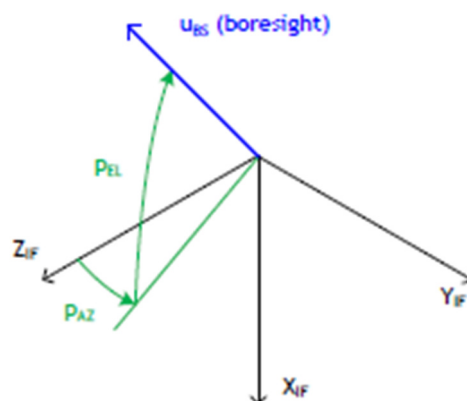


Figure 5-1: boresight orientation in Inertial Reference System (IRF)

The antenna pointing is defined by the orientation of the boresight with respect to a fixed reference system at the interface (SRF or conversely IRF). Moreover, the orientation of the boresight ( $u_{BS}$ ) can be defined by two angles: AZIMUTH ( $p_{AZ}$ ) and ELEVATION ( $p_{EL}$ ), as it is depicted in Figure 5.1. The definition of these angles ( $p_{AZ}$ ,  $p_{EL}$ ) is independent of any rotation axes.

The ADPM provides two rotation axes: AZIMUTH AXIS ( $u_{AZ}$ ) and ELEVATION AXIS ( $u_{EL}$ ). In ideal conditions:

- The rotation about the AZIMUTH AXIS ( $r_{AZ}$ ) would be equal to the AZIMUTH ANGLE ( $p_{AZ}$ ):  $r_{AZ} = p_{AZ}$  (in ideal conditions)
- The rotation about the ELEVATION AXIS ( $r_{EL}$ ) would be equal to the ELEVATION ANGLE ( $p_{EL}$ ):  $r_{EL} = p_{EL}$  (in ideal conditions)

Unfortunately, the axes misalignment breaks these equalities, and two error quantities can be defined for each axis as follows:

AZIMUTH ERROR:  $e_{AZ} = r_{AZ} - p_{AZ}$

ELEVATION ERROR:  $e_{EL} = r_{EL} - p_{EL}$

The detected inner source of misalignments is the so-called *perpendicularity error* ( $R$ ).

Figure 5.2 illustrates the more relevant aspects of this problem, it means the effect of a not perfect perpendicularity between the AZIMUTH ( $u_{AZ}$ ) and ELEVATION ( $u_{EL}$ ) axes. The *perpendicularity error* ( $R$ ) is the angular error between the IDEAL ELEVATION AXIS ( $u_{EL\_ideal}$ ) and the ACTUAL ELEVATION AXIS ( $u_{EL\_act}$ ) and it consists of 0.00878583 deg. The pointing error appears when the actuator moves the antenna from its initial orientation. The ideal trajectory is swept by a cyan vector, while the actual trajectory is swept by a yellow vector.

After a rotation about the ELEVATION AXIS ( $r_{EL}$ ), the ideal orientation will differ from the actual one. The difference can be described by a VECTOR ERROR ( $e_{VEC}$ ) and can be decomposed into the AZIMUTH ERROR ( $e_{AZ}$ ) and the ELEVATION ERROR ( $e_{EL}$ ) components. It is evident how the error grows with the misalignment error ( $R$ ) and the rotation in ELEVATION ( $r_{EI}$ ).

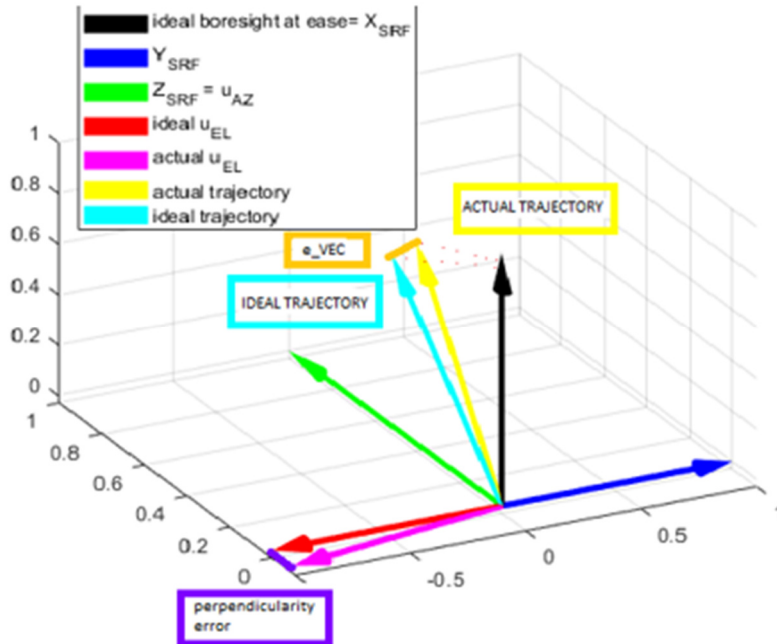


Figure 5-2: error induced by ADPM axes misalignment.

Fortunately, the misalignment error can be calibrated. The aim of this calibration is to recover the mapping between the axis rotation ( $r_{AZ}$ ,  $r_{EL}$ ) and the boresight orientation ( $p_{AZ}$ ,  $p_{EL}$ ).

The calibration process can be divided in two parts: *Extraction* and *Correction*.

The *Extraction* part refers to the characterization activities including the estimation of the *perpendicularity error*.

The *Correction* part refers to the correction algorithms. The proposed solution is to introduce a well-designed polynomial law of 3rd order which translates ADPME commanded angles in motor-steps and the other way around steps in angles. In this manner, ADPME electronics do not need to be changed and it is going to control the antenna with ideal targets while on motor side the misalignment between nominal u\_AZ and u\_EL can be reduced. However, this implies that if only one axis rotation is intended to be driven, both axes need to be moved. Here the Polynomial Correction Law is presented:

### DIRECT\_POLYNOMIAL: FROM DEG TO STEP

$$APM1 = A_3 AZ + B_3 EL + C_3 AZ^2 + D_3 AZ EL + E_3 EL^2 + F_3 AZ^3 + G_3 AZ^2 EL + H_3 AZ EL^2 + I_3 EL^3 + AB_3$$

$$APM2 = A_4 AZ + B_4 EL + C_4 AZ^2 + D_4 AZ EL + E_4 EL^2 + F_4 AZ^3 + G_4 AZ^2 EL + H_4 AZ EL^2 + I_4 EL^3 + AB_4 = B_4 EL$$

$$AZ\_motor\_corrected = APM1/160$$

$$EL\_motor\_corrected = APM2/160$$

### INVERSE\_POLYNOMIAL: FROM STEP TO DEG

$$AZ = A_1 APM1 + B_1 APM2 + C_1 APM1^2 + D_1 APM1 APM2 + E_1 APM1^2 + F_1 APM1^3 + G_1 APM1^2 APM2 + H_1 APM1 APM2^2 + I_1 APM2^2 + AB_1$$

$$EL = A_2 APM1 + B_2 APM2 + C_2 APM1^2 + D_2 APM1 APM2 + E_2 APM1^2 + F_2 APM1^3 + G_2 APM1^2 APM2 + H_2 APM1 APM2^2 + I_2 APM2^2 + AB_2 = B_2 APM2$$

Thanks to a reverse-engineering investigation, now my goal is to analyze the polynomial law effect on Azimuth and Elevation variables and then compare the pointing performance with and/or without antenna correction. Out of scope is to verify the Sener's assessment which leads to the polynomial law.

## 5.3. Analysis of Polynomial Law effect

First of all, an immediate evidence is to represent how the Polynomial Law changes the motor commands characterizing the distances e\_AZ and e\_EL.

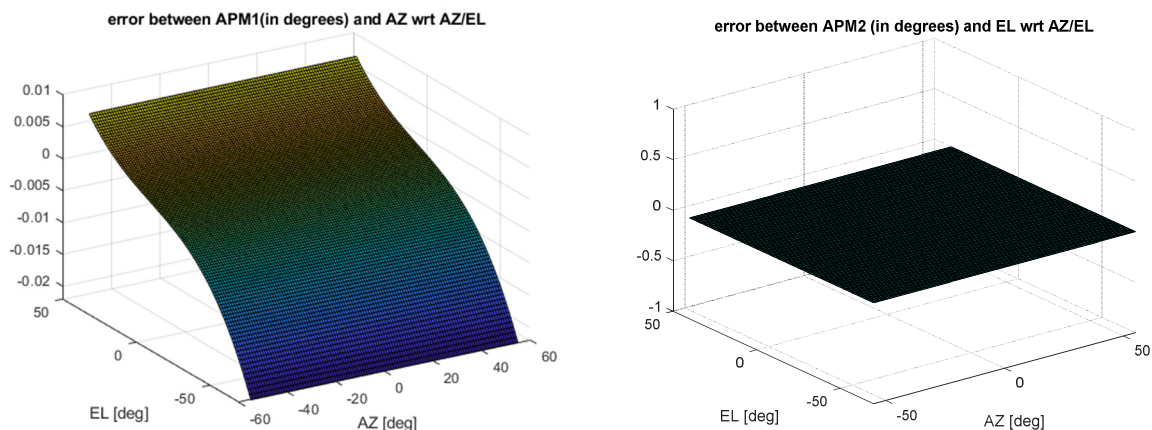


Figure 5- 3: e\_AZ (left), e\_EL (right)

It is clear from Figure 5.3 the misalignment between axes does not affect the elevation. That is why the error in elevation is zero ( $EL\_ERR = 0$ ). This means the rotation about the actual elevation axis ( $EL\_ROT$ ) coincides the actual elevation angle ( $EL\_ACT$ ) so that it holds the relation:

$$EL\_ERR = EL\_ROT - EL\_ACT = 0 \Rightarrow EL = EL\_ROT = EL\_ACT$$

On the other hand, the azimuth angle is affected by the misalignment between axes. In particular, the EL angle directly influences the  $AZ\_ERR$  such that it enters in its polynomial approximation for Azimuth motor step calculation in this way:

$$\begin{aligned} AZ\_ERR &= AZ\_ROT - AZ\_ACT \\ AZ\_ERR &\text{ approximated by 3}^{\text{rd}} \text{ order polynomial with } EL\_ROT \text{ as independent variable} \\ AZ\_ACT &= AZ\_ROT - AZ\_ERR \\ AZ\_ROT &= (AZ\_STEP/160) \cdot (\pi/180) \\ EL\_ROT &= (EL\_STEP/160) \cdot (\pi/180) \\ AZ\_ACT &= INVERSE\_POLYNOMIAL (AZ\_STEP, EL\_STEP) \end{aligned}$$

Further step is to compare three scenarios:

- *ideal case;*
- *misalignment without correction case;*
- *misalignment with correction case.*

In order to describe the antenna boresight in each situation, a mathematical model is been developed. Transformation matrices are matrices that post-multiply a column point vector to produce a new column point vector. A series of transformation matrices may be concatenated into a single matrix by matrix multiplication. A transformation matrix may represent each of the operations of translation, scaling, and rotation.

However, if such matrix is a three by three orthogonal, normalized, square matrix, it may be used to specify an isometric rotation that can be used to relate two frames of reference, i.e. two co-ordinate systems. Here, an isometric rotation is taken to mean a transformation in which the distance between any two points on an object remains invariant under the transformation.

These transformation matrices can be easily derived either from geometry, or from trigonometric identities. In accordance with the rules of linear algebra, the first rotation matrix is written to the right with the next rotation being written to its left and so on. Such rotations are termed passive as each successive rotation is applied to the newly rotated system.

An amount of 5 reference frames have been identified:

1. Guidance Reference Frame (GRF) that can be assimilated to the SC Reference Frame SRF
2. AZ ref frame, integral with the static part of the azimuth motor
3. AZ rot ref frame, integral with the rotation part of the AZ motor
4. EL ref frame, integral with the static part of the EL motor
5. EL rot ref frame, integral with the rotation part of the EL motor

Then the four rotation matrices are:

1. Frm5to4:  $rot\_EL$  – It is a rotation due to El motor angle;

2. Frm4to3: EL2AZ\_RF – Misalignment between AZ motor and EL motor. In theory this is recovered through ADPME calibration polynomial;
3. Frm3to2: rot\_AZ – It is a rotation due to AZ motor angle;
4. Frm2to1: AZ2SC\_RF – Misalignment of the AZ motor wrt the SRF.

The antenna boresight in the EL rot ref frame is expressed as:

$$b_{HGA-ELRF} = \begin{bmatrix} \cos\alpha \cos\beta \\ \sin\alpha \cos\beta \\ \sin\beta \end{bmatrix} \sim \begin{bmatrix} 1 \\ \alpha \\ \beta \end{bmatrix} \quad (\text{where alpha and beta are small angles})$$

The correct pointing is obtained when the real boresight of the HGA is rotated into the spacecraft reference frame SRF:

$$b_{SRF} = AZ2SC\_RF \cdot rot\_AZ \cdot EL2AZ\_RF \cdot rot\_EL \cdot b_{HGA-ELRF}$$

Considering only the *perpendicularity error* R, the computations become easier since AZ2SC\_RF is considered as an identity matrix while alpha, beta are null angles so that  $b_{SRF} = [1 \ 0 \ 0]$ .

Let's analyze what happens in the three cases under investigation:

- *'ideal'* case:  $b_{SRF} = rot\_AZ \cdot rot\_EL \cdot b_{ELRF}$

$$rot\_AZ = \begin{bmatrix} \cos(AZ) & -\sin(AZ) & 0 \\ \sin(AZ) & \cos(AZ) & 0 \\ 0 & 0 & 1 \end{bmatrix} \quad (u\_AZ // \text{axis } z \text{ of EL reference frame})$$

$$rot\_EL = \begin{bmatrix} \cos(-EL) & 0 & \sin(-EL) \\ 0 & 1 & 0 \\ -\sin(-EL) & 0 & \cos(-EL) \end{bmatrix} \quad (u\_EL \text{ antiparallel axis } y \text{ of EL reference frame})$$

- *'misalignment without correction'* case:  $b_{SRF} = rot\_AZ \cdot M \cdot b_{ELRF}$   
where M is a rotation matrix determined with axis  $u\_EL\_actual=[0 \ -1 \ -R]$  and rotation angle EL:

$$\begin{bmatrix} \cos(EL) + u(1)^2 * (1 - \cos(EL)) & u(1) * u(2) * (1 - \cos(EL)) - u(3) * \sin(EL) & u(1) * u(3) * (1 - \cos(EL)) + u(2) * \sin(EL) \\ u(2) * u(1) * (1 - \cos(EL)) + u(3) * \sin(EL) & \cos(EL) + u(2)^2 * (1 - \cos(EL)) & u(2) * u(3) * (1 - \cos(EL)) - u(1) * \sin(EL) \\ u(3) * u(1) * (1 - \cos(EL)) - u(2) * \sin(EL) & u(3) * u(2) * (1 - \cos(EL)) + u(1) * \sin(EL) & \cos(EL) + u(3)^2 * (1 - \cos(EL)) \end{bmatrix}$$

Conversely, M can be seen as product of EL2AZ\_RF and rot\_el:

$$EL2AZ\_RF = \begin{bmatrix} 1 & 0 & 0 \\ 0 & \cos(R) & -\sin(R) \\ 0 & \sin(R) & \cos(R) \end{bmatrix}$$

- *'misalignment with correction'* case:  $b_{SRF} = rot\_AZ \cdot EL2AZ\_RF \cdot rot\_EL \cdot b_{ELRF}$

but substituting angles in rot\_az and rot\_el with the resultants coming from the Inverse\_Polynomial.

Considering for example the case AZ=0, EL=0:

Boresigth ideal = [1.000000E+00 0.000000E+00 0.000000E+00]  
 Boresigth w/o corr = [1.000000E+00 0.000000E+00 0.000000E+00]  
 Boresigth with polynomial corr = [1.000000E+00 -7.713188E-07 0.000000E+00]

It seems that at the ease test, the best result with respect to the ideal one is that without correction but if the AZ/EL values are varying in the whole range, it is achieved:

Max angular error wrt ideal case without correction: 4.953588E-01 [arcmin]  
 Max angular error wrt ideal case with polynomial correction: 4.324772E-02 [arcmin]

Clearly, max angular error with correction is by far smaller (an order of magnitude) than max angular error without correction.

Figure 5.4 provides a graphical evaluation of the different VECTOR ERRORS (e\_VEC) for 'misalignment without correction' and 'misalignment with correction' cases and their comparison:

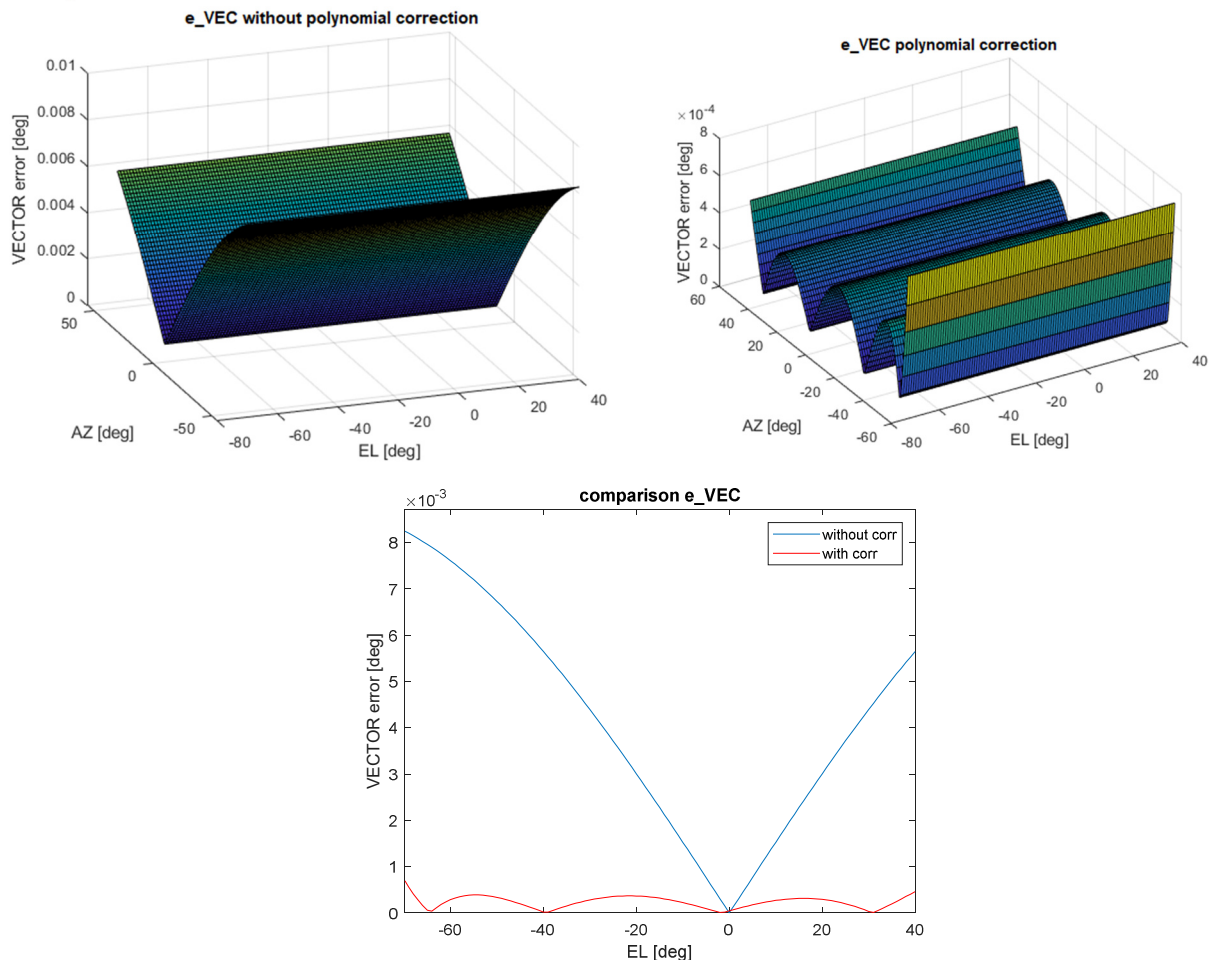


Figure 5-4: on the top e\_VEC without correction (left), e\_VEC with correction (right); on the bottom their comparison is depicted

## 5.4. Analysis of results

What has been done reveals the following conclusions:

- The error mainly depends on the misalignment magnitude  $R$  and angular excursion of the rotation in ELEVATION ( $r_{EL}$ ). The error does not vary with the rotation in AZIMUTH ( $r_{AZ}$ ). This simplifies the subsequent analyses.
- The error component in ELEVATION ( $e_{EL}$ ) can be neglected.
- The perpendicularity error between AZIMUTH/ELEVATION axes ( $R$ ) generates a VECTOR error ( $e_{VEC}$ ) and an AZIMUTH error ( $e_{AZ}$ ) that grow with the rotation in ELEVATION ( $r_{EL}$ ).
- The polynomial law correctly succeeds in dropping the discrepancy coming from lack of perpendicularity between motor axes.

These outcomes match with Sener's conclusions.



# Chapter 6

## Study of 'in-flight' HGA Calibration

When strict directivity or high-gain in a certain direction are needed, every non-omnidirectional antenna requires a pointing procedure to obtain good performance. In fact, so much the pointing is fine, so far the efficiency of the HGA is optimal in terms of electromagnetic transmitted power and, as a consequence, much more the quality signal received on ground is robust in terms of SNR (signal to noise ratio).

Typically the goodness of pointing procedure is inversely proportional to its sensitivity with respect to misalignment errors. Unfortunately, the *perpendicular error* is only one of the possible misalignment errors due to the fact that many factors like orbit knowledge error, antenna deformation after launch, aging, thermoelastic distortion in HGA elements, not modeled nonlinearities, not-exact pointing strategies, systematic errors and random errors can always worsen data delivery exceeding the expected error budget (remember the global requirement of 24 arcmin otherwise see Annex 1 to go in detail). On the basis of this consideration, an 'in-flight' calibration is essential. It is extremely important even because it is foreseen to be implemented only one time in the mission lifetime.

### 6.1. Scope and Purposes

The previous geometrical space model is going to be reviewed taking into account new misalignment errors and calibration minimization problem will be deeply studied in order to obtain an ad-hoc HGACL\_Par, a 6x1 vector with all 'in-flight' calibration parameters. Furthermore, some choices will be discussed trying to improve calibration results.

### 6.2. Calibration procedure [17]

The Ground Station (GS) vector is computed on-board considering the EME2000 reference frame (Earth's Mean Equator and Equinox at Julian date 2000) and the SC attitude quaternion, so it is the ideal direction of the HGA boresight. However there are several misalignments that needs to be recovered or the HGA cannot point the GS with the required accuracy.

The calibration procedure is defined as follows:

- 1) Taking into account the Sun-SC-Earth Angle of the moment when the HGA calibration is performed, not all the AZ-EL tuples can be reached.
- 2) Considering the reachable tuples, a number of calibration points are selected.
- 3) For each tuple, the relevant angles are commanded to the ADPME.
- 4) A target attitude quaternion is commanded to the SC such that the Earth and the HGA boresight are aligned.
- 5) The satellite will be programmed in order to offset the direction of transmission over an angular grid (this will be obtained by changing the on-board attitude, the steerable high gain antenna remaining fixed in its position). The angular grid will be explored in such a way that the orientation stays on each individual point for a prescribed duration.
- 6) The Euclid satellite will be tracked by a 35m ESA deep space antenna (either Malargüe or Cebreros, both stations simultaneously if possible from a station visibility point of view) during a scheduled pass, with the constraint of clear sky

conditions and antenna elevation between 20 degrees and 80 degrees during the whole exercise. The satellite will transmit an unmodulated K-Band signal through the high gain antenna, using the same on-board transmit power as used when transmitting science data. Ground aim is to measure the HGA carrier.

- 7) The boresight position wrt attitude reference frame is measured by using the loss function measured on ground.
- 8) Points from 3 to 7 are repeated for each AZ-EL tuple.
- 9) All the measures are used to estimate the calibration parameters HGACL\_CalPar, in table 6.1 called k1, k2, k3, k4, k5, k6.

Table 6.1: for each measure from ground, this set of data is obtained

A						B
$k_1$	$k_2$	$k_3$	$k_4$	$k_5$	$k_6$	
0	$S_{ELM}$	$-C_{AZm}S_{ELM}$	$S_{AZm}S_{ELM}$	$-S_{AZm}S_{ELM}$	$S_{AZm}$	$GS_{SRF1AZt} - C_{AZm}C_{ELM}$
$S_{ELM}$	0	$-S_{AZm}S_{ELM}$	$-C_{AZm}S_{ELM}$	$C_{AZm}C_{ELM}$	$C_{AZm}S_{ELM}$	$GS_{SRF2AZt} - S_{AZm}C_{ELM}$
$S_{AZm}S_{ELM}$	$-C_{AZm}C_{ELM}$	$C_{ELM}$				$GS_{SRF3AZt} - S_{ELM}$

In this part of the problem the unknowns are the  $\mathbf{k}$ , while the AZ\_m and EL\_m are the ones commanded, and the vector contains the vector  $\mathbf{B}$  contains the components of the measured GS vector in SRF.

Based on number of tuples, you have a calibration matrix  $\mathbf{A}$  [n. of tuples\*3 rows, 6 columns] and a vector  $\mathbf{B}$  [n. of tuples\*3 rows, 1 column], then you have to find the parameters that minimize the residuals  $\mathbf{k}$  [6 rows, 1 column]:  $\|Ak-B\|^2$

Although this is the exact procedure, Chapter 6 is going to highlight only the minimization problem discussing some important boundary conditions. Instead, Chapter 7 will be the place where a complete simulation of calibration is performed.

### 6.3. Study of minimization problem and its boundary conditions

#### 6.3.1. General Mathematical Model

As far as it concerns misalignments, the previous considered mathematical model is renewed in this general way:

$$b_{SRF} = AZ2SC\_RF \cdot rot\_AZ \cdot EL2AZ\_RF \cdot rot\_EL \cdot b_{HGA-ELrRF}$$

$$b_{HGA-ELrRF} = \begin{bmatrix} \cos\alpha\cos\beta \\ \sin\alpha\cos\beta \\ \sin\beta \end{bmatrix} \sim \begin{bmatrix} 1 \\ \alpha \\ \beta \end{bmatrix}$$

where alpha and beta are small angles but not null:

$$HGA\_boresight\_error = [0.07 \ 0.07] \cdot randn(1,2)$$

An amount of 5 reference frames have been identified:

1. Guidance Reference Frame (GRF) that can be assimilated to the SC Reference Frame SRF
2. AZ ref frame, integral with the static part of the azimuth motor
3. AZ rot ref frame, integral with the rotation part of the AZ motor
4. EL ref frame, integral with the static part of the EL motor

---

5. EL rot ref frame, integral with the rotation part of the EL motor

Then the four rotation matrices are:

1. Frm5to4: rot\_EL – It is a rotation due to EL motor angle;
2. Frm4to3: EL2AZ\_RF – Misalignment between AZ motor and EL motor. In theory this is recovered through ADPME calibration polynomial. In RPY representation:  

$$\text{EL2AZ\_RF\_err} = [0.02 \ 0.02 \ 0.02] \cdot \text{randn}(1,3) + [R \ 0 \ 0];$$
3. Frm3to2: rot\_AZ – It is a rotation due to AZ motor angle;
4. Frm2to1: AZ2SC\_RF – Misalignment of the AZ motor wrt the SRF. In RPY representation:  $\text{AZ2SC\_RF\_err} = [0.033 \ -0.033 \ 0.033] \cdot \text{randn}(1,3)$ .

Now, the same case related to comparison of boresights with/without polynomial correction of Chapter 5 is tested once again. These are the results for a given simulation:

Max angular error Alignment with polynomial correction: 1.130651E+01 [arcmin]

Max angular error Alignment without correction: 1.155354E+01 [arcmin]

Despite of the strict dependency of the results regarding the random vector errors EL2AZ\_RF\_err, AZ2SC\_RF\_err and HGA\_boresight\_error variation, it is a constant the presence of a narrow difference between with/without correction cases. The reason seems to be the equivalence in dimensions between random errors and the measured perpendicularity error (R) so that the ad-hoc polynomial law effect for a general case is negligible.

### 6.3.2. Errors in GS vector Estimation

Another source of error in calibration procedure emerges in the estimation of GS vector from ground (Err\_measure\_angles). Indeed, the minimization problem is actually trying to reduce distance between the boresight achieved using the rotation matrices (it means the one commanded by ADPME) and the real GS position (the one estimated from ground).

It is supposed to have a value of  $70\text{mdeg} \cdot \text{rand}(1,1)$  and must be related to AZ and EL of each tuple.

### 6.3.3. Calibration Points

Further step is to proceed with calibration study focusing on the role of AZ/EL tuple in the procedure. Some key-questions are: all possible series of AZ/EL tuples achieve the same calibration results or does it exist a particular set of points such that the outcome is optimal? Does the number of AZ/EL tuples influence the calibration and, if yes, how does is this related to the performance?

To verify the first hypothesis, 4 different sets of AZ/EL tuple will be considered:

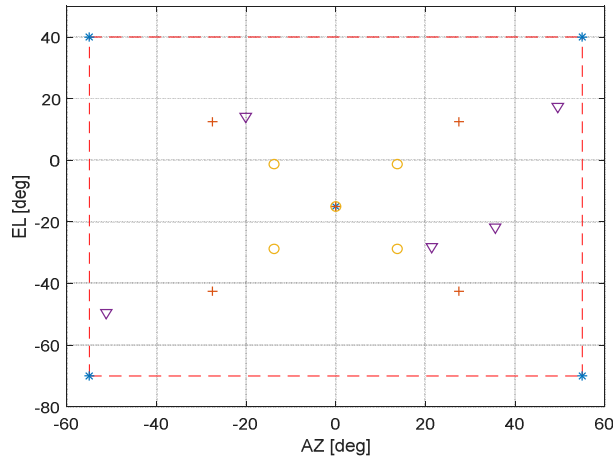


Figure 6-1: domain of AZ/EL points

In Figure 6.1, the first set of tuples is represented by 5 blue '\*' and the points are located at the edge of domain and one in the center; the second set of tuples is represented by 5 red '+' and the points are selected in the middle of the domain and one in the center; the third set of tuples is represented by 5 yellow 'o' and the points are located near to the center and one in the center; finally the fourth alternative is 5 purple lower triangles chosen in a random way.

In order to verify the second hypothesis, the calibration results will be investigated by using different number of points in AZ/EL domain considering the same initial conditions as always.

### 6.3.4. Calibration Minimization Problem

At first, the initial conditions shall be established, it means the random vectors errors EL2AZ\_RF\_err, AZ2SC\_RF\_err and HGA\_boresight\_error are defined, ADPME delivered AZ and EL commands (suitably modified by the Polynomial Law) according an appropriate tuple and GS estimation vector errors are given.

Once it is all settled, the algorithm calculates the predicted HGA boresight in SRF (spacecraft reference frame) thanks to AZ\_motor, EL\_motor and total rotation matrix obtained from EL2AZ\_RF\_err, AZ2SC\_RF\_err and HGA\_boresight\_error. While from Err\_measure\_angles, the measured position of the same HGA boresight is attained. As predictable, these two vectors do not match and furthermore none of them is actually describing the intended HGA boresight position since they are heavily affected by not-negligible errors.

So that a minimization problem of type  $\|Ak-B\|^2$  is needed where **A** is the calibration matrix, **B** contains the difference between measured HGA and commanded position and **k** as unknown shall be designed as residual coefficients vector HGACL\_CalPar. In order to determine such problem, FMINCON is chosen as solver [17].

A						B
$k_1$	$k_2$	$k_3$	$k_4$	$k_5$	$k_6$	
0	$S_{ELM}$	$-C_{AZM}S_{ELM}$	$S_{AZM}S_{ELM}$	$-S_{AZM}S_{ELM}$	$S_{AZM}$	$GS_{SRF2AZ} - C_{AZM}C_{ELM}$
$S_{ELM}$	0	$-S_{AZM}S_{ELM}$	$-C_{AZM}S_{ELM}$	$C_{AZM}C_{ELM}$	$C_{AZM}S_{ELM}$	$GS_{SRF2AZ} - S_{AZM}C_{ELM}$
$S_{AZM}S_{ELM}$	$-C_{AZM}C_{ELM}$	$C_{ELM}$				$GS_{SRF2AZ} - S_{ELM}$

Some mathematical considerations are now presented. A least square problem is a rough formulation of the problem as far as it concerns theoretical aspects; on the contrary the usage of Gauss-Markov estimate (also called BLUE estimator) seems more fitting but such model requires the definition of a covariant matrix which is quite difficult to gain from scientific data at the state of art of the mission.

Once obtaining the intended 6x1 vector **k**, the calibration coefficients enter in the algorithm calculating once again the HGA boresight position but by adapting furtherly AZ/EL target commands. At the end, the maximum angular error between the resultant final HGA boresight and the ideal HGA boresight is considered as benchmark.

To have some sort of statistical results, 400 cases with different initial conditions are been executed and investigated for three options:

- 1- NO CALIBRATION;
- 2- CALIBRATION WITHOUT POLYNOMIAL CORRECTION LAW;
- 3- CALIBRATION WITH POLYNOMIAL CORRECTION LAW.

### 6.3.5. Analysis of Comparison

First of all, it is important to establish the best procedure among no calibration and calibration with/without polynomial correction.

Presenting hereafter just some of the 400 cases though it is possible to abstract a global behavior.

For the same initial conditions furnished to both three methods, these are the distributions of maximum angular errors of antenna boresight with respect to the ideal one in all AZ/EL domain:

Table 6-2: Tests Description

Tests	Description	Goal
1	$EL2AZ\_RF\_err = [0.0804 \quad 0.0554 \quad -0.0270]$ $AZ2SC\_RF\_err = [0.1002 \quad -0.0239 \quad -0.0021]$ $HGA\_boresight\_error = [0.0500 \quad -0.0143]$ $Err\_measure\_angles = \begin{bmatrix} -4.27e-5 & 5.22 \\ -8.37e-5 & 4.71 \\ -1.58e-4 & 2.02 \end{bmatrix}$	<ul style="list-style-type: none"> <li>Check the Max Angular Err Boresight on the whole domain in case of: no cal, cal without polynomial corr, cal with polynomial corr</li> </ul>
2	$EL2AZ\_RF\_err = [0.0063 \quad 0.0298 \quad 0.0282]$ $AZ2SC\_RF\_err = [0.0468 \quad -0.0222 \quad -0.0398]$ $HGA\_boresight\_error = [0.0502 \quad 0.1141]$ $Err\_measure\_angles = \begin{bmatrix} 2.39e-5 & 4.61 \\ -8.38e-4 & 3.20 \\ -5.34e-4 & 4.46 \end{bmatrix}$	<ul style="list-style-type: none"> <li>Check the Max Angular Err Boresight on the whole domain in case of: no cal, cal without polynomial corr, cal with polynomial corr</li> </ul>
3	$EL2AZ\_RF\_err = [0.0186 \quad 0.0207 \quad 0.0145]$ $AZ2SC\_RF\_err = [-0.0100 \quad -0.0097 \quad -0.0260]$	<ul style="list-style-type: none"> <li>Check the Max Angular Err Boresight on the whole domain in case of: no cal,</li> </ul>

	HGA_boresight_error = [0.0622 -0.0803]  Err_measure_angles = $\begin{bmatrix} 4.53e-5 & 3.97 \\ -3.85e-4 & 4.92 \\ -5.46e-4 & 5.89 \end{bmatrix}$	cal without polynomial corr, cal with polynomial corr
4	EL2AZ_RF_err = [-0.0126 -0.0162 -0.0589] AZ2SC_RF_err = [0.0475 -0.0107 -0.0249] HGA_boresight_error = [0.0959 -0.1198]  Err_measure_angles = $\begin{bmatrix} -4.07e-5 & 5.02 \\ 6.35e-5 & 3.65 \\ -1.59e-4 & 4.02 \end{bmatrix}$	<ul style="list-style-type: none"> <li>Check the Max Angular Err Boresight on the whole domain in case of: no cal, cal without polynomial corr, cal with polynomial corr</li> </ul>

### TEST 1

Max Angular Err Boresight on the whole domain[arcmin]

NO CAL	7.21
CAL	2.41
CAL with Polynomial Corr	2.85

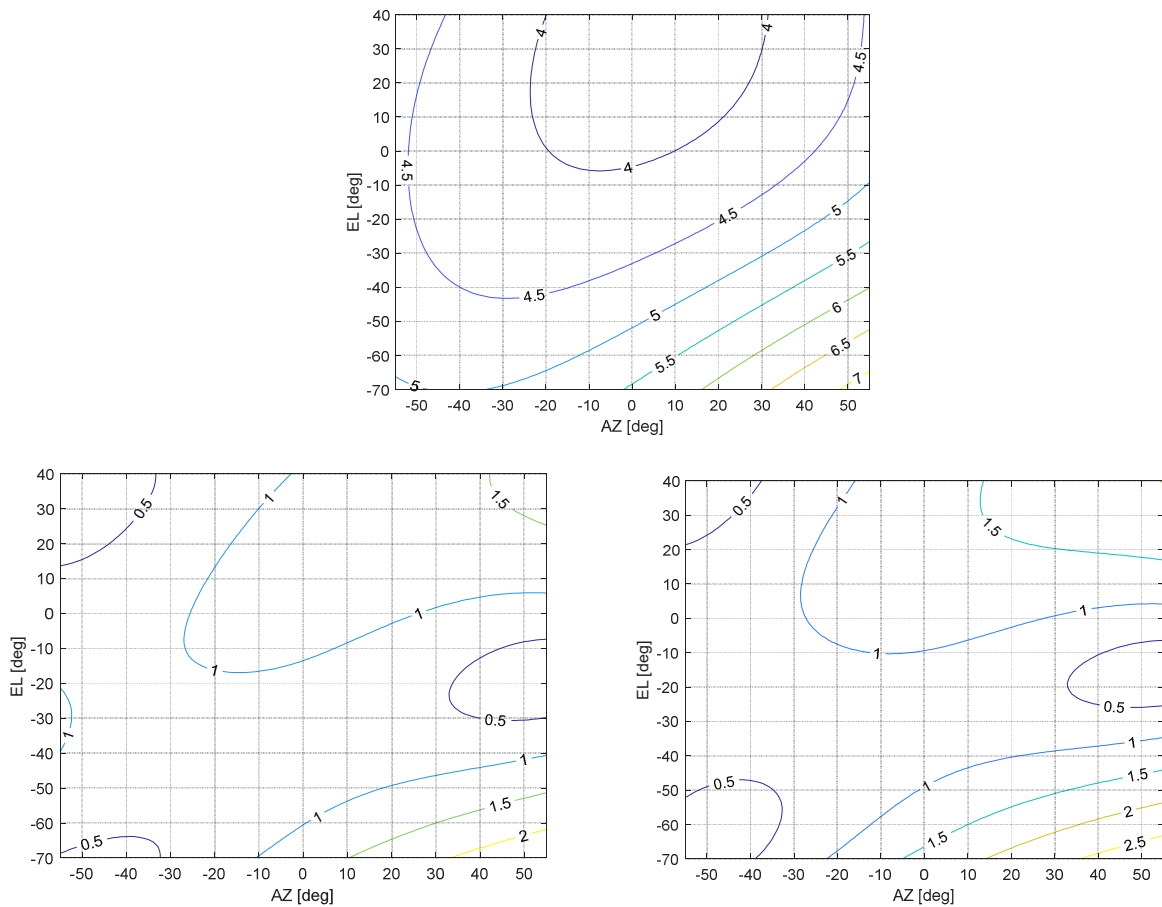


Figure 6-2: on top, the 'no-calibration' method results, on the bottom 'calibration' method (left), 'calibration with polynomial corr' method (right) results in AZ/EL points domain

## TEST 2

Max Angular Err Boresight on the whole domain [arcmin]

NO CAL	5.80
CAL	2.07
CAL with Polynomial Corr	1.99

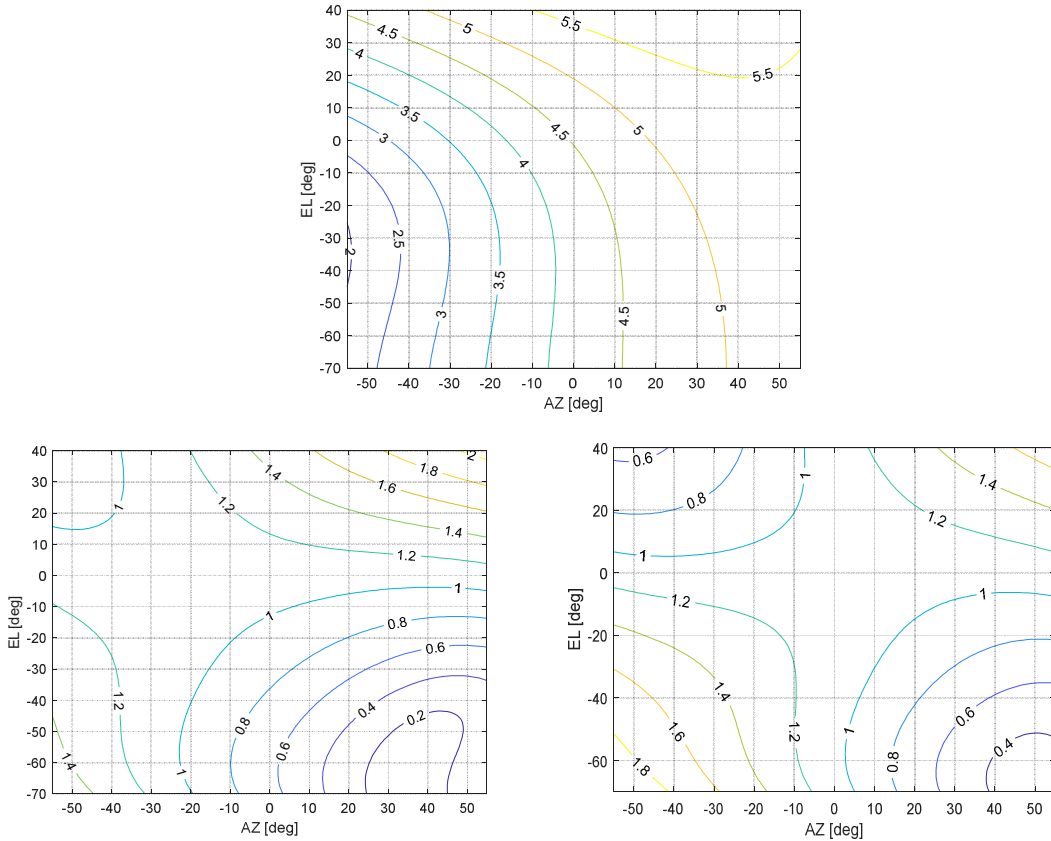
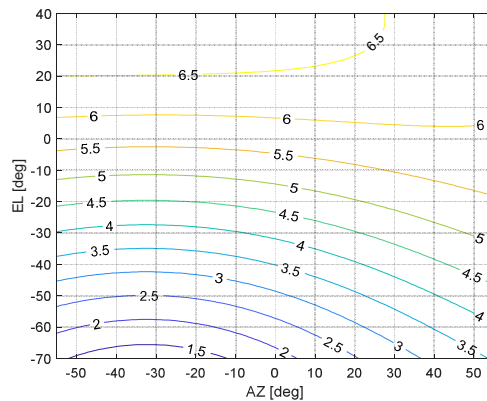


Figure 6-3: on top, the 'no-calibration' method results, on the bottom 'calibration' method (left), 'calibration with polynomial corr' method (right) results in AZ/EL points domain

## TEST 3

Max Angular Err Boresight on the whole domain  
[arcmin]

NO CAL	6.95
CAL	1.56
CAL with Polynomial Corr	1.14



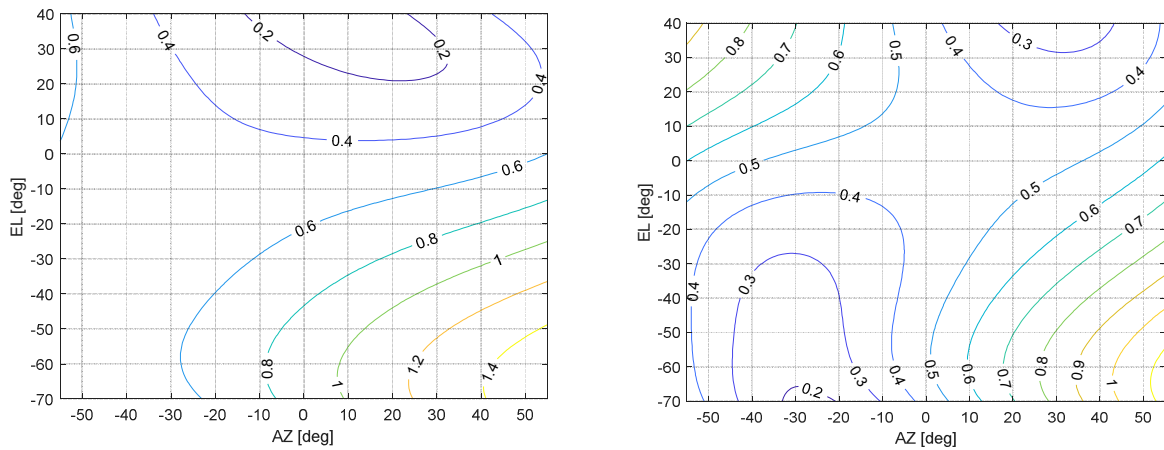


Figure 6- 4: on top, the 'no-calibration' method results, on the bottom 'calibration' method (left), 'calibration with polynomial corr' method (right) results in AZ/EL points domain

### TEST 4

Max Angular Err Boresight on the whole domain [arcmin]

NO CAL	12.67
CAL	2.05
CAL with Polynomial Corr	1.85

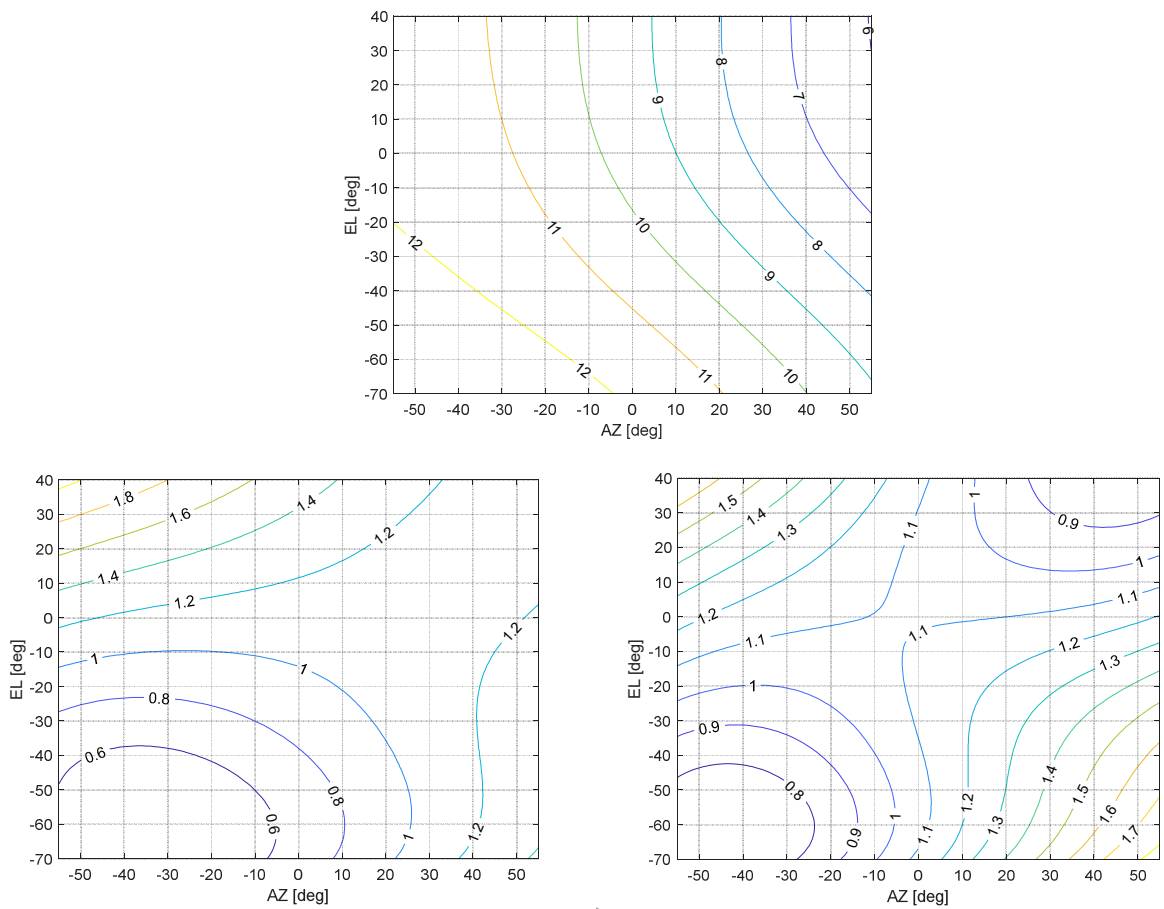


Figure 6-5: on top, the 'no-calibration' method results, on the bottom 'calibration' method (left), 'calibration with polynomial corr' method (right) results in AZ/EL points domain

From these few examples, it is evident how different errors involve different consequences on final boresight both without/with calibration but they show in common an unquestionable advantage of methods with calibration in comparison with 'no calibration' scenario (in particular note the improvement in TEST 4: from 12 arcmin down to 2 arcmin). Regarding the differences between 'calibration' and 'calibration with polynomial correction', in some cases the latter option seems to be more accurate while in other cases (see TEST 1) the only 'calibration' option is better. As said, the reason is attributable to the dimension of perpendicular error which is comparable with possible random errors occurring in actual space working conditions.

From another point of view, the comparison between cumulative distribution functions suggests the same relationship of the three methods in Figure 6.6:

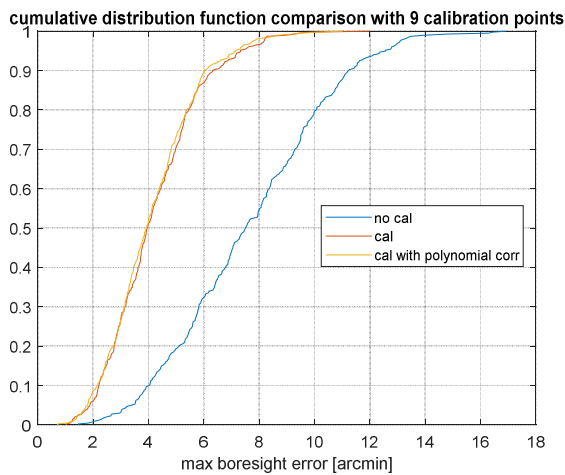


Figure 6-6: cumulative distribution functions obtained considering 400 cases

From now on, between the two, only the 'calibration with polynomial correction' case will be considered.

### 6.3.6. Are performances affected by the number of Calibration Points?

Now the hypothesis of influence of number of calibration points on calibration results is developed.

In particular, the cases with 'no-calibration', [3 4 5 7 9 11 15 18 27] calibration points will be under investigation. The statistical approach based on the study of the relative cumulative distribution function is followed.

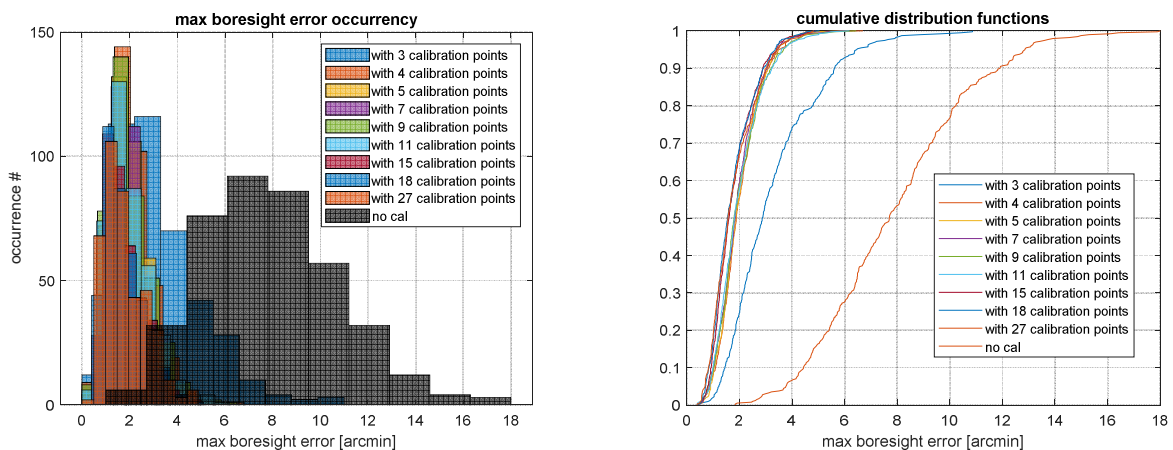


Figure 6-7: histogram of the errors occurred (left); cumulative distribution functions obtained considering 400 cases (right)

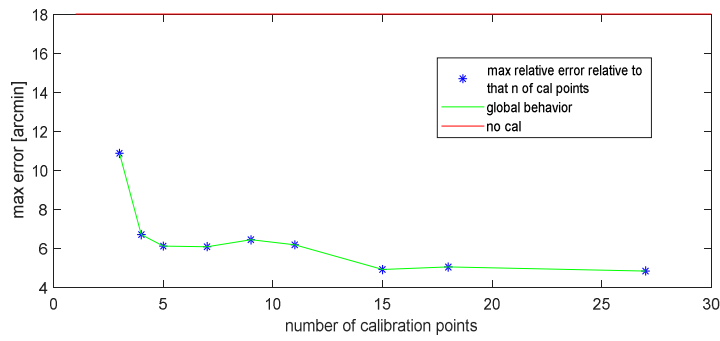


Figure 6- 8: global behavior of the errors occurred considering 400 cases

Just a glimpse is sufficient to underline how great is the improvement in calibration with only 3 points. As expected, as much you increase the number as much the calibration performances are remarkable but the step-advance is not more conspicuous as initially it is. Furthermore, the more the points are, the more the process is heavy to accomplish from a time-consuming point of view.

Regarding this point, ESA (European Space Agency) demands for a 3 points calibration. However such assumption could be discussed at least in the previous example considering the resultant maximum angular error is still around 11 arcmin (pay attention outcome depends on particular choice of calibration points). As alternative, see Figure 6.9 in comparison with another choice of calibration points.

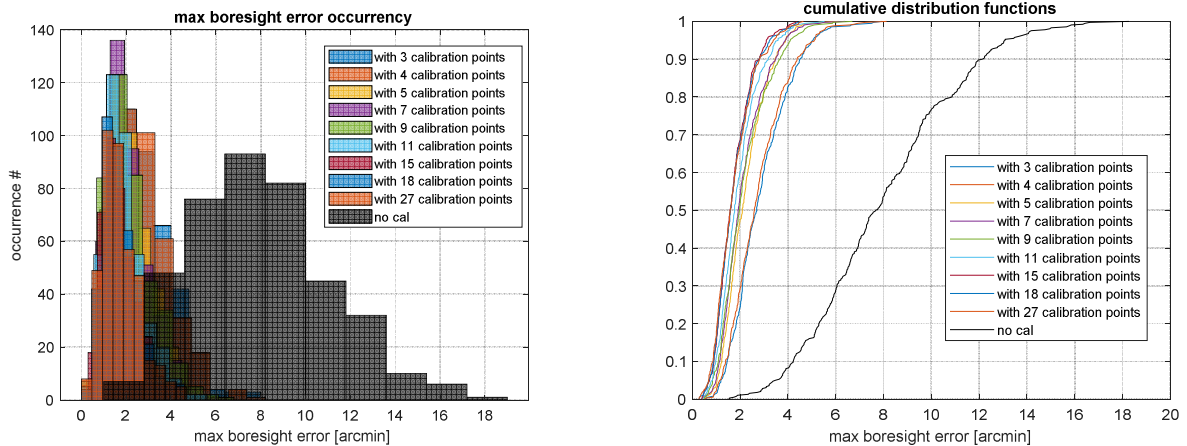


Figure 6-9: histogram of the errors occurred (left); cumulative distribution functions obtained considering 400 cases (right)

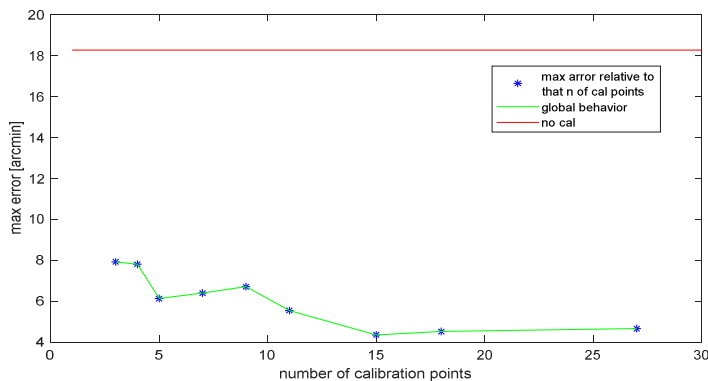
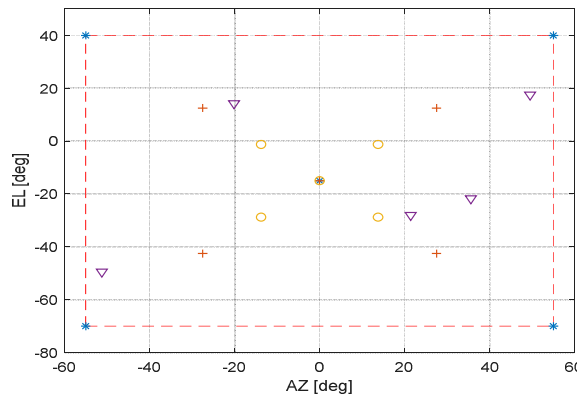


Figure 6-10: global behavior of the errors occurred considering 400 cases

A 4 or 5 points calibration should be recommended in my opinion. Generally, they both are more precautionary choices regarding pointing performance and still not so time-consuming alternatives.

### 6.3.7. Are performances affected by different choice of Calibration Points?

Aim of this segment is to discuss the way the Calibration Points influence the calibration. For sake of simplicity, the following outcomes are proposed fixing the initial conditions and assuming the 4 sets of 9 Calibration Points proposed in paragraph 6.3.3 (see Figure 6.1 here resubmitted) with 'calibration with polynomial correction':



Re-proposal of Figure 6-1: the first set of tuples is represented by 5 blue \* and the points are located at the edge of domain and one in the center; the second set of tuples is represented by 5 red + and the points are selected in the middle of the domain in a circular way and one in the center; the third set of tuples is represented by 5 yellow circles and the points are located near to the center and one in the center; finally the fourth alternative is 5 purple lower triangles chosen in a random way.

**INITIAL OUTCOME** - Distribution in the whole domain AZ/EL of the angular error boresight obtained without antenna calibration:

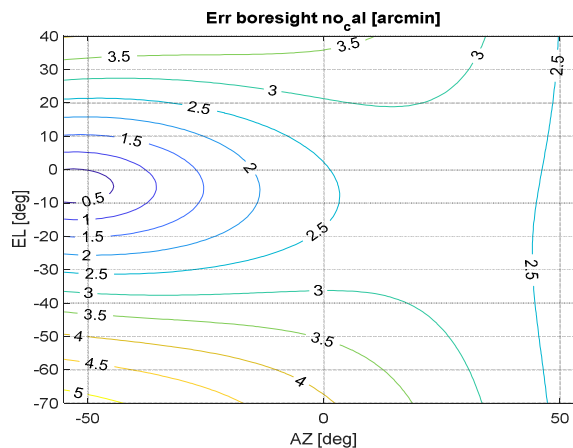


Figure 6-11

**OUTCOME DERIVED FROM THE 1<sup>st</sup> SET**- Distribution of the angular error boresight obtained with antenna calibration gained thanks to the points on the edge of AZ/EL domain:

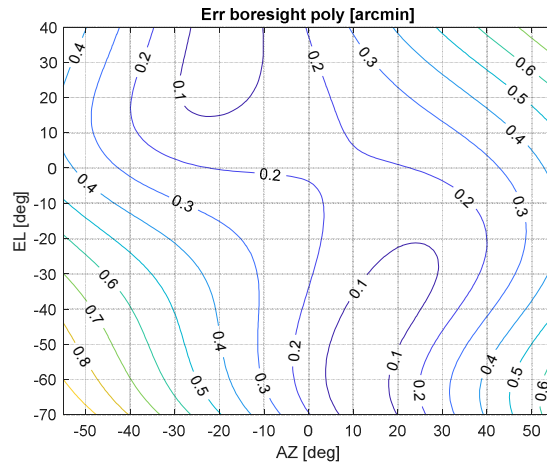


Figure 6-12

**OUTCOME DERIVED FROM THE 2<sup>nd</sup> SET-** Distribution of the angular error boresight obtained with antenna calibration gained thanks to the points in the middle of AZ/EL domain:

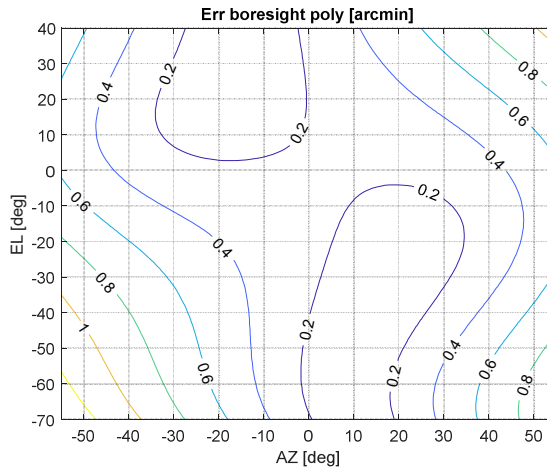


Figure 6-13

**OUTCOME DERIVED FROM THE 3<sup>rd</sup> SET-** Distribution of the angular error boresight obtained with antenna calibration gained thanks to the points near the center of AZ/EL domain:

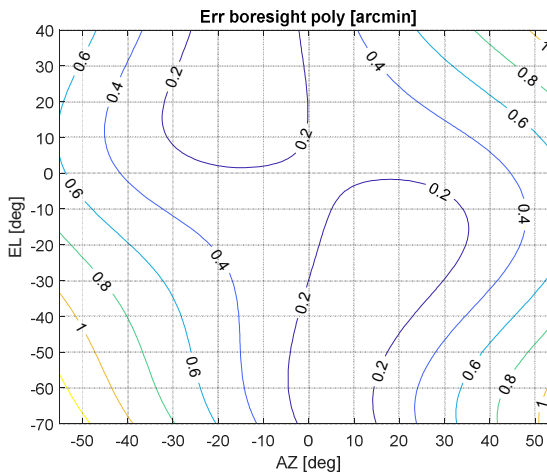


Figure 6-14

**OUTCOME DERIVED FROM THE 4<sup>th</sup> SET-** Distribution of the angular error boresight obtained with antenna calibration gained thanks to the points chosen randomly in AZ/EL domain:

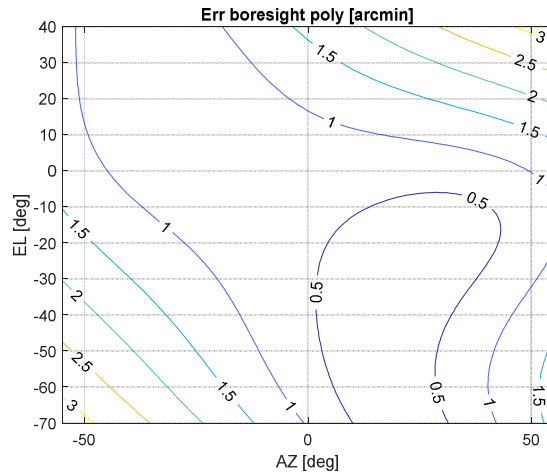


Figure 6-15

Once again, it is confirmed each calibration guarantees better performances in comparison with 'no calibration' scenario. Nevertheless, among the four sets of calibration points the first option reveals the best one concerning the global error minimization. Even the second and third options prove their goodness in the central region but the error grows on the extremities. The worst option is the random set.

Finally, the reader should understand how it urges a criterion in choosing the most fitting calibration points and nothing should be left to chance. Nevertheless, a 3-points calibration could reveal fitting, as ESA requires, if an accurate strategy in picking tuples is followed.

### 6.3.8. How to choose the optimal Calibration Points

A constraint for HGA, not treated till now, is related to variation in time of the Sun-Spacecraft-Earth angle (SSCE). In fact, the spacecraft moves around in its orbit trying to avoid direct sun-light on its instruments by exploiting the protection of solar panels which in addition absorb sun-energy in the meanwhile. Doing such maneuvers, the antenna domain is restricted as Figure 6.16 points out.

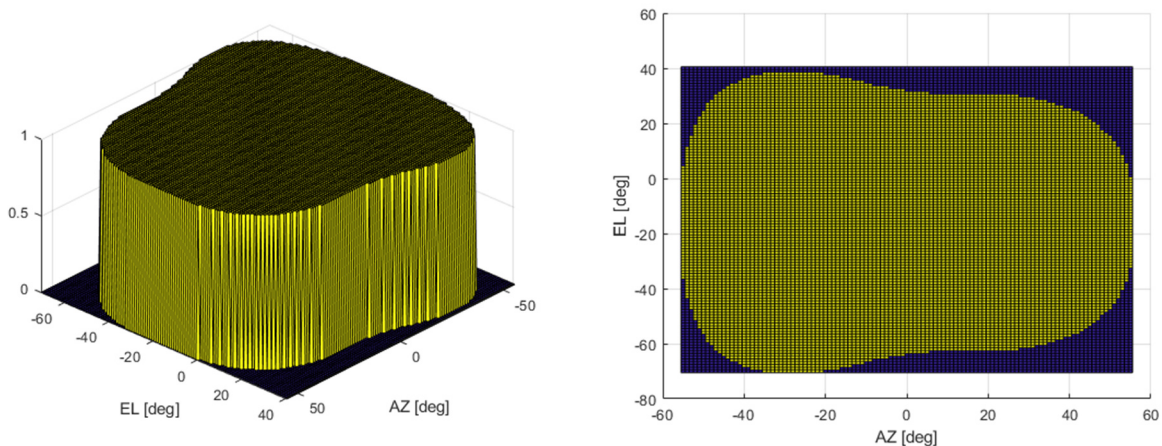


Figure 6-16: region covered by SSCE variation from 36° to 7° (left); relative top view (right)

It is been estimated SSCE shall vary approximately between  $[8^\circ, 35^\circ]$  during mission lifetime (even if an interval of  $[7^\circ, 36^\circ]$  has been considered to be more relaxed). This consideration shall be coherent with the optimal choice of calibration points. In this way, a possible distribution of angular error of the boresight after calibration becomes as it follows:

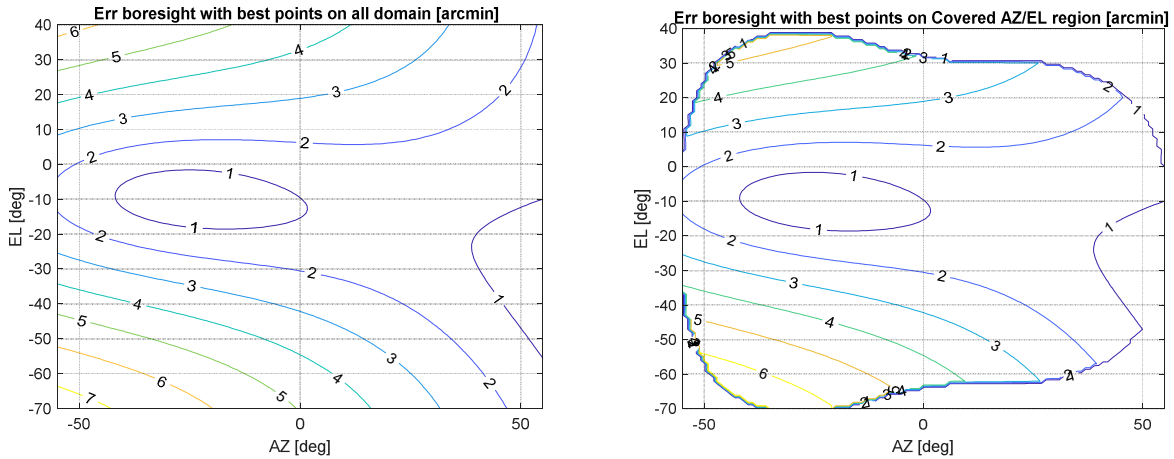


Figure 6- 17: actual AZ/EL domain considering SSCE constraints (right)

As far as it deals with search of calibration points, the central problem is always the same:

A						B
$k_1$	$k_2$	$k_3$	$k_4$	$k_5$	$k_6$	
0	$S_{ELM}$	$-C_{AZM}S_{ELM}$	$S_{AZM}S_{ELM}$	$-S_{AZM}S_{ELM}$	$S_{AZM}$	$GS_{SRF1EXT} - C_{AZM}C_{ELM}$
$S_{ELM}$	0	$-S_{AZM}S_{ELM}$	$-C_{AZM}S_{ELM}$	$C_{AZM}C_{ELM}$	$C_{AZM}S_{ELM}$	$GS_{SRF2EXT} - S_{AZM}C_{ELM}$
$S_{AZM}S_{ELM}$	$-C_{AZM}C_{ELM}$	$C_{ELM}$				$GS_{SRF3EXT} - S_{ELM}$

Nevertheless, now the key-role is the choice of the optimal calibration points among all the reachable AZ/EL domain points. On this basis, the unknown  $\mathbf{k}$  vector will be calculated and after calibration, the max angular error on boresight will be established. This algorithm is going to be reiterated looking for the minimization of the max angular error on boresight based on specific choices of AZ<sub>m</sub> and EL<sub>m</sub> which represent the new unknowns in this step.

The not-convexity of the problem implies an intrinsic effort in finding the global minimum or otherwise the best solution set of points. The optimization can assure only a greedy solution with a certain level of confidence, so several strategies are been implemented. Some of the worst initial conditions (EL2AZ\_RF\_err, AZ2SC\_RF\_err, HGA\_boresight\_error and Err\_measure\_angles) among the 400 cases shall be considered in the process.

Attempt after attempt, the reader has the chance to go through some of the solvers used to reach a plausible result. Hereafter a brief description is presented:

### FMINCON

At first, *fmincon* is implemented as nonlinear programming solver to find the minimum. Due to the presence of many local minima, this method is not satisfying in global optimization. Indeed, the solution is normally stacked in different points each time a new initial points guess is proposed.

---

### **GLOBAL SEARCH (Matlab Global Optimization Toolbox) [12]**

The *global search* solver applies to problems with a multi-start approach by starting a local solver such as *fmincon* from a variety of random start points. Then it compares the outcomes of different local solvers and it furnishes the best one as result.

### **DIRECT SEARCH (Matlab Global Optimization Toolbox) [12]**

*Direct search* is a method for solving optimization problems that does not require any information about the gradient of the objective function. A direct search algorithm searches a set of points around the current point, looking for one where the value of the objective function is lower than the value at the current point. You can use direct search to solve problems for which the objective function is not differentiable or is not even continuous.

At each step, the algorithm searches a set of points, called a *mesh*, around the *current point*—the point computed at the previous step of the algorithm. The mesh is formed by adding the current point to a scalar multiple of a set of vectors called a *pattern*. If the pattern search algorithm finds a point in the mesh that improves the objective function at the current point, the new point becomes the current point at the next step of the algorithm.

### **GENETIC ALGORITHM (Matlab Global Optimization Toolbox) [12]**

Such method solves smooth or nonsmooth optimization problems with any types of constraints including integer constraints. It is a stochastic, population-based algorithm that searches randomly by modifying the starting population imitating genetics rules: crossover, mutation, scaling factor and selection.

The following outline summarizes how the *genetic algorithm* works:

1. The algorithm begins by creating a random initial population.
2. The algorithm then creates a sequence of new populations. At each step, the algorithm uses the individuals in the current generation to create the next population. To create the new population, the algorithm performs the following steps:
  - Scores each member of the current population by computing its fitness value. These values are called the raw fitness scores.
  - Scales the raw fitness scores to convert them into a more usable range of values. These scaled values are called expectation values.
  - Selects members, called parents, based on their expectation.
  - Some of the individuals in the current population that have lower fitness are chosen as *elite*. These elite individuals are passed to the next population.
  - Produces children from the parents. Children are produced either by making random changes to a single parent—*mutation*—or by combining the vector entries of a pair of parents—*crossover*.
  - Replaces the current population with the children to form the next generation.
3. The algorithm stops when one of the stopping criteria is met.

### **PARTICLE SWARM (Matlab Global Optimization Toolbox) [12]**

*Particle swarm* is a population-based algorithm. In this respect it is similar to the genetic algorithm. A collection of individuals called particles move in steps throughout a region. At each step, the algorithm evaluates the objective function at each particle. After this

evaluation, the algorithm decides on the new velocity of each particle. The particles move, then the algorithm reevaluates.

The inspiration for the algorithm is flocks of birds or insects swarming. Each particle is attracted to some degree to the best location it has found so far, and also to the best location any member of the swarm has found. After some steps, the population can coalesce around one location, or can coalesce around a few locations, or can continue to move.

### **SURROGATE OPTIMIZATION (Matlab Global Optimization Toolbox) [12]**

A surrogate is a function that approximates an objective function. The surrogate is useful because it takes little time to evaluate. So, for example, to search for a point that minimizes an objective function, simply evaluate the surrogate on thousands of points, and take the best value as an approximation to the minimizer of the objective function. Surrogate optimization is best suited to time-consuming objective functions. The objective function need not be smooth, but the algorithm works best when the objective function is continuous.

*Surrogate optimization* attempts to find a global minimum of an objective function using few objective function evaluations. To do so, the algorithm tries to balance the optimization process between two goals: exploration and speed.

The algorithm has been proven to converge to a global solution for continuous objective functions on bounded domains.

#### **6.3.8.1. Simulation**

For our purposes, two different tests with some of the worst initial conditions (EL2AZ\_RF\_err, AZ2SC\_RF\_err, HGA\_boresight\_error and Err\_measure\_angles) for a 3-points calibration are going to be investigated in order to check similarities and/or discrepancies.

### **TEST 1**

EL2AZ\_RF\_err = [0.0293 -0.0024 0.0017] rad

AZ2SC\_RF\_err = [-0.0012 0.131 0.0766] rad

HGA\_boresight\_error = [-0.018 -0.0637] rad

$$\text{Err\_measure\_angles} = \begin{bmatrix} -4.27e-5 & 5.22 \\ -8.37e-5 & 4.71 \\ -1.59e-4 & 2.02 \end{bmatrix} \text{ rad}$$

In Figure 6.18, Max\_Err\_poly\_opt\_region with 3 random points calibration = 9.53 arcmin

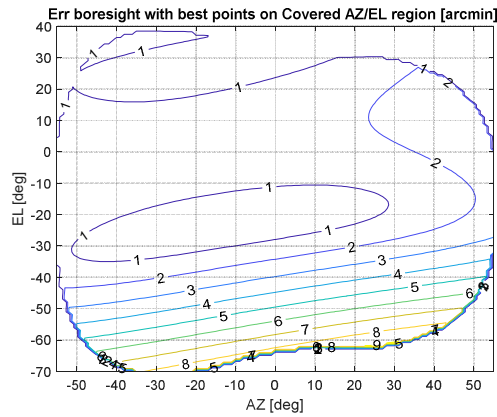


Figure 6-18: boresight error considering SSCE constraints

**FMINCON**

Since it is a local solver, two attempts are proposed:

**RUN 1:**

- INITIAL GUESS =  $x_0 = [-20 \ -20; -10 \ 25; -30 \ -10]$ ;
- FINAL RESULT= $[-15.64 \ -10.51; -6.14 \ 4.75; -47.71 \ -42.46]$ ;
- Max\_Err\_poly\_opt\_region = 5.77 arcmin

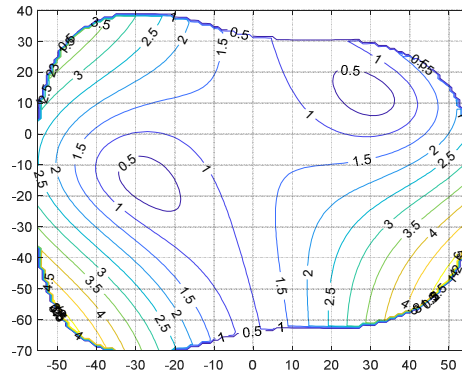


Figure 6-19: boresight error considering SSCE constraints

**RUN 2:**

- INITIAL GUESS=  $x_0 = [20 \ -40; -30 \ 20; 30 \ 0]$ ;
- FINAL RESULT=  $[31.16 \ -51.35; -29.67 \ 12.08; 39.90 \ 10.45]$ ;
- Max\_Err\_poly\_opt\_region = 3.58 arcmin

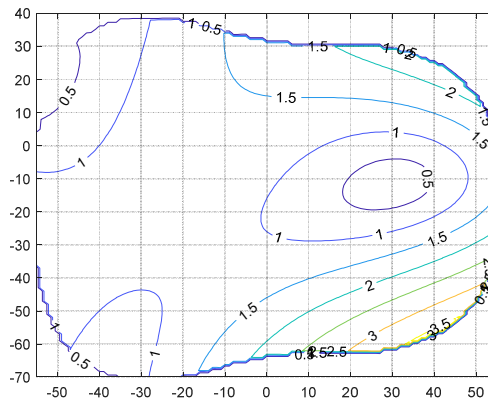


Figure 6-20: boresight error considering SSCE constraints

**GLOBAL SEARCH**

- FINAL RESULT= [ -38.8112 -53.2177; -4.2110 -62.6261; 31.8236 -50.9206];
- Max\_Err\_poly\_opt\_region = 2.11 arcmin

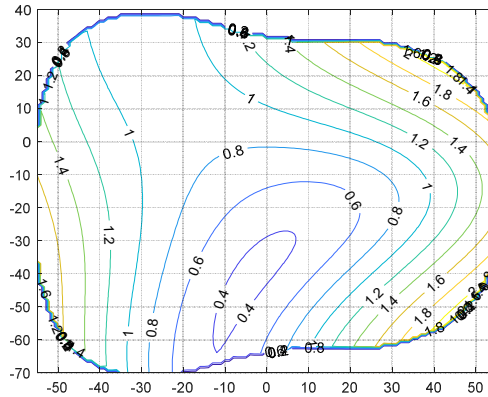


Figure 6-21: boresight error considering SSCE constraints

**DIRECT SEARCH**

- FINAL RESULT= [40.30 -40.78; -38.12 -1.0; -7.0 -40.0];
- Max\_Err\_poly\_opt\_region = 2.44 arcmin

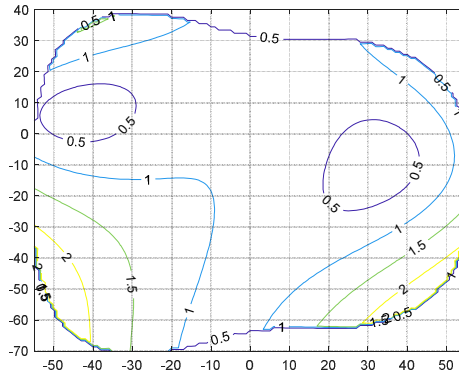


Figure 6-22: boresight error considering SSCE constraints

**GENETIC ALGORITHM**

- FINAL RESULT= [19 -36; 46 4; 48 -35];
- Max\_Err\_poly\_opt\_region = 2.07 arcmin

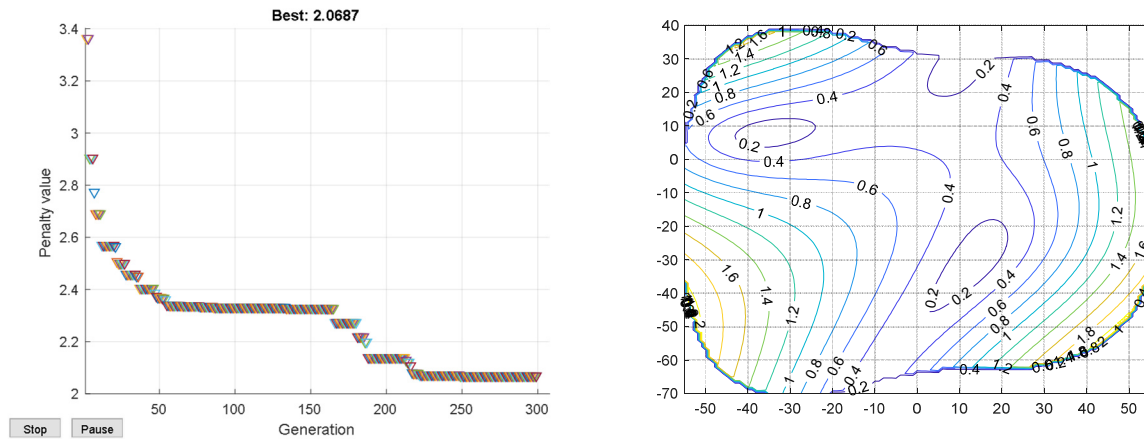


Figure 6-23: GA path solution (left); boresight error considering SSCE constraints (right)

### PARTICLE SWARM

- FINAL RESULT= [-47.50 -56.50; 6.42 -56.50; 39.50 -56.50];
- Max\_Err\_poly\_opt\_region = 1.63 arcmin

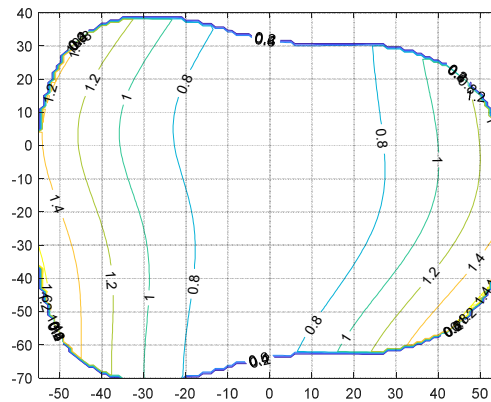


Figure 6-24: boresight error considering SSCE constraints

### SURROGATE OPTIMIZATION

- FINAL RESULT= [-3.80 -16.51; -3.93 -16.43; -3.83 -16.53];
- Max\_Err\_poly\_opt\_region = 2.75 arcmin

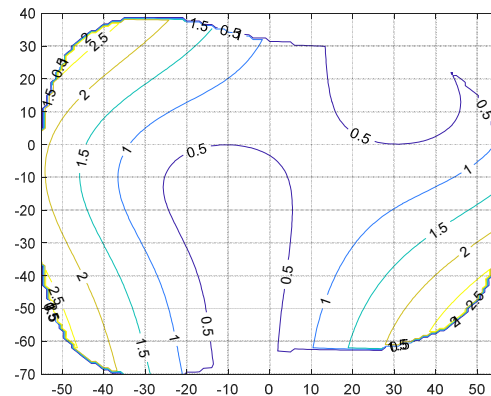


Figure 6-25: boresight error considering SSCE constraints

### TEST 2

EL2AZ\_RF\_err = [-0.0093 -0.0025 0.0034] rad

AZ2SC\_RF\_err = [-0.056 0.0792 0.0288] rad

HGA\_boresight\_error = [-0.033 -0.0803] rad

Err\_measure\_angles =  $\begin{bmatrix} 7.17e-5 & 3.88 \\ 2.82e-5 & 5.97 \\ 5.55e-4 & 2.66 \end{bmatrix}$  rad

Max\_Err\_poly\_opt\_region with 3 random points calibration = 8.96 arcmin

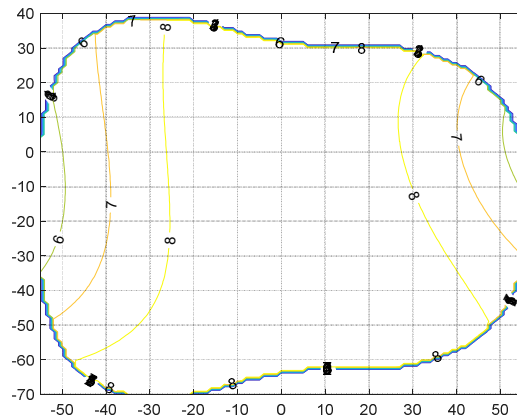


Figure 6-26: boresight error considering SSCE constraints

**FMINCON**

Since it is a local solver, two attempts are proposed:

**RUN 1:**

- INITIAL GUESS =  $x_0 = [-20 \ -20; -10 \ 25; -30 \ -10]$ ;
- FINAL RESULT =  $[-31.49 \ -18.60; 33.68 \ 15.70; -3.65 \ -0.97]$ ;
- Max\_Err\_poly\_opt\_region = 5.22 arcmin

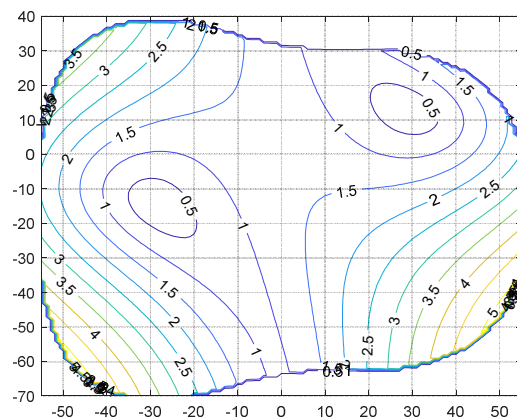


Figure 6-27: boresight error considering SSCE constraints

**RUN 2:**

- INITIAL GUESS =  $x_0 = [20 \ -40; -30 \ 20; 30 \ 0]$ ;
- FINAL RESULT =  $[-9.74 \ -54.84; 27.90 \ 11.87; 33.52 \ -18.14]$ ;
- Max\_Err\_poly\_opt\_region = 5.16 arcmin

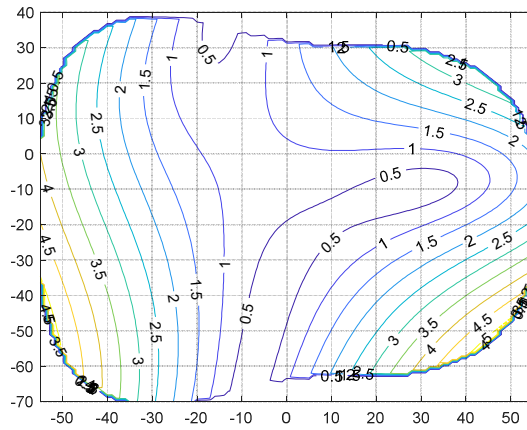


Figure 6- 28: boresight error considering SSCE constraints

**GLOBAL SEARCH**

- FINAL RESULT=[ -39 9; 28 -20; -2 -51];
- Max\_Err\_poly\_opt\_region = 5.01 arcmin

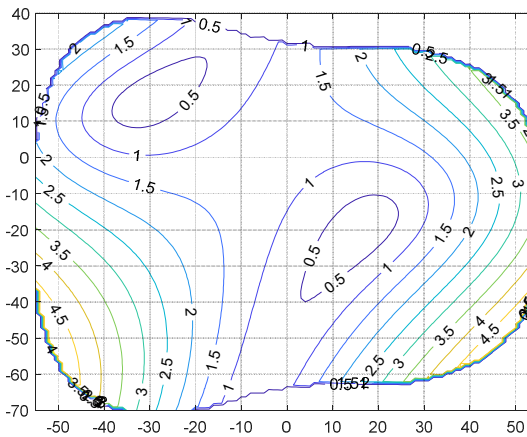


Figure 6-29: boresight error considering SSCE constraints

**DIRECT SEARCH**

- FINAL RESULT= [-8 -45; 14 -33; 1 30];
- Max\_Err\_poly\_opt\_region = 5.31 arcmin

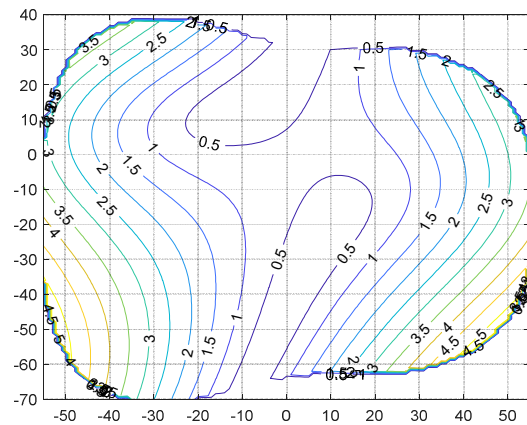


Figure 6- 30: boresight error considering SSCE constraints

**GENETIC ALGORITHM**

- FINAL RESULT= [ -55 -9; 53 -17; -5 -62];
- Max\_Err\_poly\_opt\_region = 4.85 arcmin

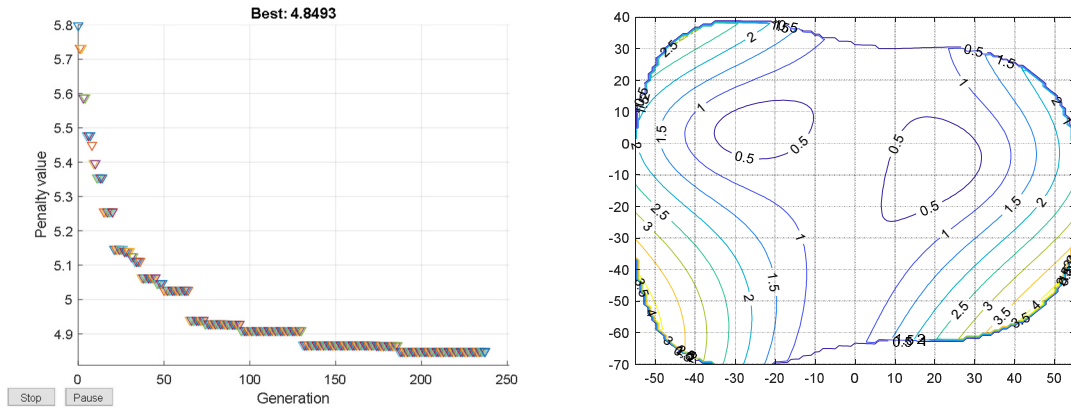


Figure 6- 31: GA path solution (left); boresight error considering SSCE constraints (right)

**PARTICLE SWARM**

- FINAL RESULT= [-47.50 -56.5; -47.5 23.50; 35.62 -55.74];
- Max\_Err\_poly\_opt\_region = 3.81 arcmin

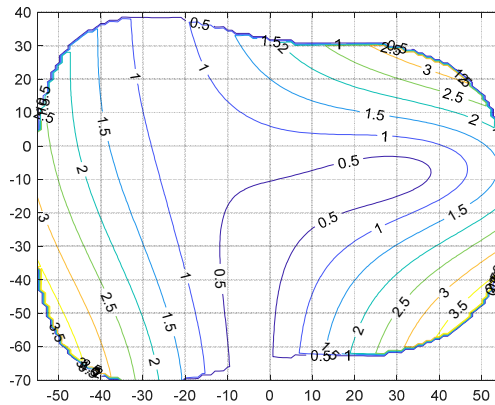


Figure 6- 32: boresight error considering SSCE constraints

**SURROGATE OPTIMIZATION**

- FINAL RESULT= [-47.50 -56.41; 39.50 22.92; 39.50 -48.86];
- Max\_Err\_poly\_opt\_region = 4.47 arcmin

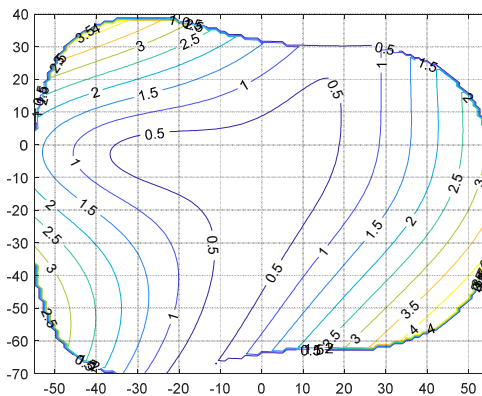


Figure 6- 33: boresight error considering SSCE constraints

### 6.3.8.2. Analysis of results

From the comparison of the two tests, it is evident how a wise selection of points can thoroughly boost the performance even with only a 3-points calibration. Nevertheless, it does not exist a general unique choice of calibration points. Unfortunately, this latter aspect is heavily affected by `EL2AZ_RF_err`, `AZ2SC_RF_err`, `HGA_boresight_error` and `Err_measure_angles` whose exact knowledge is prevented and they can only be estimated.

As far as it concerns the solvers, *fmincon* fails in finding a global minimum due to its local characteristics while each of Matlab Optimization Toolbox solvers accomplished its duty. At least in these two test-cases, both of the best optimizations are achieved through *particle swarm* algorithm.

## 6.4. Conclusions about the study

To sum up, many considerations can be assumed helpful for mission scopes:

- Calibration is an essential procedure to dramatically improve the pointing performance;
- The Polynomial Correction Law reveals efficient in 'on-ground' calibration but if plausible errors occurring during mission lifetime are added, a more general 'in-flight' calibration is needed;
- Many factors like SSCE angle, the number and/or the choice of calibration points in AZ/EL domain are relevant;
- In ESA opinion, a calibration by means of 3 points is a good trade-off between improvement of performance and time-consuming operation. A 4/5 points calibration is a more time-consuming but relaxed choice, instead;
- Fixed the number of points and the initial conditions, a criterion for an optimal choice of calibration points shall be identified. Such type of problem is not convex and only a greedy solution can be found. However if a good estimation of the result is identified, then even a 3-points calibration manages to meet more comfortably the DTCP pointing requirement.



# Chapter 7

## Simulation of an ‘in-flight’ HGA Calibration

In the frame of the Euclid mission, it has been planned to calibrate in flight the on-board pointing error by use of measurements performed on ground with the ESA deep space antennas. The purpose of the calibration is to estimate the angular misalignment between on-board antenna boresight and commanded orientation. In this note the calibration procedure is going to be fully analyzed, and all error contributors affecting the final estimate are considered, in order to check whether the desired accuracy of the end result can be achieved.

It is worth to remember the calibration procedure is defined as follows:

1. Taking into account the Sun-SC-Earth Angle of the moment when the HGA calibration is performed, not all the AZ-EL tuples can be reached.
2. Considering the reachable tuples, a number of calibration points are selected.
3. For each tuple, the relevant angles are commanded to the ADPME.
4. A target attitude quaternion is commanded to the SC such that the Earth and the HGA boresight are aligned.
5. The satellite will be programmed in order to offset the direction of transmission over an angular spiral grid (this will be obtained by changing the on-board attitude, the steerable high gain antenna remaining fixed in its position). The angular spiral grid will be explored in such a way that the orientation stays on each individual point for a prescribed duration.
6. The Euclid satellite will be tracked by a 35m ESA deep space antenna (either Malargüe or Cebreros, both stations simultaneously if possible from a station visibility point of view) during a scheduled pass, with the constraint of clear sky conditions and antenna elevation between 20 degrees and 80 degrees during the whole exercise. The satellite will transmit an unmodulated K-Band signal through the high gain antenna, using the same on-board transmit power as used when transmitting science data. Ground aim is to measure the HGA carrier.
7. The boresight position wrt attitude reference frame is measured by using the loss function measured on ground.
8. Points from 3 to 7 are repeated for each AZ-EL tuple.
9. All the measures are used to estimate the calibration parameters HGACL\_CalPar which till now have been considered null.

From hereafter, only aspects related to the thesis scope are going to be pointed out in the simulation results.

### 7.1. Preliminary Steps

First of all, the orbit environment and EUCLID initial parameters are furnished to HGACL\_ESE Simulink model.

Once the Sun-SC-Earth Angle (SSCE) at that time is extracted and the mechanical errors (EL2AZ\_RF\_err, AZ2SC\_RF\_err and HGA\_boresight\_error) are supposed, three tuples for a 3-points calibration are chosen among the reachable tuples to command the ADPME. In this case, the set is the following: [-17 -32; -10 0; -20 -20].

As procedure prescribes, for the first tuple, ADPME drives the motors to align the antenna in that exact position while EUCLID acts on its attitude to align as much accurate as possible the HGA boresight to Earth (Cebreros ground station will be considered in the calculation). From now on, its on-board attitude varies in given time performing a 26-points spiral and referring to a series of target quaternions (see Figure 7.1 and Figure 7.2).

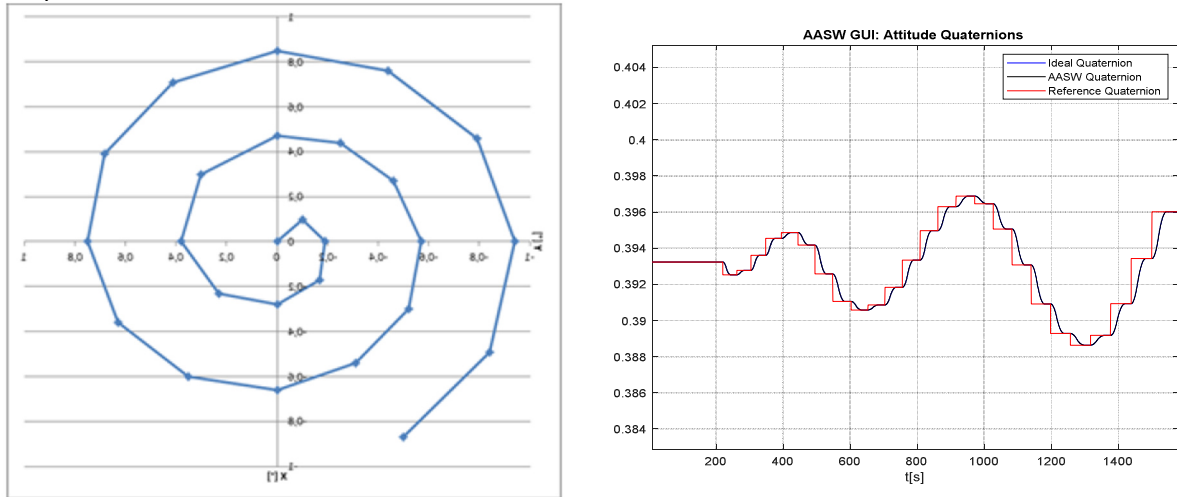


Figure 7-1: calibration spiral (left) and example of one component of target quaternions (right)

These passages are repeated for the rest of tuples. The following figures represent the result after all these steps are executed.

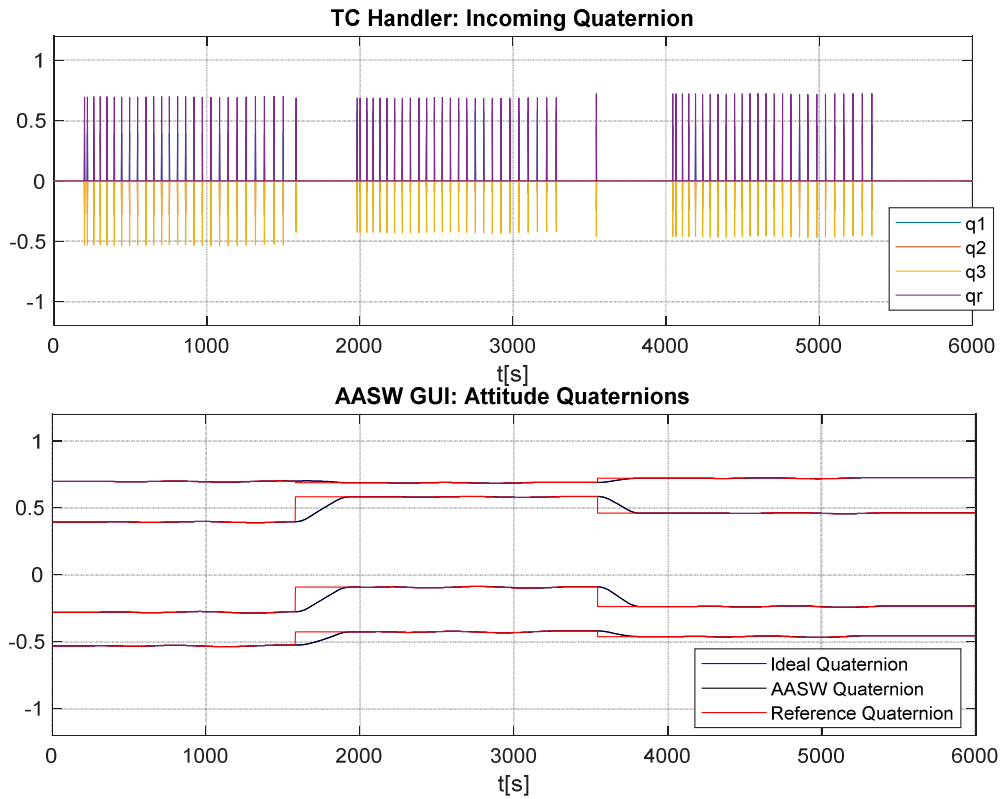


Figure 7-2: target quaternions

## Chapter 7 - Simulation of an 'in-flight' HGA Calibration

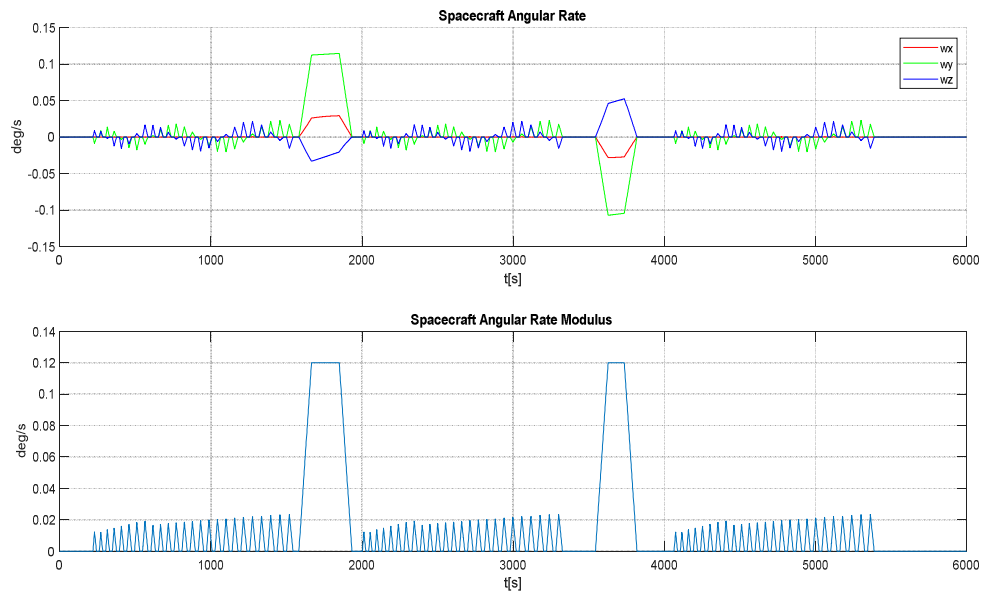


Figure 7-3: SC angular rate

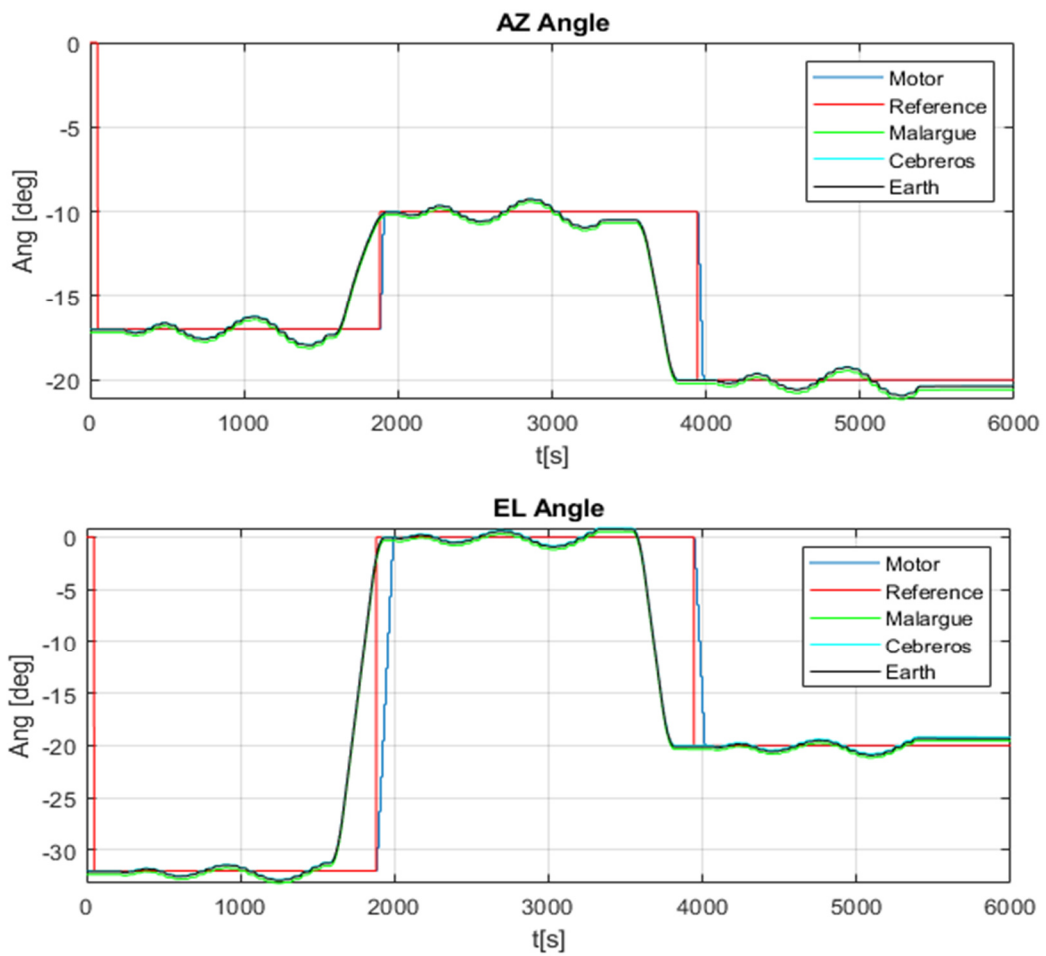


Figure 7-4: AZ/EL behavior

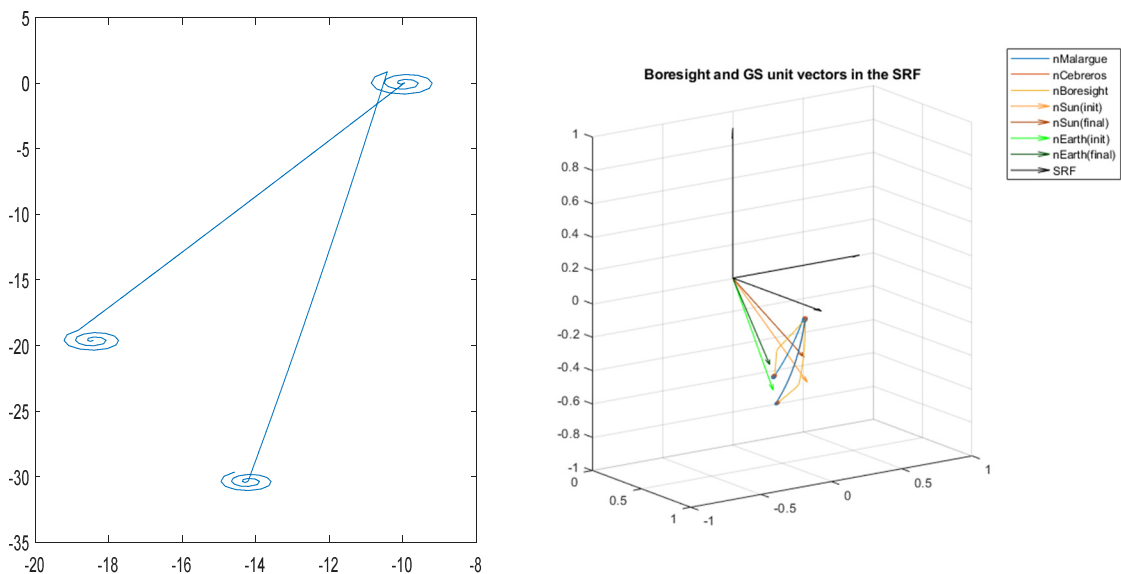


Figure 7- 5: 3-spirals accomplishment

As shown, each spiral expends more or less 1500 sec to be accomplished successfully with a further time-interlude where the spacecraft needs to reach the next target attitude quaternion (as Figure 7.3 denotes with the two trapezoidal speed profile at maximum velocity or as Figure 7.2. implies with step variation in attitude quaternion in the meanwhile). In total, almost 1 h 30 m is required to perform this section of Calibration Procedure which is the most time-consuming part. On the contrary, a 4-points calibration should request almost 2 h, while more than 2 h for a 5-points calibration. Reasonably if only a limited time constraint is reserved for Calibration in the mission timeline, then ESA must take into account such values.

Figure 7.4 reveals Azimuth and Elevation behaviors while Cebros Ground Station varies its position in spacecraft reference frame (SRF).

Instead, Figure 7.5 highlights 3-spirals movement from different point of views.

## 7.2. Measurements from Ground

During this step, the last elements, essential in minimization problem definition, have been measured: `Err_measure_angles`.

The normal purpose of a measurement process is to characterize the radiation pattern at a very great, or infinite, distance with reference to an angular, or other co-ordinate set, with respect to a carefully defined mechanical interface. Once acquired, this data can then be utilized to establish the extent to which the instrument fulfils its requirements which is often accomplished by comparing the measured performance with a theoretical prediction.

Once boresight carrier is received on the delivered ground station (Cebros), a certain additive error has to be considered in the estimation. Such mistakes come from different sources, although two main categories can be summarized: APE (Absolute Pointing Error) and KME (Knowledge Measurement Error). Obviously, APE depends not exclusively but mainly on misalignments already mentioned. On the other hand, KME relies on aspects apart from antenna as for example poor signal detection due meteorological conditions (outdoor temperature, relative humidity, barometric pressure, wind speed and direction, cloud presence in the sky) or low-signal amplification issues.

To get the point, Figure 7.6 describes the angular distance between actual and ideal boresights from SRF and in the meanwhile Figure 7.7 indicates the same fault between measured and ideal boresights on ground.

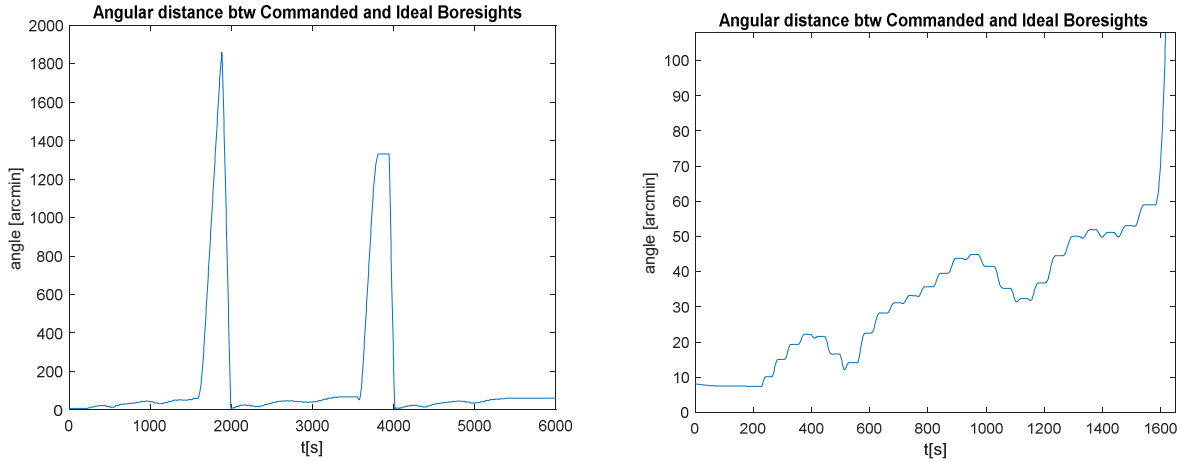


Figure 7-6: boresight error in SC reference frame (left); zoom of a single spiral (right) where the angle increases coherently while the spiral goes far from the center.

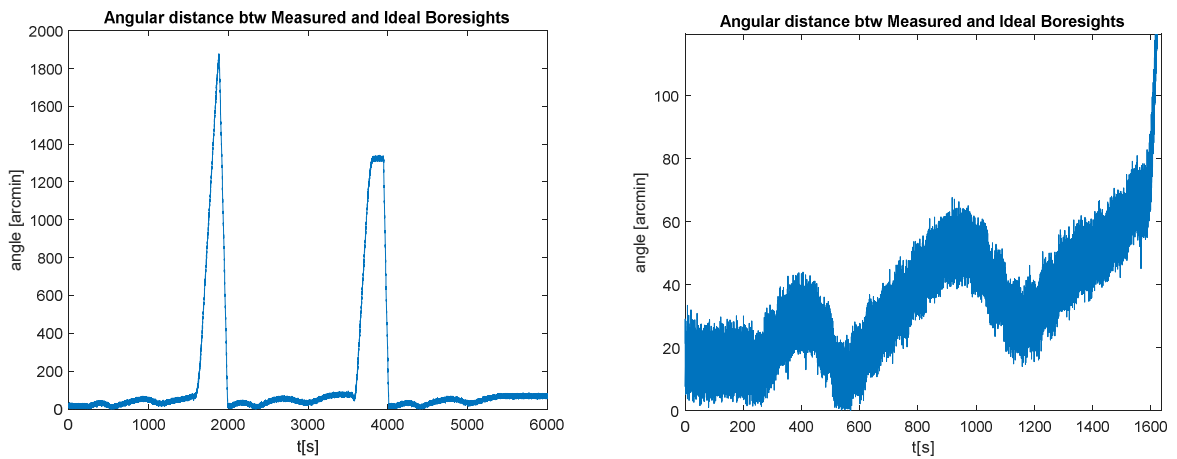


Figure 7-7: boresight error on ground (left); zoom of a single spiral (right)

Out of scope is to explain the ESA technical notes ([5],[18]) about this argument but a rough explanation is suggested to explain what it is been reused in my analysis to get Err\_measure\_angles.

The signal level at the input of the measuring systems operating at intermediate frequency is studied by adopting a loss function as follows:

$$S = \frac{P_T G_T}{L_T L_{PT}} \left( \frac{c}{4\pi R f} \right)^2 \frac{1}{L_{POL} L_{MED}} \frac{G_R}{L_{PR}} \frac{1}{L_R G_B}$$

where:

- $P_T$  is the on-board transmit power level defined at the transmitter output port;
- $G_T$  is the maximum on-board antenna gain;
- $L_T$  is the loss from transmitter output to antenna input port;
- $L_{PT}$  is the on-board antenna pointing loss;
- $R$  is the distance between transmitting and receiving antennas (m);
- $c$  is the speed of light (m/s);
- $f$  is the signal frequency (Hz);

- $L_{MED}$  is the transmission media loss (essentially the loss due to the transit through the atmosphere);
- $L_{POL}$  is the polarization loss between the two antennas;
- $G_R$  is the maximum receive antenna gain, defined at antenna output port;
- $L_{PR}$  is the receive antenna pointing loss;
- $L_R$  is the loss from antenna output port to the input;
- $G_B$  is the gain between input and interface at the detection system, including all cable losses and gain of the frequency conversion system.

Based on the above,  $L_{PT}$  is the only term which actually contains key information to be retrieved through calibration procedure. Furthermore, it has to be clear the pointing error measured on ground includes contributions both from antenna misalignments as well as from inaccuracy of the satellite attitude control and the two contributions are harsh to be discriminated.

As a consequence, means have to be employed to minimize the inaccuracy due to attitude control well below the overall accuracy requirement leaving then to calibration the duty to correct the rest of residuals by relying on information transmitted through the telemetry.

### 7.3. Final Calibration Outcome

Finally, all the measures have been gathered and the minimization problem can be solved to estimate the calibration parameters vector HGACL\_CalPar.

The criterion developed in Chapter 6 is adopted in search of calibration points by means of *genetic algorithm* usage in this case.

For the sake of a better global comprehension, two simple tests will certify the resultant performances after calibration.

Three study-cases will be checked out in some of the most demanding error-conditions:

EL2AZ\_RF\_err=[0.0293 -0.0024 0.0017] rad;

AZ2SC\_RF\_err=[-0.0012 0.131 0.0766] rad;

HGA\_boresight\_error=[-0.018 -0.0637] rad;

- 1) No Calibration: HGACL\_CalPar = [0 0 0 0 0];
- 2) 3-points Calibration: HGACL\_CalPar = [9.08e-05 2.27e-05 0.0015 -0.001 0.0031 -0.0021];
- 3) 5-points Calibration: HGACL\_CalPar = [-2.56e-05 0.0011 -0.0015 0.0004 0.0017 -0.0013];

### TEST 1: dither slew)

SAA\_start= 100.2°    SAA\_end = 98°    (87° ≤ SAA ≤ 121° in mission lifetime)

AA\_start= 1.7°    AA\_end= 7°    (-8° ≤ AA ≤ 8° in mission lifetime)

SSCE= 13,8°    (8° ≤ SSCE ≤ 35° in mission lifetime)

Spacecraft maneuvers are perfectly accomplished through all the three options as shown in Figure 7.8:

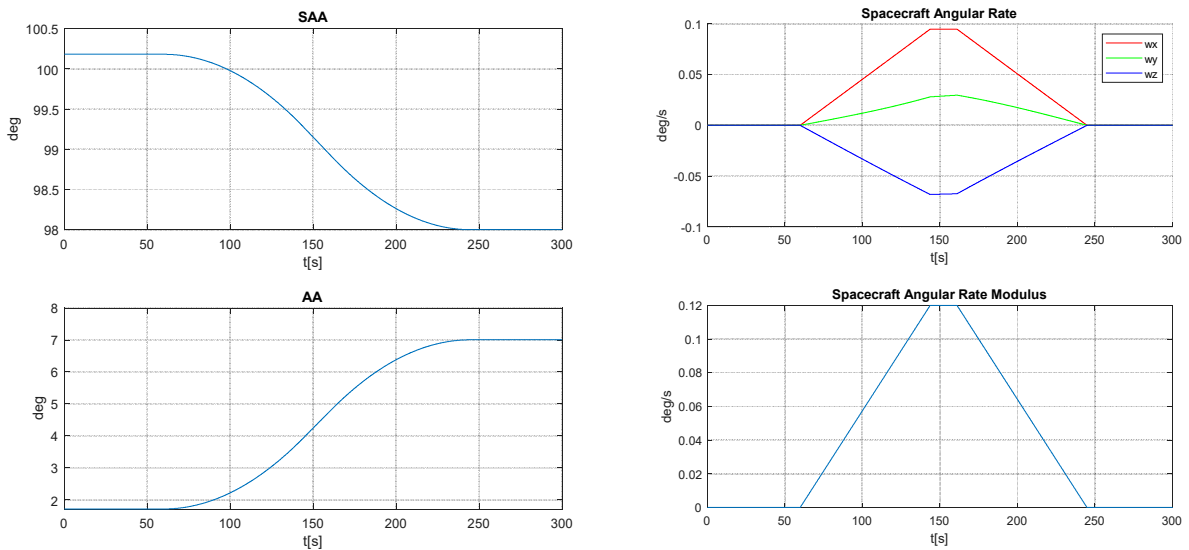


Figure 7-8: SAA and AA behavior (left); x-y-z spacecraft angular rate components and spacecraft angular rate modulus (right)

As far as it concerns the alignment between HGA boresight and Cebberos position in SRF, an exhaustive comparison is furnished in Figure 7.9.

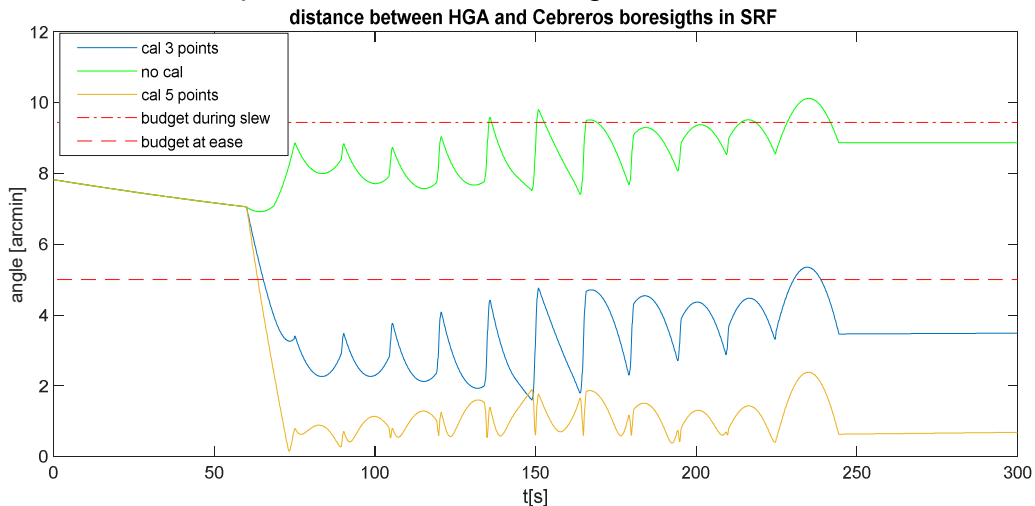


Figure 7-9: alignment btw HGA and Cebberos boresights after calibration

It can be seen how the antenna after 50 sec starts to move since the dither slew command is just sent. As expected, the 5-points calibration guarantees the best performance in absolute even if the 3-points calibration manages to stay below the budget of 5 arcmin in static condition at 250 sec (see Annex 1). Only the not calibrated curve exceeds the budget requested both in dynamic and static condition.

## TEST 2: go to GS and slew)

SAA\_start= 121°    SAA\_end = 87°    ( $87^\circ \leq SAA \leq 121^\circ$  in mission lifetime)  
 AA\_start= -8°    AA\_end= 8°    ( $-8^\circ \leq AA \leq 8^\circ$  in mission lifetime)  
 SSCE= 33,5°    ( $8^\circ \leq SSCE \leq 35^\circ$  in mission lifetime)

Spacecraft maneuvers are perfectly accomplished through all the three options as shown in Figure 7.10:

## Chapter 7 - Simulation of an 'in-flight' HGA Calibration

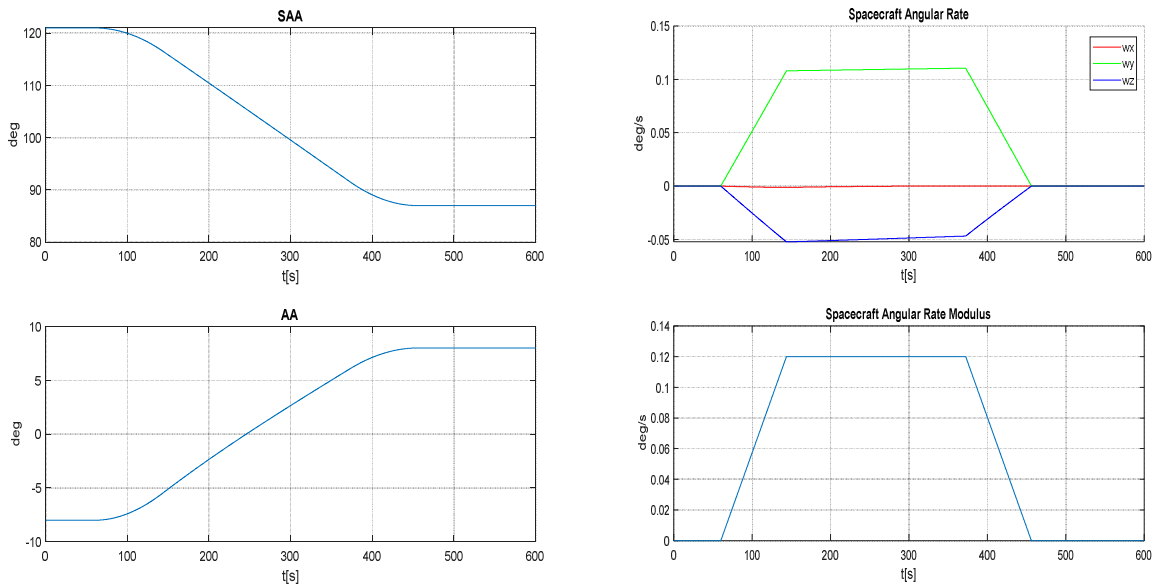


Figure 7-10: SAA and AA behavior (left); x-y-z spacecraft angular rate components and spacecraft angular rate modulus (right)

As far as it concerns the alignment between HGA boresight and Cebberos position in SRF, an exhaustive comparison is furnished in Figure 7.11.

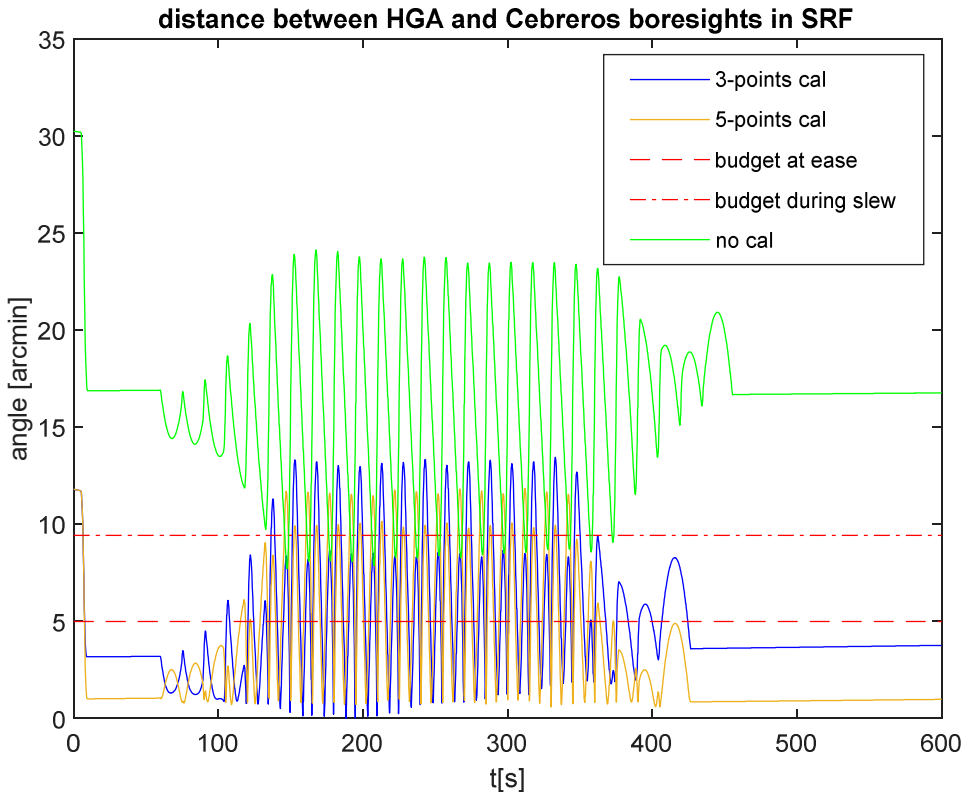


Figure 7-11: alignment btw HGA and Cebberos boresights after calibration

It can be seen how the antenna goes in Go\_to\_GS mode after 5 sec and from 60 sec on a dither slew is executed. As expected, the 5-points calibration guarantees the best performance in absolute even if the 3-points calibration manages to stay below the budget of 5 arcmin in static condition (see Annex 1). It is interesting the fact that both calibrated

curves exceed the budget requested in dynamic condition (see Annex 1). However, this is verified to happen only in particular circumstances where a so large variation of SAA and AA angles (very rear in actual situation) excites the high dynamics of the spacecraft as proposed in this test.

A possible solution consists of lowering the maximum angular rate of spacecraft of  $0.12^\circ/\text{s}$  (note the angular rate modulus in Figure 7.10) to an adapt velocity as it can be proved hereafter in Figures 7.12 and 7.13. Taking as example the 3-points calibrated curve, by decreasing the velocity from  $0.12^\circ/\text{s}$  to  $0.10^\circ/\text{s}$  as result the error remains under the dynamic budget with the only cons of a slight increasing in the amount of time spent along the maneuvers.

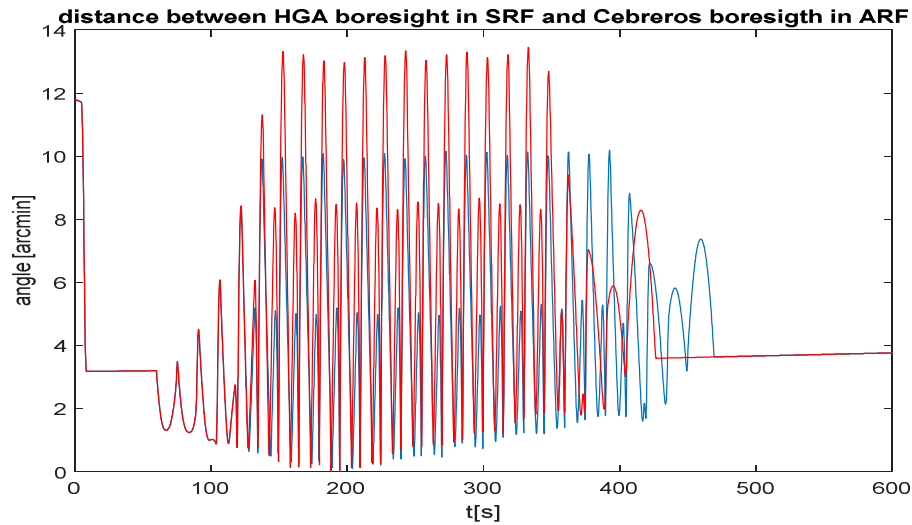


Figure 7-12: considering 3-points calibration, the red curve is obtained with  $0.12^\circ/\text{s}$ , the blue curve with  $0.10^\circ/\text{s}$

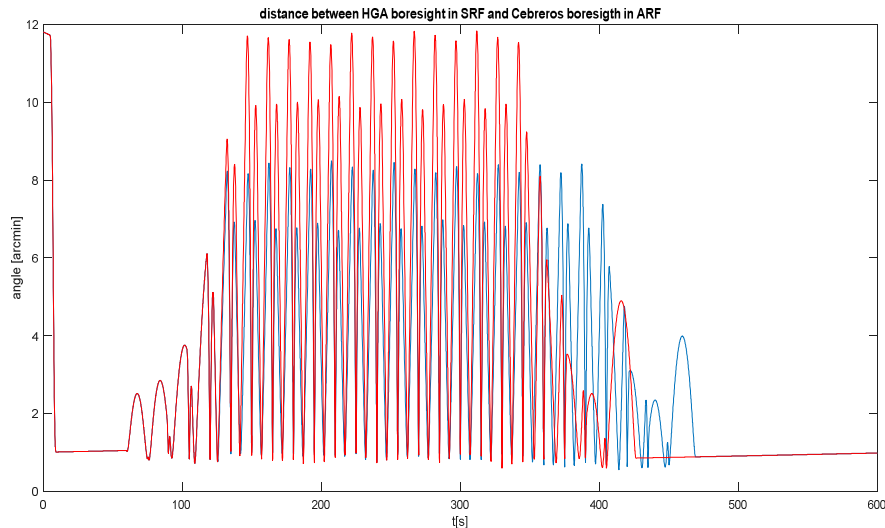


Figure 7-13: considering 5-points calibration, the red curve is obtained with  $0.12^\circ/\text{s}$ , the blue curve with  $0.10^\circ/\text{s}$

## 7.4. Conclusions of Chapter 7

In conclusion, the whole calibration procedure reveals fulfilling every constraint imposed by requirements. In particular, even a 3-points calibration succeeds in doing that (as ESA suggests) although some additional precautions must be held about the choice of optimal tuples and/or adjustment of spacecraft maximum angular rate modulus.



# Chapter 8

## Final Conclusions

This paper describes the additional post processing that is required to yield alignment corrected far field data from an acquisition of an imperfectly aligned antenna.

In fact, if Thales Alenia Engineering Group was investigating HGA in its functionalities supposing to orientate the downlink antenna perfectly aligned, my purpose through this thesis is to verify HGA pointing performance in case of misalignments in a simulated environment.

Either due to the size of the antenna or a limitation of the mechanical mounting structure, there are often considerable difficulties inherent with positioning the assembly with the degree of accuracy and precision required. The use of rigorous alignment correction methods can attain very accurate antenna alignment where alternative strategies would perhaps fail or require the use of additional mechanical support equipment.

So that, after the verification and validation of ADPME Simulink block model i.e. the electronics commanding antenna motors (see Chapter 4), at first the Polynomial Law designed by Sener and then Calibration procedure have been considered as available alignment correction methods.

The first option reveals a valid strategy only when dealing with the measured angular distance between AZ/EL motor axes known as Perpendicularity Error (see Chapter 5).

On the contrary, the Calibration procedure is the most general and accurate option to recover from any misalignments coming from both manufacture and related-mission variables (for example after-launch SC shaking, orbit and attitude control errors, thermoelastic distortion and so on; see Annex 1 for Pointing Error Budget in FPM and SCM modes).

In Chapter 6, an exhaustive analysis is carried out on calibration optimization problem. Furthermore, some elements are highlighted since they could heavily affect the calibration outcome. In details, the results denounce a critical importance in choosing the right number of points in AZ/EL domain and the optimal selection of AZ/EL tuples. Concerning the optimal selection of AZ/EL tuples, some of Matlab Global Optimization Toolbox solvers are been compared: genetic algorithm and particle swarm specifically earn credits for the goodness of their optimizations.

Finally, in Chapter 7 a complete Calibration procedure is tested on Thales Alenia HGACL Simulink Environment described in Chapter 3.

As far as it concerns the most compelling results, hereafter some of them are been listed:

- ADPME Simulink model testing, at least the version where I worked on, put in evidence some limits related to the boundary conditions;
- The polynomial law correctly succeeds in dropping the discrepancy coming from lack of perpendicularity between motor axes but if otherwise further random errors estimated to occur are added in the mathematical model, its beneficial effect on boresight alignment dramatically reduces;
- A more general correction method is essential as it is the Calibration procedure. The objective is to have a 6-parameters vector HGACL\_CalPar, according to which ADPME will adjust motor commands nullifying each not idealities and staying within the delivered pointing error budget;

- During calibration, carefully evaluate the SSCE value, number of calibration-points and optimal choice of tuples in AZ/EL domain;
- As ESA demands, a 3-points calibration should be a suitable trade-off between pointing performance and time-consuming procedure. Otherwise a 4 or 5 points calibration is a more conservative option;
- It does not exist a general fitting HGACL\_CalPar, since it changes according different working conditions;
- After calibration, if the angular error between HGA boresight and Ground Station position vector in SRF continues to exceed the budget foreseen in dynamic conditions, then SC must decrease its working angular rate modulus. Instead, it is mandatory the performance always stays within the budget in static conditions.

# ANNEX 1

## Pointing Error Budget

It is furnished a general insight in Pointing Error Budget. Specifically, in the analysis of results of Chapter 7, it will be considered *Residual Calibration* as budget in static condition while the root sum square of *Residual Calibration* and *Antenna Control* as budget in dynamic condition. Note that the following is just the pointing error budget in FPM and SCM slews whereas different pointing error budgets exists for other mission modes which are however out of scopes of this document.

	<b>Error contribution</b>	<b>FPM and SCM slews Worst Case [arcmin]</b>
<b>Deterministic Errors</b>	1) <i>Thermoelastic distortion (of antenna and other SC components)</i> 2) <i>Earth motion (position drift and rotation) + systematic error GS position</i>	~ 10
	3) <i>Residual Calibration</i>	~ 5
<b>Stochastic Errors</b>	4) <i>HGAMA and SC APE (Absolute Pointing Error)</i> 5) <i>Orbit knowledge error</i>	~ 6
<b>Antenna Control</b>	6) <i>Allocated error to HGACL</i>	~ 8
<b>TOTAL</b>		~24

*Pointing budget during only FPM and SCM slews*

The total is given by  $\sqrt{\text{Total Deterministic}^2 + \text{Total Stochastic}^2} + \text{Antenna control}$



# BIBLIOGRAPHY

- [1] G.D.Racca, R.Laureijs, L.Stagnaro, *Euclid mission status*  
<http://proceedings.spiedigitallibrary.org/> on 02/24/2015 Terms of Use: <http://spiedl.org/terms>
- [2] G.D.Racca, R.Laureijs, L.Stagnaro, *The Euclid mission Design*  
Proceedings Volume 9904, Space Telescopes and Instrumentation 2016: Optical, Infrared and Millimeter Wave; 99040O (2016); <https://doi.org/10.1117/12.2230762>
- [3] ESA/SRE(2011)12, *Euclid: Mapping the geometry of the dark Universe - Definition Study Report*, ESA/ESTEC, September 2011 (Revision 1);
- [4] EOPORTAL, <https://directory.eoportal.org/web/eoportal/satellite-missions/e/euclid>.  
Retrieved from <https://directory.eoportal.org>.
- [5] ESA. (2017). *Calibration of Euclid antenna pointing by ground measurements*.
- [6] ESA. <http://sci.esa.int/euclid/>. Retrieved from <http://sci.esa.int/home/>.
- [7] ESA. <http://sci.esa.int/euclid/42267-science/>. Retrieved from <http://sci.esa.int>.
- [8] ESA. <http://sci.esa.int/euclid/45403-mission-status/>. Retrieved from <http://sci.esa.int>.
- [9] ESA. <http://sci.esa.int/euclid/46661-mission-operations/>. Retrieved from <http://sci.esa.int>.
- [10] ESA. <http://sci.esa.int/euclid/61403-three-dark-fields-for-euclid-deep-survey/>. Retrieved from <http://sci.esa.int>.
- [11] *Euclid Space Mission: building the sky survey*, Statistical Challenges in 21<sup>st</sup> century Cosmology, Proceedings IAU Symposium No. 306, 2014 A.C. Editor, B.D. Editor & C.E. Editor, eds.
- [12] MATLAB (2019), *Global Optimization Toolbox, User's Guide*.
- [13] Sener (2017) (reserved material), *EUCLID Antenna Deployment and Pointing Mechanism, Polynomial Correction of ADPM Misalignment*.
- [14] Sener (2017) (reserved material), *EUCLID Antenna Deployment and Pointing Mechanism, POLYNOMIAL LAW TEST REPORT*.
- [15] Thales Alenia Space (2017) (reserved material), *ADPME Model Test Report*.
- [16] Thales Alenia Space (2018) (reserved material), *EUCL-TAST\_TN-2-045\_is1\_HGACL\_ESE\_Description\_And\_Simulation\_Results*.
- [17] Thales Alenia Space(2018) (reserved material), *EUCL-TAST-RP-2-072\_is2\_draft\_HGACL\_Design\_and\_Justification\_Report\_2018\_11\_13*.
- [18] S.F.Gregson, C.G.Parini, J.McCormick, *FAST AND ACCURATE ANTENNA ALIGNMENT CORRECTION PERFORMED USING A VECTOR ISOMETRIC ROTATION*, 2007  
Loughborough Antennas and Propagation Conference
- [19] Marco Rotondo (2019), thesis: *Euclid AOCS: Fine Guidance Sensor modeling and simulation*